**Università degli Studi di Torino**
Doctoral School of Sciences and Innovative Technologies
PhD Program in Chemical and Materials Sciences XXXIII Cycle

# CHARACTERIZATION OF VEHICLE AND LABORATORY AGED COMMERCIAL THREE WAY CATALYST: A CORRELATION BETWEEN REAL AND SIMULATED AGEING

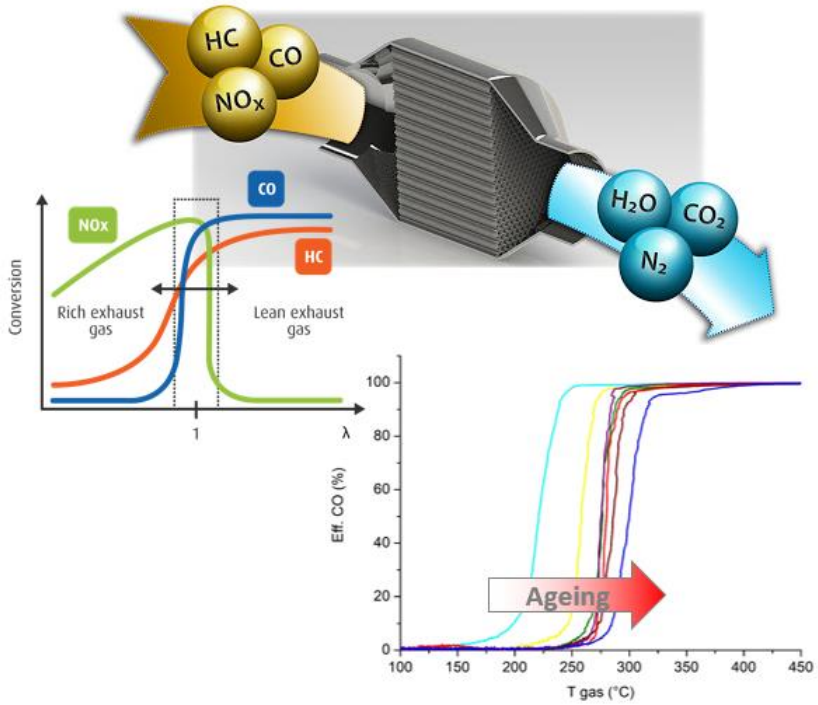


**Mattia Giuliano**

Supervisor:
Prof. Gabriele Ricchiardi

**Università degli Studi di Torino**

Doctoral School of Sciences and Innovative Technologies

PhD Program in Chemical and Materials Sciences XXXIII cycle

# CHARACTERIZATION OF VEHICLE AND LABORATORY AGED COMMERCIAL THREE WAY CATALYST: A CORRELATION BETWEEN REAL AND SIMULATED AGEING


Candidate: **Mattia Giuliano**

Supervisor: Prof. **Gabriele Ricchiardi**

Jury Members: Prof. **Samir Bensaid**
Politecnico di Torino
DISAT – Department of Applied Science and Technology

Dr. **Yakoumis Iakovos**
MONOLITHOS Catalysts & Recycling Ltd.

Prof. **Giuseppe Spoto**
University of Torino
Department of Chemistry

Head of the Doctoral School: Prof. Massimo Maffei
PhD Programme Coordinator: Prof. Bartolomeo Civalleri


Torino, 26/03/2021

# Summary

# Abbreviation Table

- TWC: three way catalyst
- CO: carbon monoxide
- HC: hydrocarbon
- $NO_x$: nitrogen oxides
- PGM: platinum group metal
- XRD: x-ray diffraction
- XPS: x-ray photoelectron spectroscopy
- BET: Brunauer–Emmett–Teller method
- TPR: temperature programmed reduction
- BAT: bench ageing time
- SSA: specific surface area
- SEM: scanning electron microscopy
- TEM: transmitted electron microscopy
- XRF: x-ray fluorescence
- EDX: energy-dispersive X-ray
- FUL: full useful life
- ICP-OES inductively coupled plasma optical emission spectrometer
- FT-IR: Fourier-transform infrared spectroscopy
- RT: room temperature
- LNT: liquid-nitrogen temperature
- TCD: thermal conductivity detector
- FE-SEM: field-emission scanning electron microscopy
- BSD: back-scattering electron detection
- OSC: oxygen storage capacity
- T50: light-off temperature

# 1 Introduction

One of the main sources of environmental pollution are vehicle emissions. Starting from the '70s one of the main challenges for vehicle manufacturers has been the compliance to the increasingly stringent regulations on emissions. This was obtained largely by means of the development of catalysts and catalytic systems. For gasoline-fueled vehicles, the main system to reduce engine emission is represented by the three-way catalyst (TWC). It can perform simultaneous oxidation of CO and unburned hydrocarbons (HC) and reduction of nitrogen oxides ($NO_x$), thanks to a well-controlled air-to-fuel ratio (A/F = 14.63→λ =1) that keeps the gaseous combustion stream close to stoichiometry. In this condition both the oxidation and reductions reactions reach the higher yield (figure 1)[1].

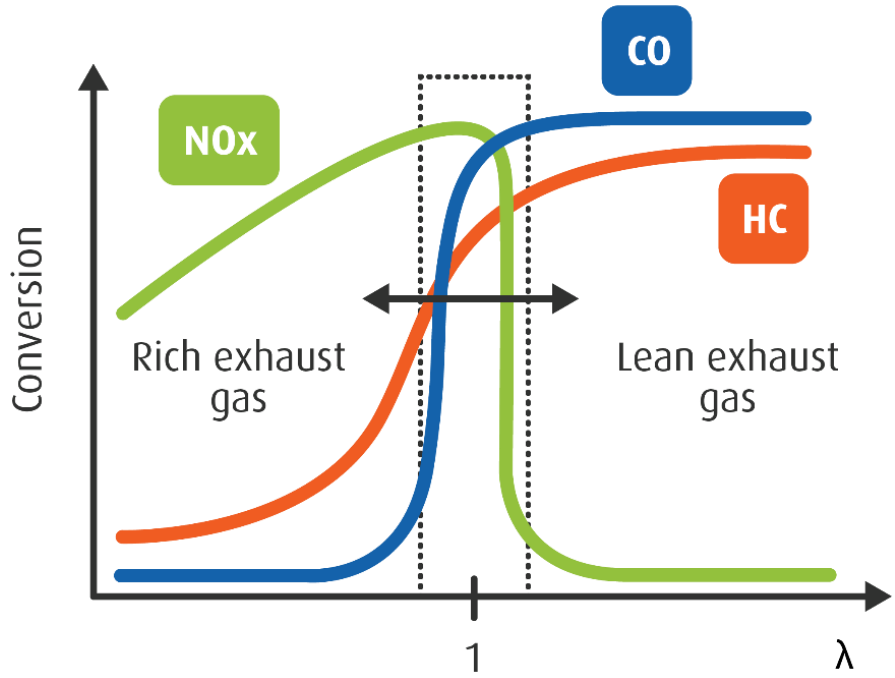


*Figure 1: Conversion efficiency vs. air-to-fuel ratio relationship in TWC[1].*

These catalysts are composed by a support structure, a ceramic honeycomb monolith (typically made of cordierite) with a high density of channels. This component has only a mechanical function and it is not involved in the catalytic processes. The walls of the

channels are coated with the catalytic material, typically called *washcoat*. It is a very complex catalytic material, composed by a porous support, with a high surface area in order to increase the contact with the reactant, by the catalytically active metals and by numerous other components, such as dopants and stabilizers, useful to enhance the performances and the service life of the catalyst[2]. The most used material for the porous support is aluminum oxide ($Al_2O_3$) and, in particular its $\gamma$-$Al_2O_3$ polymorph, thanks to its high specific surface area and relatively high thermal stability. Due to the requirement of reaching quickly an acceptable conversion already at low temperature, at the so called "cold-start" of the vehicle, the "close-coupled-catalyst" technology has been develop. In this solution, the catalyst is installed near the engine, in order to exploit its heat to warm-up the catalyst and reach easily the optimal working condition. Being the catalyst mounted on the exhaust manifold, it also experiences very high temperatures, which may exceed 1000°C, above the limits of the thermal stability of alumina. For this reason, the most advanced technologies contain numerous type of stabilizing agents. In particular alkaline earth metal or rare earth oxides are used, for example BaO, $La_2O_3$, but the most important is Cerium oxide ($CeO_2$) [3]. The role of ceria inside the catalytic automotive technologies is not only to increase the stability of the porous structure, but it is fundamental to increase the reactivity of the material. In particular ceria is able to store and release oxygen as a function of the environmental conditions due to its redox properties ($Ce^{4+} \leftrightarrow Ce^{3+}$)[4]. The TWC works in a constant oscillation between lean (air rich, air-to-fuel ratio >1) and rich conditions (fuel rich, air-to-fuel ratio <1), so ceria allows to store oxygen during lean phases and release it during rich steps. This property is called Oxygen Storage Capacity (OSC) and leads to an increasing of TWC efficiency by enlarging the air-to-fuel operating window [5]. To enhance the thermal stability and the redox properties, nowadays Ce oxide is stabilized with Zr oxide. Ce-Zr mixed oxides are more stable at high temperature and the insertion of $ZrO_2$ in the crystal lattice of $CeO_2$ generates a structural modification, with the generation of highly mobile lattice oxygens, that improves the oxygen storage capacity of the material[6]. The catalytic function is obtained by highly dispersed precious metals like Pt, Pd, Rh (PGM, Platinum Group metals) dispersed in the washcoat by impregnation to form a uniform distribution of particles with a diameter of a few nm. These noble metals have good thermal stability

(compared to the base metals) and relatively resistant to sulphur poisoning. Moreover, some noble metals as Ru, Os and Ir have been excluded due to their tendency to form volatile oxides [7]. PGM nanoparticles are affected by the high temperatures, which leads to a decrease of the dispersion, but the stabilizing agents help to limit this effect, reducing the mobility of the metal atoms. The high surface area of the support and the high dispersion of PGM particles are crucial for the catalyst activity, increasing its contact with engine-out gases and allowing to exploit effectively the noble metals.

## 1.1 Ageing and deactivation of TWC

Automotive catalysts usually work in extreme conditions: at high temperature due to the exhaust temperature and to exothermic reactions involved, with local peaks above 1000-1100°C. They also operate in a very variable environment, in constant oscillation between oxidant and reducing conditions, and in presence of water vapor in the stream. Furthermore, they are in contact with numerous chemical species, which can react with catalyst components producing some unwanted products. These phenomena, called *thermal* and *chemical ageing* respectively, are the primary sources of catalyst deactivation [8]. Chemical ageing is linked to the deposition on the catalyst of foreign elements carried by exhaust gases, generated by the combustion of oil and fuel additives (Zn, P, Ca, S), which can react with oxides and noble metals present in the washcoat. These reactions can lead to the formation of less active compounds, and then decrease catalysts performance, or to the deposition of a superficial layer that makes it impossible for the reactants to access the porosity of the washcoat [9]. Thermal ageing is the major way of catalyst deactivation. The high temperature induces a series of physical processes that lead to sintering of washcoat components and of PGM particles and water vapor accelerates these phenomena. The sintering is associated to the loss of active surface via structural modification, which is usually driven by the high temperature. In the automotive catalyst the main phenomenon affecting the porous supports a phase transformation from $\gamma$-$Al_2O_3$, characterized by high porosity and high surface area, to other more thermodynamically stable forms of alumina with lower surface area ($\delta$, $\theta$, $\alpha$). The rate of this transformation increases with increasing of the temperature. Another

driving force of sintering is the lowering of the surface energy and the transport of material leads to coalescence of particles, particle growth and elimination of the pores, due to condensation of hydroxyl groups residing on adjacent particles. Temperature and the atmosphere are the main parameters controlling the sintering of a given oxide. The result of support sintering in catalysis is the loss of surface area of the carrier [10].

Highly dispersed noble metals particles undergo similar processes, with aggregation via coalescence of the particles and metal atoms migration. Sintering occurs trough migration of both atoms and crystallites on surface support and their coalescence, forming lager agglomerations, reducing the surface exposed to reactants. PGM particles can be also involved in the sintering process of the alumina support, suffering encapsulation of particles due to the collapse of the porous structure. The metal sintering obviously depends on the nature of metal and on the temperature and, to a lower extent, on the reaction atmosphere. The sintering of Pt is higher in oxidizing environment compared to sub-stoichiometric conditions [11]. Pd differs from Pt in a way that it is more active in oxide form (PdO). However, at high temperature PdO decomposes to metallic Pd, which results in decreased catalytic activity. Lowering the temperature a re-oxidation of Pd take place, but it is not complete due to major rate sintering particles of metallic palladium. Metallic Pd at high temperature form larger agglomerates, which are re-oxidized at low temperature only on the surface, while the bulk remains in Pd form, due to the higher dimensions of the particles [12]. Rh is not affected by sintering, but high temperatures promote the formation of irreducible oxides ($RhO_2$ and $Rh_2O_3$) and the reaction between Rh and $Al_2O_3$, forming a phase that renders Rh progressively inaccessible [13].

As said previously, Ce and Zr mixed oxides have the fundamental capacity to stabilize the support and PGM particles, giving stability and durability. Stabilization of the alumina support is due to the interaction between their crystal structures, which makes the support more stable to the high temperature. These effects are reported in numerous publications, like the work of Wu et al. [14] where a comparison between sample of pure γ-alumina and alumina mixed with Ce and Zr oxides, fresh and after thermal ageing (1000°C) is made. Morphological and X-ray diffraction results highlighted that samples containing Ce-Zr oxides did not form the α-$Al_2O_3$, polymorph with lowest porosity and

the specific surface area measurements showed that the reduction of surface after thermal ageing in these mixed samples was lower than in pure alumina samples. Stabilization of noble metals is related to the formation of strong PGM-O-Ce interactions, which inhibits the sintering of metal particles [15]. Cao et al. [16] used $H_2$-TPR to verify the dispersion of noble metal and TEM microscopy was employed to measure the particles dimensions. The results show a larger dispersion of PGM in Ce-Zr supported sample in all ageing conditions, with a limited growth of their dimensions (>20 nm). On supports made of alumina only thermal ageing leaded to a serious growth of particles (smaller than 100 nm). Ceria can suffer the effects of thermal ageing, deteriorating its properties. The sintering of $CeO_2$ leads to a loss in surface area, hindering its oxygen storage capacity, and to a decrease of contact between the precious metal and ceria. Adding $ZrO_2$ in appropriate way can form a Ce-Zr oxides solid solution that can improve the oxygen storage capacity and durability of this phase [17]. In addition, Ce-Zr mixed oxides undergo to thermal ageing and sintering phenomena. In particular, sintering leads to a growth of the particles which hinders oxygen migration from the bulk to the surface, decreasing the quantity available to release in the reaction atmosphere [18]. Other dopants useful to stabilize the washcoat structure and properties are the rare earth oxides (La, Nd, Pr, and Y). For example La oxide, a trivalent cation, can stabilize the solid solution of Ce-Zr mixed oxide, and at high temperature it can form compounds with alumina helping to stabilize the porous structure and preventing the sintering process.

Heo et al. [20] proposed an overall ageing and deactivation mechanism for automotive three-way catalysts. This scheme was based on an extensive characterization of four catalysts coming from vehicles with different mileage (20000-100000 km). They identified two steps for the deactivation: the initial, where the activity of TWC decreases due to sintering of noble metal particles, Ce-Zr mixed oxides (with separation of phases in this case) and poisoning by P and S contained in engine exhaust gas. The second step is represented by a gradual deactivation due to a progressive poisoning and to the encapsulation of noble metal particles in sintered support.

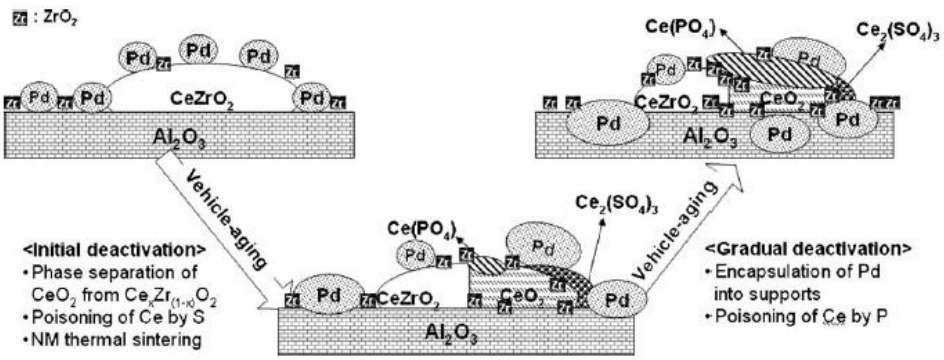


*Figure 2: Schematic deactivation process of Pd TWCs [20]*

## 1.2 Ageing simulation in automotive application

Long-term compliance with automotive exhaust gas emission regulations is one of the challenges faced by the automotive industry. The increasingly stringent limits require high performances also at high mileage (up to 160000 km), so the catalysts needs to be designed to guarantee that yield for the whole life of the component. Despite the progressive transition to electric mobility, the interest on emission control of gasoline vehicle is high, being the hybrid technology still based on this type of engine. Furthermore, the catalysts of hybrid vehicles are exposed to the additional stress deriving from an engine shut down after a warm up at low driver torque demand, creating a high temperature lean environment in the TWC.

To test the catalyst durability and useful life, automotive manufacturers need to define accelerated ageing methods. Ageing and testing directly on road using a real vehicle is not economically feasible and requires too long time for testing. For this reason accelerated engine test benches and laboratory accelerated ageing protocols were developed. Engine bench tests consists in obtaining the same deactivation in a reduced time using an accelerated ageing method, in which the catalyst is exposed to a high temperature exhaust stream produced by an engine-dynamometer set-up which follows prescribed sequences of operating conditions to provide specific conditions of λ and

temperature of engine out gas[21]. These methods can be very useful to simulate the ageing condition for high mileage samples, but these are expensive in terms of time and cost.

The second solution is to simulate the engine out gas condition at laboratory scale, using facilities, which create synthetic a gas mixture (air and water vapor in the easiest layout) and feed it at high temperature for long times through the sample catalysts, using special furnaces. This is a very flexible solution, but a complex and expensive facility is required in order to simulate the heterogeneous stresses produced by vehicle aging.

The definition of simulated ageing protocols requires the knowledge of the effects of ageing in different operating conditions, and the ability to correlate them to the real on road ageing. To make this comparison is not easy. A first problem is the difficulty to obtain significant samples of identical catalysts on identical vehicles used in comparable conditions over very long mileages. Furthermore, to re-create the same engine-out gases conditions at laboratory scale is complicated because they have a complex composition and are very variable [22]. This is valid above all for the three-way catalyst, which works constantly in oscillating conditions around the stoichiometric air-to-fuel ratio, fluttering between oxidant and reducing environment. Numerous studies have tried to understand the impact of different environments on automotive catalysts components and to correlate real vehicle ageing with accelerated ageing methods: Stenbom *et al.* studied the thermal deactivation path of TWC in different conditions and temperatures. That study found that high temperature lean (oxidant) conditions were particularly detrimental to the catalyst. On the other hand, rich condition (reducing) did not show any effect, except at very high temperature (>1100°C); but these results were not easily comparable with real vehicle ageing [23]. Hietikko *et al.* [24] and Lassi *et al.* [25] performed a similar study on thermal ageing, correlating their results with a vehicle-aged and an engine-aged samples, characterizing them using XRD, XPS, BET surface area and measuring their activity. The results showed a good correlation between a real sample and a sample aged in reducing condition in terms of structural changes, but from the performance point of view the best correlation was achieved with oxidizing conditions. Kallinen *et al.* compared catalyst samples aged on engine bench, in static oven and in dynamic condition using an IR furnace. The oxidant atmosphere of the static oven resulted more detrimental for the

catalysts, but the dynamic ageing, designed to replicate the change in temperature and environment typical of the engine working condition, correlates well with the engine-aged sample, but with some problem linked to the shortness of the lab-ageing cycle [26]. In addition, the correlation between the results of different accelerated ageing methods are also difficult. Blades *et al*. tried to correlate lab ageing in static air condition with engine bench results. Their aim was to understand if the BAT (bench ageing time), equation adopted by US EPA to calculate the appropriate length of time to age a catalyst at determined temperature, to yield an equivalent deterioration as vehicle on an approved road cycle, works well in all the simulated condition. Their result underlined that static ageing caused stronger dependence from temperature of the ageing process then that predicted by the BAT model, but a lesser dependence on time, probably due to high oxygen concentration of static ageing atmosphere [27].

- REFERENCES:


1. González-Velasco, J. R.; Botas, J. A.; Ferret, R.; Pilar González-Marcos, M.; Marc, J.-L.; Gutiérrez-Ortiz, M. A. Thermal Aging of Pd/Pt/Rh Automotive Catalysts under a Cycled Oxidizing–Reducing Environment. *Catalysis Today* **2000**, *59* (3–4), 395–402. https://doi.org/10.1016/S0920-5861(00)00304-7.
2. Kašpar, J.; Fornasiero, P.; Hickey, N. Automotive Catalytic Converters: Current Status and Some Perspectives. *Catalysis Today* **2003**, *77* (4), 419–449. https://doi.org/10.1016/S0920-5861(02)00384-X.
3. Kašpar, J.; Fornasiero, P.; Graziani, M. Use of CeO2-Based Oxides in the Three-Way Catalysis. *Catalysis Today* **1999**, *50* (2), 285–298. https://doi.org/10.1016/S0920-5861(98)00510-0.
4. Gong, J.; Wang, D.; Li, J.; Kamasamudram, K.; Currier, N.; Yezerets, A. An Experimental and Kinetic Modeling Study of Aging Impact on Surface and Subsurface Oxygen Storage in Three-Way Catalysts. *Catalysis Today* **2019**, *320*, 51–60. https://doi.org/10.1016/j.cattod.2017.11.038.
5. Vidal, H.; Kašpar, J.; Pijolat, M.; Colon, G.; Bernal, S.; Cordón, A.; Perrichon, V.; Fally, F. Redox Behavior of CeO2–ZrO2 Mixed Oxides. *Applied Catalysis B: Environmental* **2000**, *27* (1), 49–63. https://doi.org/10.1016/S0926-3373(00)00138-7.
6. Kašpar, J.; Di Monte, R.; Fornasiero, P.; Graziani, M.; Bradshaw, H.; Norman, C. Dependency of the Oxygen Storage Capacity in Zirconia–Ceria Solid Solutions upon Textural Properties. *Topics in Catalysis* **2001**, *16/17* (1/4), 83–87. https://doi.org/10.1023/A:1016682831177
7. Gandhi, H. S.; Graham, G. W.; McCabe, R. W. Automotive Exhaust Catalysis. *Journal of Catalysis* **2003**, *216* (1–2), 433–442. https://doi.org/10.1016/S0021-9517(02)00067-2.
8. Winkler, A.; Ferri, D.; Hauert, R. Influence of Aging Effects on the Conversion Efficiency of Automotive Exhaust Gas Catalysts. *Catalysis Today* **2010**, *155* (1–2), 140–146. https://doi.org/10.1016/j.cattod.2008.11.021.
9. Shelef, M.; Otto, K.; Otto, N. Poisoning of Automotive Catalysts. *Adv. Catal*. **1979**, *27*, 311–365, doi:10.1016/s0360-0564(08)60059-0.
10. Neyestanaki, A. K.; Klingstedt, F.; Salmi, T.; Murzin, D. Y. Deactivation of Postcombustion Catalysts, a Review. *Fuel* **2004**, *83* (4–5), 395–408. https://doi.org/10.1016/j.fuel.2003.09.002.

11. Flynn, P. Experimental Studies of Sintering of Supported Platinum Catalysts. *Journal of Catalysis* **1975**, *37* (3), 432–448. https://doi.org/10.1016/0021-9517(75)90180-3.
12. Farrauto, R. J.; Hobson, M. C.; Kennelly, T.; Waterman, E. M. Catalytic Chemistry of Supported Palladium for Combustion of Methane. *Applied Catalysis A: General* **1992**, *81* (2), 227–237. https://doi.org/10.1016/0926-860X(92)80095-T.
13. Marchionni, V.; Newton, M. A.; Kambolis, A.; Matam, S. K.; Weidenkaff, A.; Ferri, D. A Modulated Excitation ED-EXAFS/DRIFTS Study of Hydrothermal Ageing of Rh/Al2O3. *Catalysis Today* **2014**, *229*, 80–87. https://doi.org/10.1016/j.cattod.2013.10.082.
14. Wu, X.; Xu, L.; Weng, D. The Thermal Stability and Catalytic Performance of Ce-Zr Promoted Rh-Pd/γ-Al2O3 Automotive Catalysts. *Applied Surface Science* **2004**, *221* (1–4), 375–383. https://doi.org/10.1016/S0169-4332(03)00938-3.
15. Shinjoh, H.; Hatanaka, M.; Nagai, Y.; Tanabe, T.; Takahashi, N.; Yoshida, T.; Miyake, Y. Suppression of Noble Metal Sintering Based on the Support Anchoring Effect and Its Application in Automotive Three-Way Catalysis. *Top Catal* **2009**, *52* (13–20), 1967–1971. https://doi.org/10.1007/s11244-009-9371-5.
16. Cao, Y.; Ran, R.; Wu, X.; Zhao, B.; Wan, J.; Weng, D. Comparative Study of Ageing Condition Effects on Pd/Ce0.5Zr0.5O2 and Pd/Al2O3 Catalysts: Catalytic Activity, Palladium Nanoparticle Structure and Pd-Support Interaction. *Applied Catalysis A: General* **2013**, *457*, 52–61. https://doi.org/10.1016/j.apcata.2013.03.002.
17. Bunluesin, T.; Gorte, R. J.; Graham, G. W. CO Oxidation for the Characterization of Reducibility in Oxygen Storage Components of Three-Way Automotive Catalysts. *Applied Catalysis B: Environmental* **1997**, *14* (1–2), 105–115. https://doi.org/10.1016/S0926-3373(97)00016-7.
18. Zhao, M.; Shen, M.; Wang, J. Effect of Surface Area and Bulk Structure on Oxygen Storage Capacity of Ce0.67Zr0.33O2. *Journal of Catalysis* **2007**, *248* (2), 258–267. https://doi.org/10.1016/j.jcat.2007.03.005.
19. Wang, Q.; Zhao, B.; Li, G.; Zhou, R. Application of Rare Earth Modified Zr-Based Ceria-Zirconia Solid Solution in Three-Way Catalyst for Automotive Emission Control. *Environ. Sci. Technol.* **2010**, *44* (10), 3870–3875. https://doi.org/10.1021/es903957e.
20. Heo, I.; Choung, J. W.; Kim, P. S.; Nam, I.-S.; Song, Y. I.; In, C. B.; Yeo, G. K. The Alteration of the Performance of Field-Aged Pd-Based TWCs towards CO and C3H6 Oxidation. *Applied Catalysis B: Environmental* **2009**, *92* (1–2), 114–125. https://doi.org/10.1016/j.apcatb.2009.07.016.
21. Ramanathan, K.; Oh, S. H. Modeling and Analysis of Rapid Catalyst Aging Cycles. *Chemical Engineering Research and Design* **2014**, *92* (2), 350–361. https://doi.org/10.1016/j.cherd.2013.06.020.
22. Kang, S. B.; Kwon, H. J.; Nam, I.-S.; Song, Y. I.; Oh, S. H. Activity Function for Describing Alteration of Three-Way Catalyst Performance over Palladium-Only Three-Way Catalysts by Catalyst Mileage. *Ind. Eng. Chem. Res.* **2011**, *50* (9), 5499–5509. https://doi.org/10.1021/ie200083f.
23. Stenbom, B.; Smedler, G.; Nilsson, P. H.; Lundgren, S.; Wirmark, G. Thermal Deactivation of a Three-Way Catalyst: Changes of Structural and Performance Properties; 1990; p 900273. https://doi.org/10.4271/900273.
24. Hietikko, M.; Lassi, U.; Kallinen, K.; Savimäki, A.; Härkönen, M.; Pursiainen, J.; Laitinen, R. S.; Keiski, R. L. Effect of the Ageing Atmosphere on Catalytic Activity and Textural Properties of Pd/Rh Exhaust Gas Catalysts Studied by XRD. *Applied Catalysis A: General* **2004**, *277* (1–2), 107–117. https://doi.org/10.1016/j.apcata.2004.09.029.
25. Lassi, U.; Polvinen, R.; Suhonen, S.; Kallinen, K.; Savimäki, A.; Härkönen, M.; Valden, M.; Keiski, R. L. Effect of Ageing Atmosphere on the Deactivation of Pd/Rh Automotive Exhaust Gas Catalysts: Catalytic Activity and XPS Studies. *Applied Catalysis A: General* **2004**, *263* (2), 241–248. https://doi.org/10.1016/j.apcata.2003.12.024.
26. Kallinen, K.; Suopanki, A.; Härkönen, M. Laboratory Scale Simulation of Three-Way Catalyst Engine Ageing. *Catalysis Today* **2005**, *100* (3–4), 223–228. https://doi.org/10.1016/j.cattod.2004.09.057.
27. Blades, L.; Douglas, R.; McCullough, G.; Woods, A. Correlation of Static Aging Effects on Automotive Catalysts. *Can. J. Chem. Eng.* **2014**, *92* (9), 1526–1530. https://doi.org/10.1002/cjce.22012.
28. Fernández-Ruiz, R.; Galisteo, F. C.; Larese, C.; Granados, M. L.; Mariscal, R.; Fierro, J. L. G. TXRF Analysis of Aged Three Way Catalysts. *Analyst* **2006**, *131* (4), 590. https://doi.org/10.1039/b513508g.

# 2 Experimental Project

The present work has the purpose to understand in deep of all the microscopic processes associated to ageing, trying to find a correlation between phenomena occurred on vehicle and accelerated ageing protocols. All these information could be useful for the future definition of new ageing protocol, able to substitute an accelerated engine bench cycle, ensuring a better correlation and reduced time and economic costs. In the first part of the study, the focus was on the characterization of a fresh and aged TWC. The aim was to study all the thermal effects occurring in the catalyst structure from the structural and morphological point of view, using different techniques [1]. Subsequently, an extensive characterization of a TWC commercial technology was undertaken, using the techniques optimized previously, covering different ageing conditions (on vehicle, on engine bench, at laboratory). Moreover, in this step a functional characterization of the samples was also performed. Using a synthetic gas facility, some efficiency tests were performed in order to observe and study the progressive deactivation of the catalyst. In this way, it was possible to interpret the relationship between structural modification and loss of conversion efficiency[2]. The last part of the study was focused on one of the central element for the catalyst functionality: the noble metal particles. In particular, the samples were studied using techniques useful to understand the dimensions and distribution of the noble metal particles in washcoat materials [3]. A brief study about chemical ageing effects was performed, in order to understand relationship with the results of the functional test. After a complete characterization of these samples, a correlation between real and laboratory aged samples was attempted.

## 2.1 Catalyst Technology

One important limitation of the studies available in the literature concerning TWC catalysts is that they are typically performed on model materials especially prepared for the purpose. This makes the transferability of the results to real commercial catalysts questionable. In this work, the analysis were made on a commercial technology, which has complex composition and high structural complexity due to the highly optimized

formulation and production method. The technology chosen were commercial formulations of TWC, based on double metals Pd/Rh technology. This is one of the most recent and widely diffused formulations for gasoline engine catalyst due to the high thermal resistance of Pd in oxidizing conditions (owing to the lower vapor pressure of the PdO)[4].

The first step of the study, concerned the optimization of the characterization protocol, and it was performed on an experimental formulation, not in production, with a loading of PGM of 70 g/ft$^3$ and ratio 0:58:12 (Pt:Pd:Rh) coated on cordierite cylindrical monolith of 1l, with channel density of 750 cpsi (channels/inch$^2$). For the second part of the study the technology chosen was a more recent one, a real commercial formulation, currently in production, with a PGM loading of 60 g/ft$^3$, ratio 0:55:5 (Pt:Pd:Rh) and washcoat loading of 2,9 g/inc$^3$. The component was a cylindrical monolith of 0,55l (4.2" x 2.5") characterized by a high density of channels (900 cpsi) with hexagonal shape. All the components were cored in order to obtain a cylindrical sample of 1.5" of diameter (Figure 3).

.

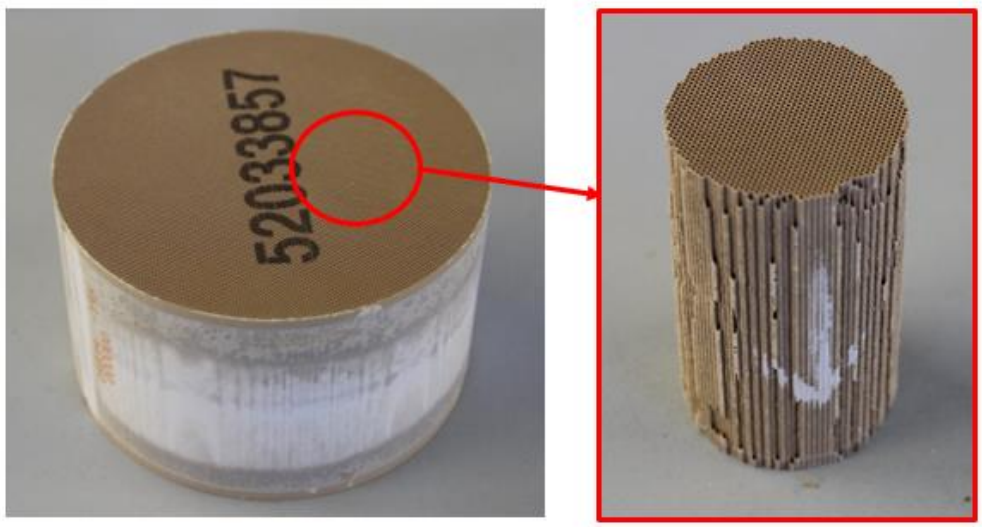


*Figure 3: TWC full-scale ceramic monolith (60 g/ft$^3$, 900 cpsi) and cored sample.*

## 2.2 Optimization of characterization methodologies.

As described before, one of the key-points of this work is to understand the processes occurring during the thermal ageing of automotive catalyst material. To do this, the first part of the project was focused on a complete characterization of a fresh and an aged TWC, in order to test and optimize the measurement protocols. In this way, besides studying the thermal behavior of this material, it was possible to optimize the analysis conditions for all the techniques applied on the topic, as SSA, XRD, SEM, TEM and Raman Spectroscopy. Three cored samples were prepared from a single fresh catalyst. One of them was aged in a static oven, at 1000 °C for 15 h. This treatment was intended to simulate the full useful life of the component. In fact, these arbitrary conditions correspond to doubling the time of the standard static ageing cycle adopted by many carmakers. Therefore, it represents a limiting case of severe ageing, near the end-of-life condition for this type of component. TWCs usually work spanning both lean and rich condition, but oxidant environments result more harmful for this material [5]. So, the use of pure static air (totally lean condition) enhance the ageing phenomena, accelerating all the thermal ageing processes.

### 2.2.1 Washcoat extraction method.

One drawback of studying real commercial catalysts instead of model systems is that the largest part of the mass of commercial catalysts is constituted by the cordierite ceramic support, which has only a mechanical function and which does not undergo significant ageing phenomena. The interesting part of the catalyst is the washcoat, which represents only 30-40% in weight of catalyst. For this reason, in the first part of this study a washcoat extraction method was developed aimed at improving the sensitivity of the characterization methods. In fact, the presence of the cordierite substrate may cause a significant dilution of sample if the entire catalyst is milled. Therefore, a practical procedure to separate the washcoat from cordierite substrate was tuned. This method is based on the detachment of the material by thermal shock, performed soaking the sample first in liquid nitrogen, then in water, repeating the operation ten times. Between the

repetitions, the samples are blown with gaseous $N_2$ to remove water residues from channels, to avoid formation of ice deposits, which can break the ceramic substrate. The solid material extracted was recovered evaporating the water and drying the material in oven. The powder obtained was weighted, as well as the sample before and after extraction, to evaluate the efficiency of the process. Washcoat extraction process was performed on four fresh and one aged samples to study also the reproducibility of the method. Before that, the samples were axially broken to observe the internal appearance before and after the process, and to obtain samples with the washcoat still coated on cordierite for the SEM and SSA analyzes. These visual analyses were performed using an optical microscope Leica S6D equipped with digital camera MC 170 HD. Scanning Electron Microscopy (SEM) was performed with a Zeiss EVO50 XVP using source of $LaB_6$ with an electron acceleration potential of 10 kV and 100 pA using a working distance of 9.5-10 mm. The images were collected using the back-scattered electron detector (BSD). The samples was metallized with Au.

### 2.2.2 Washcoat powder characterization.

Moving to the characterization of the washcoat powder, the composition of the fresh sample was investigated with a semi-quantitative elemental analysis using X-ray fluorescence (XRF) with a Panalytical Axios, which used an Rh tube source. To observe the microstructural variation due to ageing, X-ray powder diffraction was performed using a Rigaku MiniFlex 600. The pattern was recorded with a Bragg-Brentano flat geometry, using a Cu-Kα radiation (λ= 1.5406 Å; 40 kV, 15 mA) at 0.02° in the range $5°<2\theta<80°$ using a scanning velocity of 1°/min. A Micromeritics ASAP 2020 was used to measure the specific surface area (SSA) according to the BET (Brunauer–Emmett–Teller) equation. Before the analysis, the sample was outgassed in vacuum (< 50 μm Hg) at high temperature (90°C for 30 min-350°C for 90 min). Three series of BET analysis were performed: one on the full material (washcoat supported on cordierite) one on washcoat powder extracted and the last on the remaining ceramic support, coming from the same samples. In this way, it was possible to evaluate the increase in the sensitivity due to the elimination of the cordierite support and estimate the quantity of residual

washcoat still present on ceramic residues. Powder Samples were also observed with transmission electron microscopy (TEM) using a JEOL JEM 3010-UHR ($LaB_6$ source, 300 kV) equipped with an EDX systemX-Stream INCA-OXFORD useful to have a compositional information of the observed area. Raman spectroscopy was employed in order to understand if this technique could be useful in the determination of ageing effects in this type of material. For this topic, the analysis was performed on the structured catalyst, composed by washcoat on ceramic substrate. The first step was to determine the best laser source for these samples. The system used is a Renishaw inVia Raman Microscope with emission line at 442, 514, 785 nm, focused on sample with a 20x ULWD objective. The idea was to make a mapping of a channel area, collecting a series of spectra from defined points of a fixed area and try to reconstruct an image of the area based on the intensity of the Raman signal.

## 2.3 Correlation between real and simulated ageing.

For the second part of the study, a step forward was made. A commercial technology, currently in production, was characterized, using all the techniques optimized previously. In order to understand the correlation between real and simulated ageing, samples of the same technology coming from different origins were analyzed. The reference real samples came from two vehicles equipped with 1.2 liter, 69 hp gasoline engines compliant with the E6b emission standard, currently in production. The ageing mileages were 25000 km and 60000 km (samples denoted as 25k and 60k in the following). A sample came from an engine bench ageing cycle: In this case, the ageing protocol was used to simulate a worst-case scenario, a catalyst aged at full useful life of the vehicle (FUL) 160000 km, in severe driving condition. For the laboratory deactivation protocol, two samples were cored from two fresh monoliths, and aged in different conditions. In both cases, a tubular oven equipped with a heated gas line was used, in order to flux the gases in the sample during the operation, with a peristaltic pump to add the water (Figure 4).

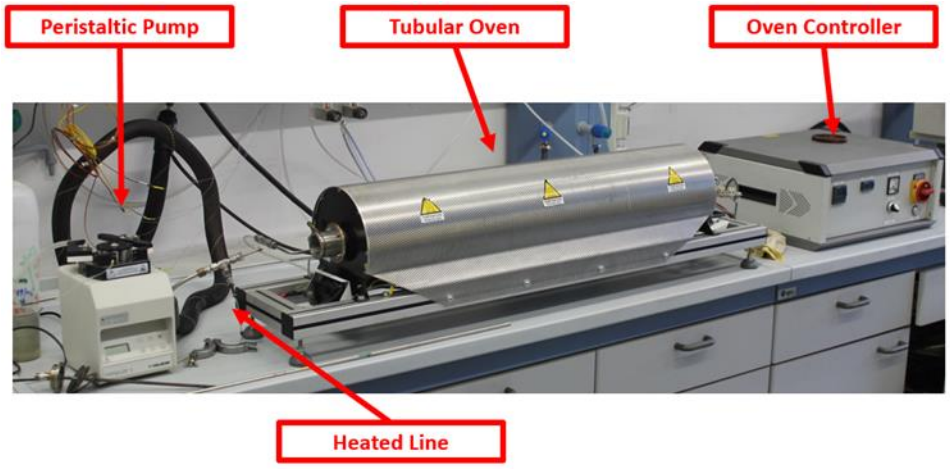


*Figure 4: Laboratory ageing system.*

The temperature and the time of ageing were the same for both the samples: 1100°C for 7h, a company standard to simulate a highly aged catalyst condition. The temperature and duration of this ageing protocol was based on literature research and on the wide experience of CRF aftertreatment department about the ageing of this components. According with the literature, the more detrimental environment of this type of catalyst is the oxidant, in presence of water [6,7]. For this reasons, two hydrothermal ageing environments were chosen: the first extremely oxidant, performed in pure air flow (4 l/min), with 10% water. In the second case, a controlled atmosphere was used, flowing a mixture of $N_2$ used as carrier gas with 2% of $O_2$ (4 l/min) and water (10%), in order to evaluate the impact of different levels of oxygen. All the samples extracted from the fresh monolith were degreened, before undergoing testing, in a static over at 650°C for 2h to eliminate any possible residue of production intermediates. A summary of the samples tested in this phase of the study is presented in Table 1.

| TWC 60 g/ft$^3$ Pd/Rh | ID |
|---|---|
| Fresh sample | Fresh |
| Vehicle aged - 25k km | 25k |
| Vehicle aged - 60k km | 60k |
| Engine bench aged | FUL |
| Lab. Aged - 1100°C 7h air + $H_2O$ | AIR |
| Lab. Aged - 1100°C 7h 2% $O_2$ + $N_2$ + $H_2O$ | 2% $O_2$ |

*Table 1: Summary of the sample tested.*

Also in this case, a complete visual analysis of the component was performed before the ceramic support removal, using optical and electronic microscopy techniques, in order to evaluate the visible effects of the ageing on the washcoat layer. Washcoat powder extracted from these samples was analyzed using all the techniques optimized in the previous step: SSA via BET equation on separated washcoat and on the full samples (to evaluate the increase of sensitivity), XRF, XRD, TEM and Raman Spectroscopy. Samples aged on the engine were in contact with numerous chemical species present in engine out gases, so may have been subjected to chemical ageing process [8]. The contribution of these phenomena was evaluated performing a quantitative chemical analysis on washcoat powder using inductively coupled plasma optical emission spectrometer (ICP-OES) with an Agilent 720 ES. The samples were dissolved using a nitric acid ($HNO_3$) solution 1:1 in water (100°C – 1h). The analysis were focused on the three principal elements coming from the combustion of fuels and engine oil as P, Ca and S.

### 2.3.1 Noble Metal Characterization Techniques

Noble metal particles sintering is one of the major deactivation pathways of automotive catalysts, due to working condition of these components. The techniques optimized in the previous step of the project were focused on the morphological modification of the washcoat, due to thermal ageing. However, noble metals are present in very low concentration (1-2 wt.%), which makes it very difficult to follow specifically their evolution. The techniques adopted for the study of the washcoat are relatively insensitive

to the changes happening at the metal particles level. For this reason in this part of the study, metal particles were studied using specific methodologies in order to understand the evolution of PGM, trying to determine their evolution in different ageing conditions. In order to characterize the surface of noble metals FT-IR probe molecule experiments were done, using CO as probe. Carbon monoxide is a very versatile molecule, widely used to probe both oxidic and metallic phases [9,10]. CO at gas phase typically present an IR absorption band at 2143 $cm^{-1}$. The interaction with surficial active sites lead to the appearance of absorption bands towards higher or lower frequency. In particular, the highest occupied molecular orbital (HOMO) of CO has a slightly anti-bonding character. So, the interaction with transition metal centers, thanks to the σ-donation and π-back-donation effects, involving the HOMO and LUMO of CO and the uppermost d states of the metallic phase, change the IR absorption behavior of CO molecules, depending on the type of bonds created with metallic active sites [11]. Both positions of the bands and their stabilities towards desorption at controlled temperatures, reflect the interaction strength between the metal and the probe. Analysis of the IR-CO spectra and assignment of the observed bands is guided by reference data, available for the metallic/oxidic phases considered in this work. Washcoat powders were compressed in self-supporting discs (~20 mg $cm^{-2}$) and placed in quartz IR cells suitable for high-temperature treatments and FT-IR analysis at room (RT) and liquid-nitrogen temperature (LNT). In order to characterize Lewis acid sites, i.e. $Pd^{n+}$ ions, at the surface of all the samples, ex situ measurements of CO adsorption at RT was performed. Before the IR measurements, the samples were pretreated, following two different protocols. The first one was a treatment in vacuum at 400 °C for 30 minutes. The second one was an activation protocol through oxidation and subsequent reduction of the material. The oxidation step was performed in a static system using dry $O_2$ on the sample at 400 °C. Oxygen was used twice, at about 40 mbar for 15 min per each step: the first treatment was useful to remove reduced species, possibly adsorbed on the surface; the second treatment was performed to ensure the oxidation. The reduction step was performed in the same way as the previous one, but the treatment was carried out in $H_2$. Hydrogen was used twice at 40 mbar for 15 min per each step. The double treatment was intended to ensure the reduction. Finally, the sample was outgassed and cooled to RT in vacuum. Absorption/transmission IR spectra

were run on a Perkin-Elmer FTIR System 2000 spectrophotometer equipped with a Hg-Cd-Te cryo-detector, working in the range of wavenumbers 7200-580 $cm^{-1}$ at a resolution of 2 $cm^{-1}$, with 60 scans. IR absorbance spectra were acquired on sample as-is, at increasing coverage of CO (θCO), using increasing CO pressure up to 20 mbar, and after a final outgassing. Infrared analyses at RT are not suitable to characterize the support, because the interaction of CO with its surface sites is too weak due to low binding energies involved. But to have a complete characterization of these materialist is worth to understand whether the aging influences the oxidic support and the oxygen storage capacity (OSC) of the material. To achieve this purpose analyses at LNT were performed, following the same protocol of RT tests. All these measurements were performed at the Chemistry Department of the University of Turin.

The distribution and the dispersion of noble metal particles in washcoat samples were analyzed via pulse CO pulse chemisorption in a plug-flow reactor. These analyses were performed at the department of Applied Science and Technology of the Politecnico of Torino using a Thermo Scientific 1100 TPDRO equipped with a thermal conductivity detector (TCD). The catalyst powder (200 mg) was placed in a quartz reactor, between two quartz wool layers. A reducing pre-treatment was carried out in a 20 ml min-1 flow of 5% $H_2$ in Ar, by heating the sample up to 300 °C with a 10 °C/min ramp and maintaining this temperature for 120 minutes. CO chemisorption was performed at room temperature, using He as carrier gas (20 ml $min^{-1}$ flow) and sending pulses of 800 µl of a mixture of 10% CO in He until saturation [12]. A TCD detector was used to measure the concentration of CO in the stream entering and leaving the reactor. Therefore, in order to detect changes in CO concentration, He must be used as a carrier gas, since it has a very different thermal conductivity. During the test He flows continuously and every 10-15 min a CO injection is made into the He flow. After a few minutes the detector detects a signal related to the CO output (the presence of this gas lowers the average thermal conductivity of the mixture) and then draws a peak. If there is chemisorption, the area of the peaks gradually increases until it becomes constant, and by calculating the missing area of the first peaks, the amount of CO chemisorbed on the sample can be calculated.

Due to the low contrast between noble metal particles and the substrate, sometimes is not possible to observe PGM nanoparticles with electron microscopy. It could probably due to the low differences between atomic weight of Pd and the elements that compose the porous support, Ce and Zr in particular, that lead to a similar behavior with the electron probe of microscope. In order to observe the particles and follow their growth during the ageing all the samples were observed using a new high resolution scanning electron microscope: a FE-SEM TESCAN S9000G equipped with a FEG source Schottky type. The detector is an In-Beam SE with a resolution of 0,7 nm at 15 keV, used in back-scattering electron detection (BSD), due to high atomic numbers of elements involved, in ultra-high resolution modality. The instrument is equipped also with an EDX detector Ultima Max OXFORD with AZTEC software.

## 2.4 Functional Characterization.

In this part of the study, another set of cored samples were prepared, extracted from the same monolith, in order to evaluate the catalytic performances of the components. The samples were tested on a synthetic gas bench, a facility present in CRF in Orbassano specifically thought for the functional testing of automotive catalysts (Figure 5). A mixture of gases, with composition that mimics the engine out gases is fed through the catalyst cored sample, which is placed in a heated metallic sample holder. The layout is presented in Figure 6.

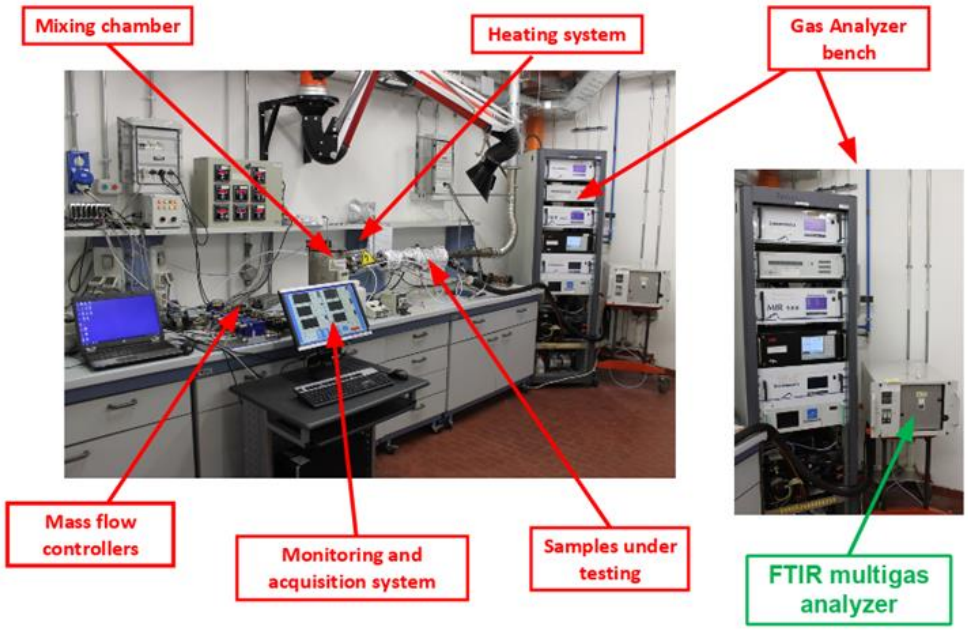


*Figure 5: Synthetic Gas Bench facilities in CRF (Orbassano)*

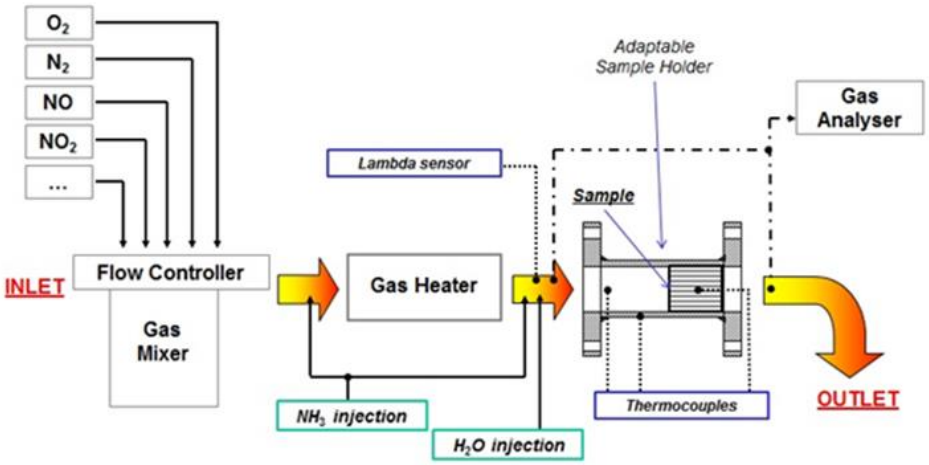


*Figure 6: Synthetic Gas Bench layout.*

The synthetic gas mixture is based on a carrier flow of $N_2$, an inert gas which does not participate into the catalytic reaction. All the gaseous species (CO, HC, $NO_x$, $SO_2$) pass

through a mixer with a controlled flow, specifically calculated and measured with single mass flow controllers in order to have the correct concertation of all the species in the final gas mixture. The synthetic engine out gas is then pre-heated and water is added during heating through a peristaltic pump, by injection in the hot gas stream. The catalyst sample (1.5"x2.5") is installed in a heated sample holder. The temperature is controlled by two thermocouples placed before and after the catalyst and other two placed inside the sample, one in a central channel and one in a lateral one. The gas mixture is analyzed using a FT-IR FTIR Multi-gas Analyzer MKS 2030 HS for the simultaneous analysis of all chemical species. The concentration measurements are recorded before and after the catalyst, in order to evaluate the gas flux composition and its variation during the reactions. For the testing of a gasoline engine catalyst, the synthetic gas mixture needs to replicate the composition of that engine exhaust gases. However, the system is not sufficiently fast to replicate the fluctuations between lean (oxidant) and rich (reducing) conditions, so it works near the stoichiometric condition ($\lambda$ =1) in slightly lean environment. The composition of the adopted gas mixture is presented in Table 2:

| $O_2$ | CO | $CO_2$ | HC | NO | $H_2O$ | SV | $\lambda$ |
|---|---|---|---|---|---|---|---|
| 0,7% vol. | 15 % vol. | 10% vol. | 1875 ppm | 600 ppm | 1% vol. | 50k $h^{-1}$ | 1,02 |

*Table 2: Synthetic Gas Mixture composition*

The $\lambda$ value of the mixture is calculated from the concentration of CO, $O_2$ and $N_2$, but is further controlled by a $\lambda$-sensor placed before the sample holder. HCs are a gas mixture of short-chain hydrocarbons, ethylene-propylene-methane (3.5/1/1) defined after a characterization of the HC content in the real gasoline engine out.

Two types of test were performed: the conversion efficiency and the evaluation of the oxygen storage capacity. The conversion efficiency test consists in the evaluation the effectiveness of catalytic converters in reducing a given gas emission. In this case, due to the slightly lean environment of the gas mixture, the test was focused on the oxidation of

CO and HCs. To evaluate the reduction of NOx the gas mixture needs to be slightly rich ($\lambda<1$), therefore NOx reduction was not analyzed in this study. The sample was mounted in the holder and the system closed. The first step was to measure the initial composition of synthetic gas mixture, sampling with the FT IR upstream respect the sample holder, in order to verify the correctness of the concentration. After that, the sampling was switched to the outlet side of the sample and the warming of the component started, using a ramp rate of 30°C/min from ambient temperature to 500°C, measured before the catalyst. The thermocouples inside and after the component are not reliable because the chemical reactions occurred during the test are exothermic, so the sensor measure higher temperatures. The FT-IR measure the progressive decrease of the concentration of CO and HC, due to the oxidation reaction occurred inside the sample, in function of the temperature. The test was repeated three times to control the variability of sample, and the results presented are average values. The results are an efficiency curve for CO and HC as a function of the increasing temperature. From this result is possible obtain another important parameter for the evaluation of catalyst functionality: the light-off temperature (T50), the temperature in which the catalyst reaches 50% CO or HC conversions [13]. The progressive deactivation of the catalyst increases this temperature. The second test performed is an evaluation of the oxygen storage capacity (OSC). This test was performed at constant temperature of 400°C. Reached that temperature a flux of 1% of $O_2$ (in nitrogen carrier) ($\lambda$ =1.04) was sent to the sample for 180 sec, in order to saturate the component with oxygen. After that, all the residues of $O_2$ not stored in the washcoat were purged using a flux of pure $N_2$. The OSC was evaluated fluxing for 180 sec. 7000-8000 ppm of CO ($\lambda$ = 0.97) and measuring the residual CO concentration downstream the catalyst (Figure 7). CO is oxidized by the $O_2$ stored in the sample in the first phase, so measuring residual quantity of CO that came out from is possible calculate the quantity of CO oxidized and, consequently, the quantity of oxygen present inside the sample. Also in this case the test was repeated three times to control the variability of the sample, and the results presented are average values.

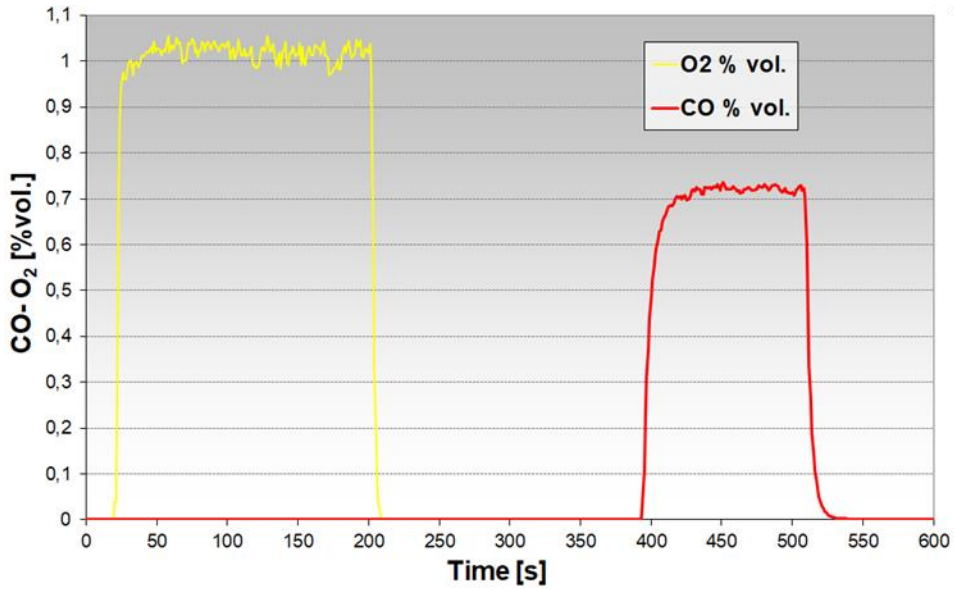


*Figure 7: OSC test time scheme.*

- REFERENCES:


1. Giuliano, Mattia, et al. "Thermal ageing effects in a commercial three-way catalyst: physical characterization of washcoat and active metal evolution." *International Journal of Automotive Technology* 21.2 (2020): 329-337.
2. Giuliano, Mattia et al. "Characterization of Vehicle and Laboratory Aged Commercial Three Way Catalyst: A Morphological and Functional Correlation between Real and Simulated Ageing", *International Journal of Automotive Technology* 2021, Vol. 22, No. 1.
3. Giuliano, Mattia, et al. "Characterization of the Evolution of Noble Metal Particles in a Commercial Three-Way Catalyst: Correlation between Real and Simulated Ageing." *Catalysts* 11.2 (2021): 247.
4. Kang, S. B.; Han, S. J.; Nam, S. B.; Nam, I.-S.; Cho, B. K.; Kim, C. H.; Oh, S. H. Effect of Aging Atmosphere on Thermal Sintering of Modern Commercial TWCs. *Top Catal* **2013**, *56* (1–8), 298–305.
5. Stenbom, B.; Smedler, G.; Nilsson, P. H.; Lundgren, S.; Wirmark, G. Thermal Deactivation of a Three-Way Catalyst: Changes of Structural and Performance Properties; 1990; p 900273.
6. González-Velasco, Juan R., et al. "Thermal aging of Pd/Pt/Rh automotive catalysts under a cycled oxidizing–reducing environment." *Catalysis today* 59.3-4 (2000): 395-402.
7. Hietikko, Marko, et al. "Effect of the ageing atmosphere on catalytic activity and textural properties of Pd/Rh exhaust gas catalysts studied by XRD." *Applied Catalysis A: General* 277.1-2 (2004): 107-117.
8. Fernández-Ruiz, R.; Galisteo, F. C.; Larese, C.; Granados, M. L.; Mariscal, R.; Fierro, J. L. G. TXRF Analysis of Aged Three Way Catalysts. *Analyst* **2006**, *131* (4), 590. https://doi.org/10.1039/b513508g.
9. Terekhina, O.; Roduner, E. FTIR Spectroscopic Investigation of Zeolite-Supported Pd–Ag Bimetallic Clusters. *J. Phys. Chem. C* **2012**, *116* (12), 6973–6979.

10. Hollins, Peter. "The influence of surface defects on the infrared spectra of adsorbed species." *Surface Science Reports* 16.2 (1992): 51-94.
11. Lynn, Matthew A., and Bruce E. Bursten. "An analysis of the bonding in some 'nonclassical'd0 and d10 metal carbonyl complexes." *Inorganica chimica acta* 229.1-2 (1995): 437-443.
12. Bergeret, G., & Gallezot, P. (2008). Particle size and dispersion measurements. *Handbook of Heterogeneous Catalysis: Online*, 738-765.
13. Kallinen, K.; Suopanki, A.; Härkönen, M. Laboratory Scale Simulation of Three-Way Catalyst Engine Ageing. *Catalysis Today* **2005**, *100* (3–4), 223–228.

# 3 Result and Discussion.

## 3.1 Washcoat extraction method optimization.

For the first test of washcoat extraction, water at room temperature was used. During the process, however, the formation of a thick layer of ice on the sample and in its channels was observed. Despite a resting phase in water to allow its elimination, this makes the method less effective in washcoat removal and causes a deterioration of the ceramic structure, whose fragments mix with the extracted washcoat. To avoid this problem, warm water (60 °C) was used reaching good yield of extraction. The separated dry washcoat represents 20 ~ 30 % of the initial weight of the samples (Table 3). The quantity of Cordierite debris in the final fine powder obtained after drying is very limited. Optical microscopy confirms this result showing low presence of washcoat residues on Cordierite after extraction in warm water (Figure 8).

| | **Extraction Method** | **Initial Weight (g)** | **Washcoat extracted (g)** | **wt. %** |
|---|---|---|---|---|
| **Fresh sample A** | Liquid $N_2$ + $H_2O$ T r.t. | 23,028 | 1,745 | 7,6% |
| **Fresh sample B** | Liquid $N_2$ + $H_2O$ T 60°C | 17,703 | 3,715 | 21,0% |
| **Fresh sample C** | Liquid $N_2$ + $H_2O$ T 60°C | 17,825 | 5,990 | 33,6% |
| **Fresh sample D** | Liquid $N_2$ + $H_2O$ T 60°C | 17,493 | 5,131 | 29,3% |
| **Aged Sample** | Liquid $N_2$ + $H_2O$ T 60°C | 13,273 | 3,310 | 24,9% |

*Table 3: washcoat extraction yield (wt. %) using water at room temperature (fresh sample A) and warm water (fresh sample B, C, D and aged).*

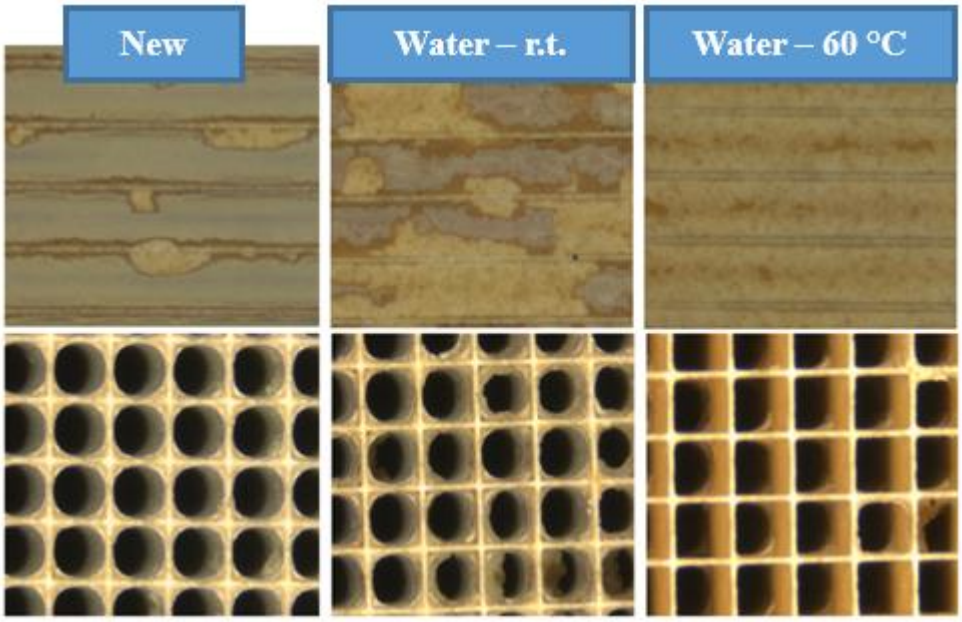


*Figure 8: Microscope images of the washcoat of a new TWC and after extraction in water at room temperature (r.t.) and at 60°C.*

Comparing XRD pattern of the washcoat powder extracted with this method and a pattern recorded on a sample obtained grinding entirely the same TWC, in the same operative condition the reduction of the contribute of cordierite is evident (Figure 9). This is very important in order to be able to focus on washcoat modification. Cordierite is the major component of the TWC monolith in weight and it is a highly crystalline ceramic material, so in the diffraction pattern its peaks are very sharp and intense (black line). However, these peaks overlap with other signals coming from the washcoat, which is characterized by a very complex composition. It contains numerous phases and a great number of dopants in low concentration but of great importance for its thermal behavior. The washcoat is in general less crystalline, with a very small crystallite size. After extracting the washcoat, a diffraction pattern subtracted of the cordierite interference (red line) can be acquired, simplifying the interpretation and identification of the remaining peaks.

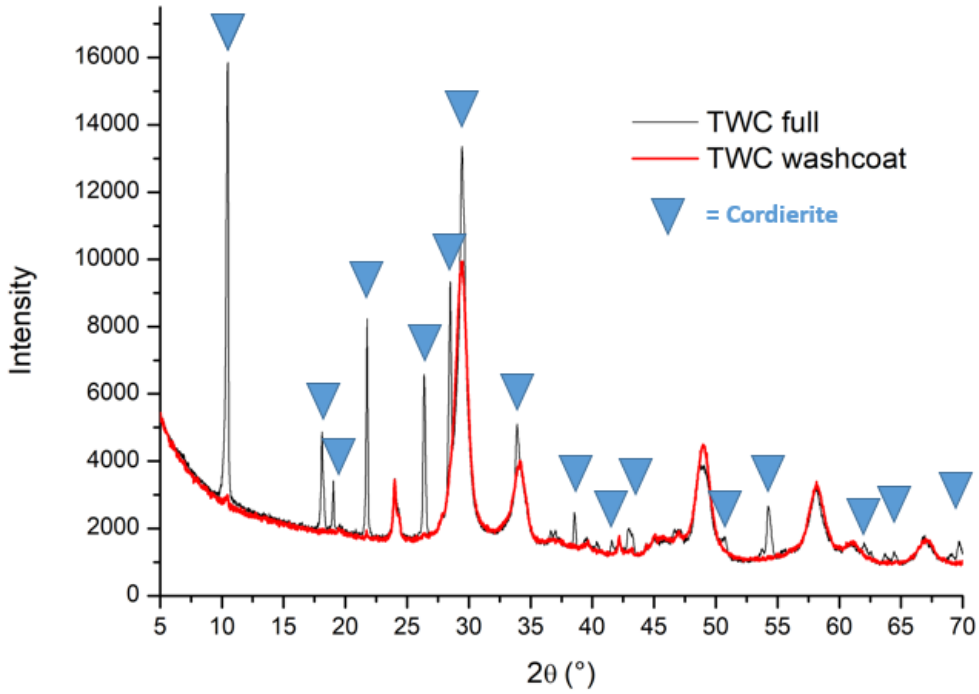


*Figure 9: Powder XRD pattern of full TWC (black line) and only washcoat after extraction (red line).*

The results of specific surface area analysis on fresh and thermally aged samples, are presented in Table 4. Three sets of measurements were performed: the first on a whole TWC (fresh and aged), the second on the washcoat powder obtained from the same samples and the last on the residual ceramic support. In general, the results highlight the structural change that take place upon thermal ageing, with a decrease of the porous structure due to sintering of the support material. The difference between BET values of the fresh and aged sample is more pronounced in the pure washcoat samples as compared to the full-TWC case. This effect is due to the dilution of these samples by the Cordierite, which has a very low specific surface area (below 1 $m^2/g$), but it represent its largest component in weight. In this case, the part that effectively changes its surface area is a small fraction of the total weight of sample, so the difference between fresh and aged is lower. The SSA of the residual ceramic support is relatively high (20,7 $m^2/g$) with respect to the expected values. This can be due to residues of washcoat on the support, not detached by the extraction. Considering the yield of washcoat extraction (25 ~ 30 % wt)

and the relative SSA of washcoat, support and complete component, the quantity of residual washcoat present on ceramic support can be evaluated to be about 5 ~ 7 % in weight, explaining the BET results.

| BET surface area ($m^2/g$) | Fresh | Aged |
|---|---|---|
| TWC (washcoat + substrate) | 50,9 | 33,8 |
| Washcoat powder | 114,0 | 54,4 |
| Substrate | 20,7 | 4,1 |

*Table 4: Specific surface area results (BET method) obtained on whole TWC, washcoat powder and residual support samples coming from fresh and aged components.*

## 3.2 Washcoat morphological characterization.

The X-ray fluorescence elemental analysis, performed on the washcoat powder separated from the fresh sample, shows that the washcoat material is mainly composed of Al, Ce and Zr oxide and relevant presence of dopants Ba, Nd, and La oxides (Table 5). XRF has also highlighted the good results of the washcoat extraction method, displaying low concentration of Si and Mg, 0,4 and 1% respectively, elements present only in the cordierite support.

| $Al_2O_3$ | $ZrO_2$ | $CeO_2$ | BaO | $Nd_2O_3$ | $La_2O_3$ | $SiO_2$ | MgO |
|---|---|---|---|---|---|---|---|
| 58,7% | 19,8% | 12,7% | 3,3% | 2,3% | 0,9% | 0,4% | 1,0% |

*Table 5: Results of x-ray fluorescence elemental analysis performed on washcoat powder sample. All the value are expressed in weight % of oxide.*

Moving to the comparison between fresh and thermally aged samples, the BET analysis results presented above (Table 4), show an important reduction of the surface area of the washcoat. In fact, it decreases by more than 50 % upon ageing. This effect is due to a phase transformation from γ-Al2O3, characterized by high porosity and high surface

area, to other more thermodynamically stable forms of Alumina with lower surface area (δ, θ, α) with increasing rate at increasing temperature (see discussion of XRD below). The sintering of particles leads to their growth, and to the elimination of pores. According with literature, this phenomenon is associated to condensation of hydroxyl group residing on adjacent particles, with a collapse of porous structure [2]. Structural degradation in aged sample is evident also in observing SEM images recorded on supported material, which shows the formation of littles cracks in the washcoat layer due to shrinking of the washcoat layer and thermal stress.

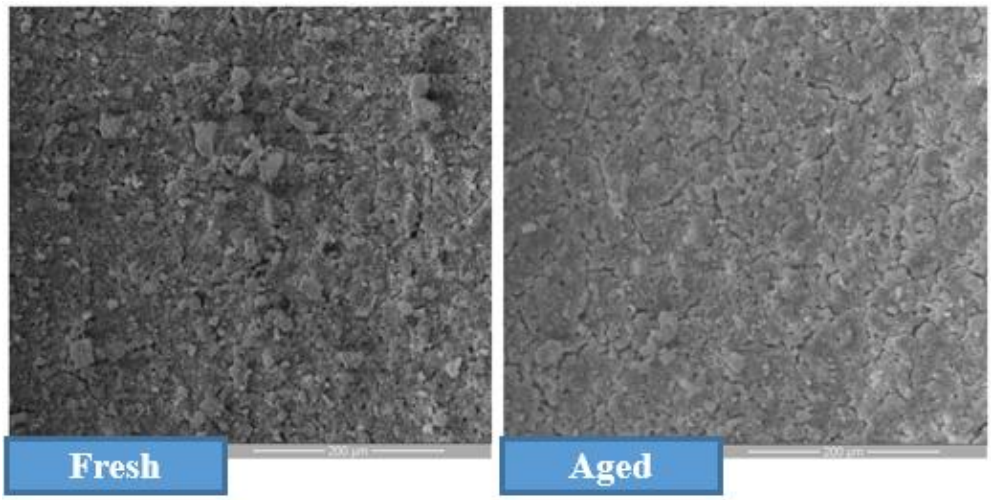


*Figure 10: SEM images of fresh (left) and aged (right) TWC.*

X-ray powder diffraction data (Figure 11) show that the support material of the catalysts is mainly composed of the oxides of Al, Ce and Zr, confirming the XRF data. The fresh material contains amorphous and/or low crystallinity phases, with small crystallite size, which cause a broadening of pattern peaks and the not negligible background signal. The pattern indicates the presence of a Ce/Zr mixed-oxide phase with cubic symmetry and fluorite structure typical of $CeO_2$, characterized by the presence of four reflections corresponding to {111}, {200}, {220}, {311} planes [3]. The very strong peak {111} at 29° can be attributed to a $Ce_{0,75}Zr_{0.25}O_2$ phase and the symmetricity of these peaks suggests a good homogeneity of this phase [4, 5]. Alumina is present only as γ polymorph, typically the highly porous form of this oxide, characterized by a distorted spinel structure and small crystalline grain, as evidenced by the broad peaks [6]. In this type of material,

Ba was added in form of Witherite, Barium Carbonate, identified by peaks at 24 and 42°, used as $NO_x$ storage compound, promoter for the water-gas-shift reaction and as stabilizer of Ce-Zr oxides, going to integrate in the mixed oxide solid solution [7].

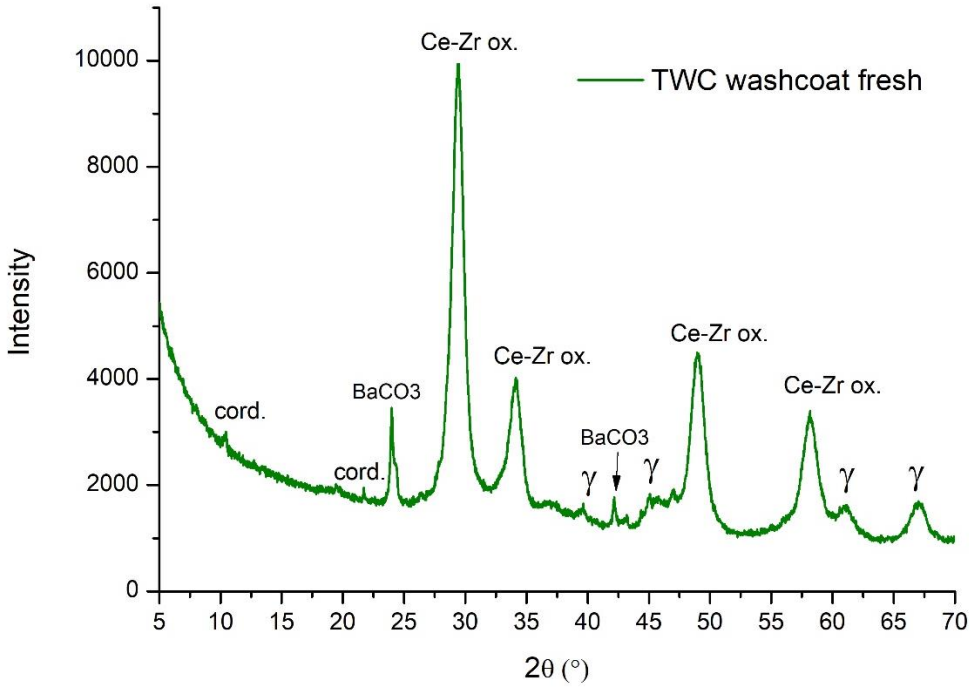

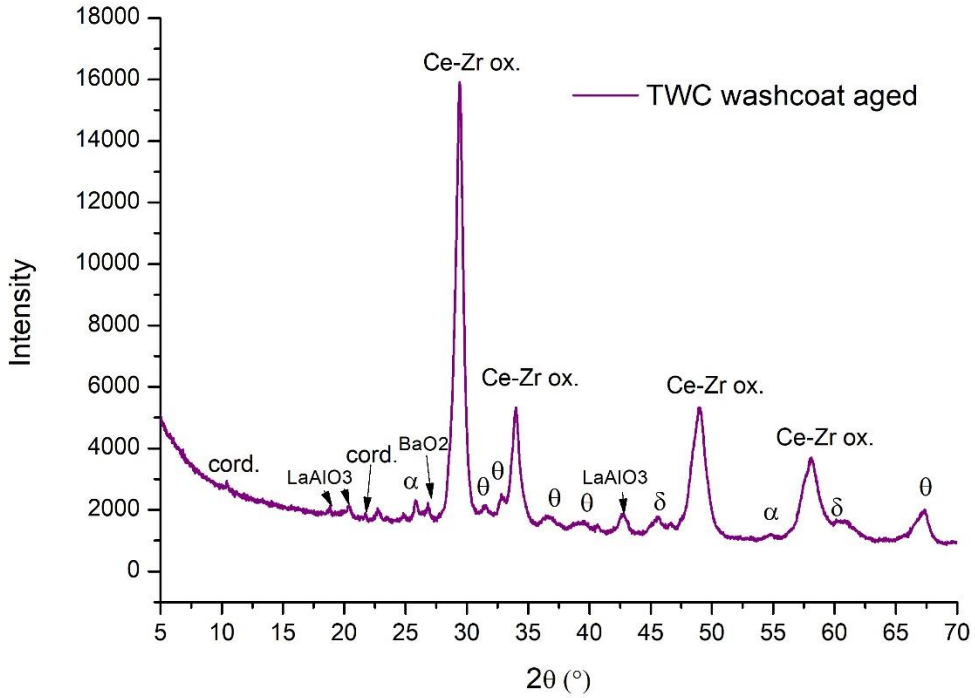


*Figure 11: XRD pattern of washcoat extracted from fresh TWC sample (green line) and aged sample (purple line).*

The XRD pattern of the aged sample (purple line) shows that the phase transitions promoted at high temperature, led to a general increase of the crystallinity of the material, with an increase of the intensity and narrowing of diffraction peaks. Ce-Zr mixed oxide phase peaks display an increase of the intensity and sharpness, with a small shift of their position but without loss in symmetry (Figure 12).

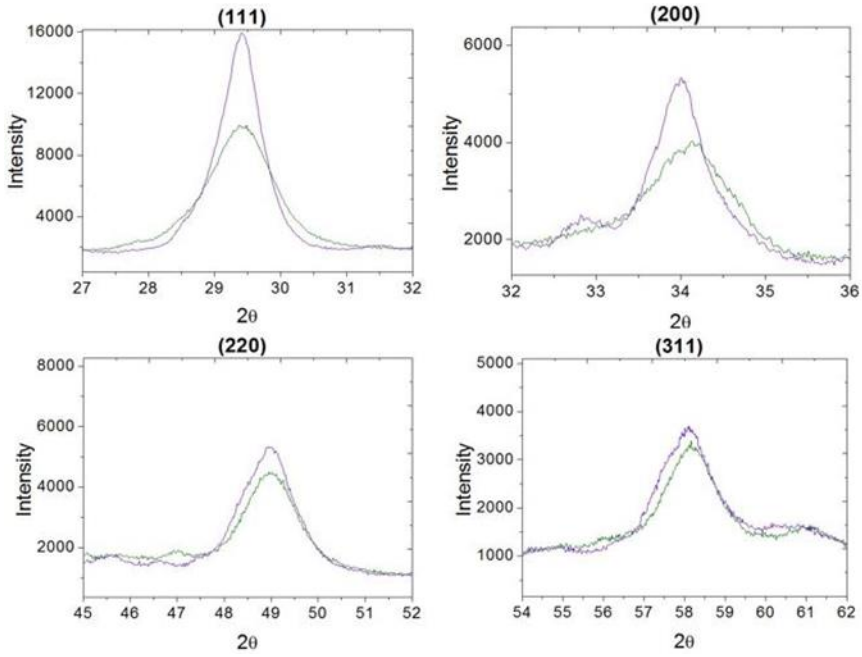


*Figure 12: Detail of fresh (green line) and aged (purple line) sample patterns focused on relative positions of typical peaks of Ce-Zr mixed oxide phase.*

This effect is probably due to a growth of crystal dimensions, without great change in the crystalline structure of this phase. The Alumina support phase results totally converted from γ to a mixture of δ, θ and α-$Al_2O_3$, identified by their typical peaks [8,9], according to the literature. $BaCO_3$ is converted to $BaO_2$, testified by the loss of carbonate typical peaks. The ageing promotes also the formation of $LaAlO_3$ by the reaction between $La_2O_3$ and γ-$Al_2O_3$, , which have the function of prevent sintering of the alumina inhibiting the α-transformation reducing the reaction rate [10], with characteristic peak at 18,8; 20,4 and 24,8° [11]. No trace is observed of the typical peaks of PdO or Pd, at 34° and 40° respectively [12] in both diffraction patterns, probably because they are too diluted in our sample.

TEM images corresponding to the fresh and aged samples are presented in Figure 13. The Fresh sample shows darker zones, labeled by red circles, which were identified to be Palladium particles using EDX analysis. They are finely dispersed in the sample with an average size smaller than 5 nm. The aged sample displays larger crystals particles, with

a well-defined crystallinity. Numerous darker zones are present in the aggregates, but only a few of them are associated with the presence of PGMs, because sintering reduces their dispersion in the sample. To identify them, the samples were scanned at low magnification using the EDX detector. In the fresh sample, a constant low level of Pd is observed, associated with the well dispersed nanoparticles observed at high magnification.

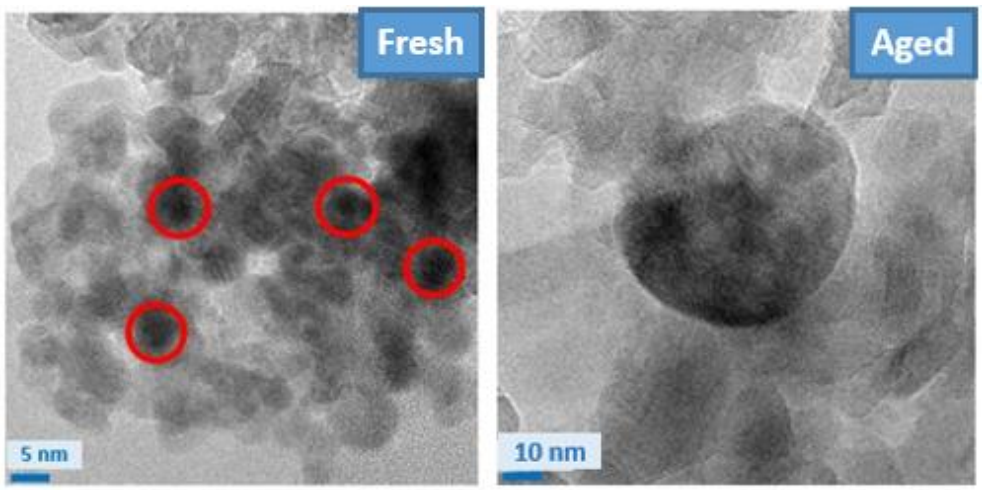


*Figure 13: TEM imagine of fresh and aged washcoat sample. Red circles in fresh sample image highlight the PdO particles.*

On the other hand, in the aged powder, numerous dark zones show no trace of Pd, and we interpret them as thick aggregates of support oxides. A few dark spots instead display a high level of noble metal, more than the average value of the fresh sample, so they are identified as noble metal particles, with dimensions of 100 nm (Figure 14). In twenty aggregates analyzed with this method, only two appear to contain Pd particles. Highly dispersed noble metal particles undergo sintering processes at high temperature, with aggregation occurring. This process occurs through migration of crystallites on the surface of the support and their coalescence, forming larger agglomerations, more stable from a thermodynamic point of view, but reducing the surface exposed to reactants [13].

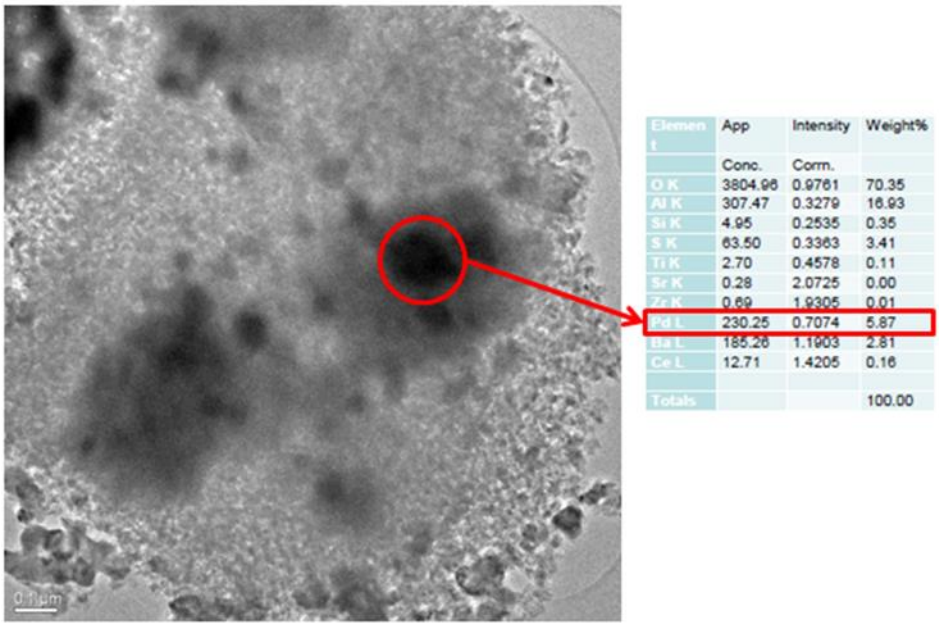


| Element | App Conc. | Intensity Corrn. | Weight% |
|---|---|---|---|
| O K | 3804.96 | 0.9761 | 70.35 |
| Al K | 307.47 | 0.3279 | 16.93 |
| Si K | 4.95 | 0.2535 | 0.35 |
| S K | 63.50 | 0.3363 | 3.41 |
| Ti K | 2.70 | 0.4578 | 0.11 |
| Sr K | 0.28 | 2.0725 | 0.00 |
| Zr K | 0.69 | 1.9305 | 0.01 |
| Pd L | 230.25 | 0.7074 | 5.87 |
| Ba L | 185.26 | 1.1903 | 2.81 |
| Ce L | 12.71 | 1.4205 | 0.16 |
| | | | |
| Totals | | | 100.00 |

*Figure 14: TEM image of aged simple. The zone labeled with red circle is the zone analyzed with EDX, which identify the presence of Pd.*

Raman Spectroscopy is a powerful technique in terms of sensitivity and applicability. The technique has been used previously to characterize automotive catalysts. Boullosa-Eiras et al. [14] have studied an $Al_2O_3/ZrO_2$ system and they concluded that some bands characteristic of $\alpha$-$Al_2O_3$ formation can be observed. However, De Oliveira et al. [15] demonstrated that these bands were in fact fluorescence peaks of alumina, due to its electronic structure, and not vibrations. Oliveira proved also that they cannot be used as markers of support ageing because their position in terms of Raman shift are dependent by the laser excitation line used.

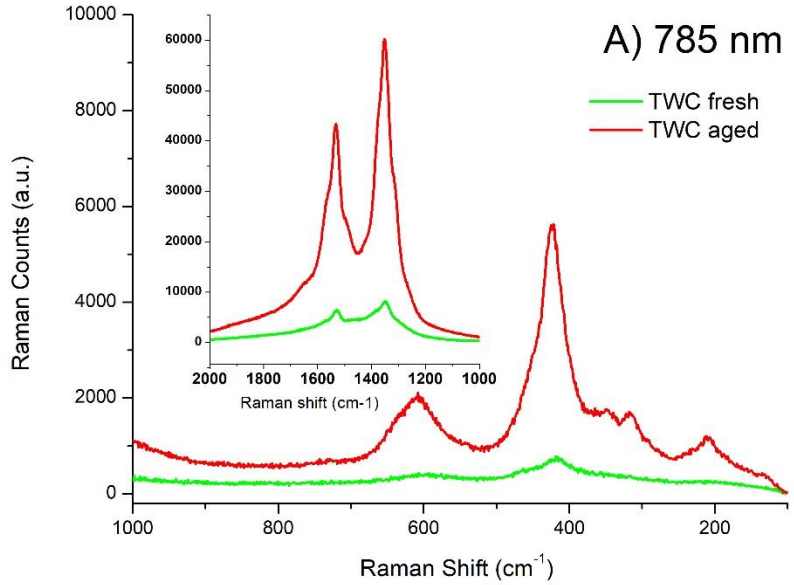
A) 785 nm
TWC fresh
TWC aged
Raman Counts (a.u.)
Raman Shift (cm-1)
Raman shift (cm-1)

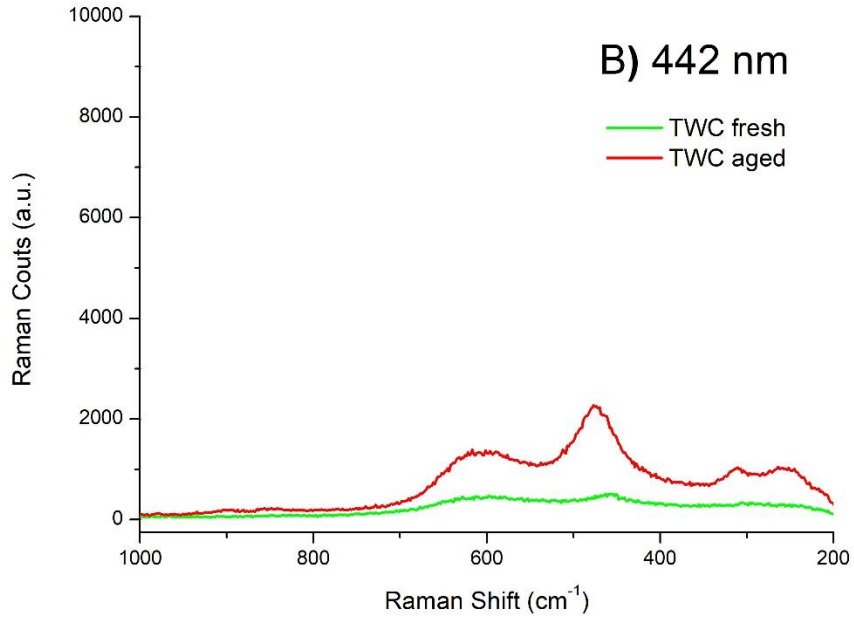
B) 442 nm
TWC fresh
TWC aged
Raman Couts (a.u.)
Raman Shift (cm-1)

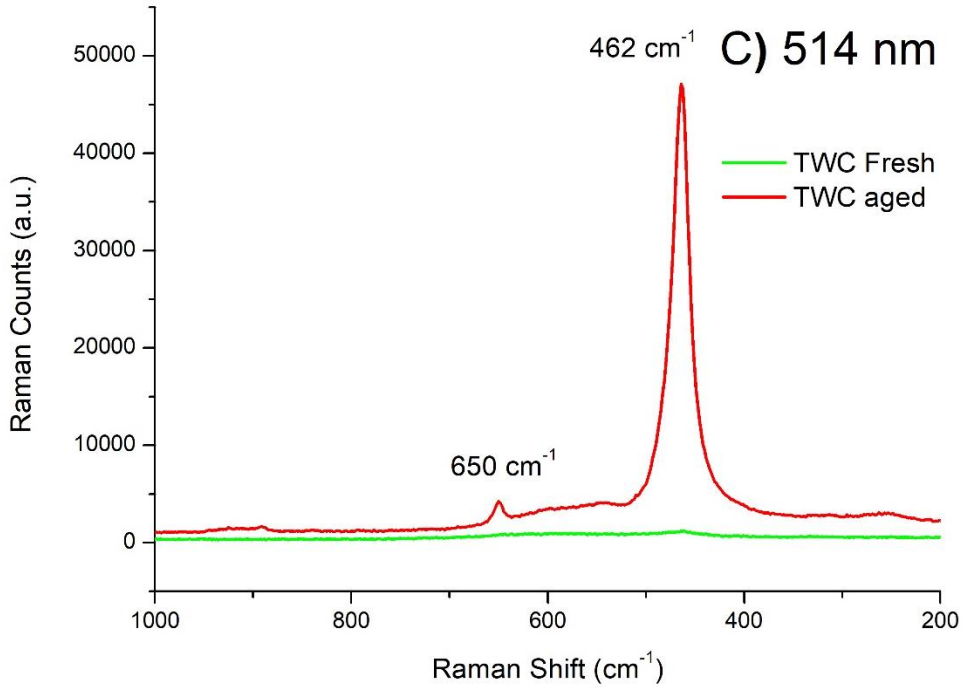


*Figure 15: Raman spectra recorded on full TWC material (washcoat+substrate, fresh and aged, using different excitation wavelengths: A) 785 nm B) 442 nm C) 514 nm.*

In order to discriminate fluorescence from real signals, we have adopted multiple excitation wavelengths: 785, 442, and 514 nm. Spectra presented in Figure 15A, coming from sample excited with 785 nm radiation, show a series of peaks above 1000 $cm^{-1}$ on both the fresh and aged samples (Figure 15A inset) corresponding to the fluorescence spectrum observed by De Oliveira and Boullosa and we will not analyze them here. Below 1000 $cm^{-1}$, 2 peaks are present: the first at 462 $cm^{-1}$, typical of the F2g Raman active mode of a fluorite-structured material like Ce and Zr oxide [3]. The second peak at 650 $cm^{-1}$ is associated with the B2g Raman mode of PdO, which is the native form of this noble metal in automotive catalysts [16]. Their intensity are low, due to the presence of very intense fluorescence peaks. Spectra recorded with the 442 nm laser (Figure 15B) display a complicated trend, with the same peaks, confused in a high background signal, probably due to fluorescence phenomena in the same region of the spectrum. Excitation radiation at 514 nm provided the best results: well defined spectra, with very intense peaks at 462

and 650 $cm^{-1}$, above all in the aged sample. Therefore, these signals can be used as markers of thermal ageing of the material. Finally, we noted that none of the spectra at different wavelengths display trace of the typical peaks of α-alumina (380 and 420 $cm^{-1}$)[6] in the aged sample, which are probably confused in the high and complicated background signal. Furthermore, some other peaks in the 100 ~ 350 $cm^{-1}$ range are difficult to assign.

The intensity of the main peaks chosen as ageing markers changes significantly varying the analysis position on samples. So, a series of Raman spectra were recorded by scanning an area of the sample. A selected area of 40 × 20 μm was divided in 27 (9 × 3) points where laser radiation performed the excitation of sample, recording 27 spectra. These operations were performed in two different points of fresh and aged TWC. All the spectra were averaged, in order to compare the results of aged and fresh samples (Figure 16). The difference between fresh and aged TWC are presented in figure 17: Raman spectra of aged sample show higher intensity and sharper peaks. The peaks of Ce-Zr mixed oxide are present also in the fresh samples, while PdO peaks appear only in aged samples, but its position is constant in all the spectra. The Ce-Zr Raman band however, changes the Raman shift slightly probably because the ageing process yields to a local change in the composition of this solid solution, with modification of Ce/Zr ratio, or a growth of the crystal. The increase of intensity of PdO peak is probably due to of metal particle growth via sintering occurred during the ageing [12].

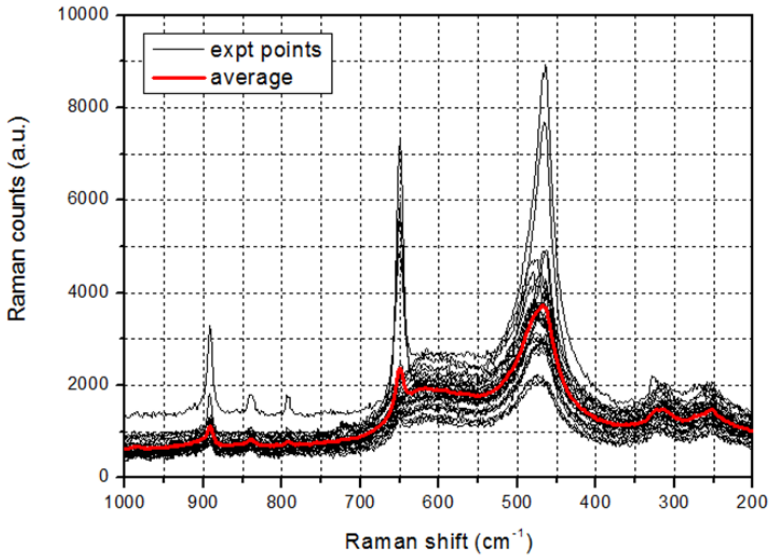


*Figure 16: Average Raman spectrum calculated starting form 27 spectra recorded in the selected area on the aged sample.*

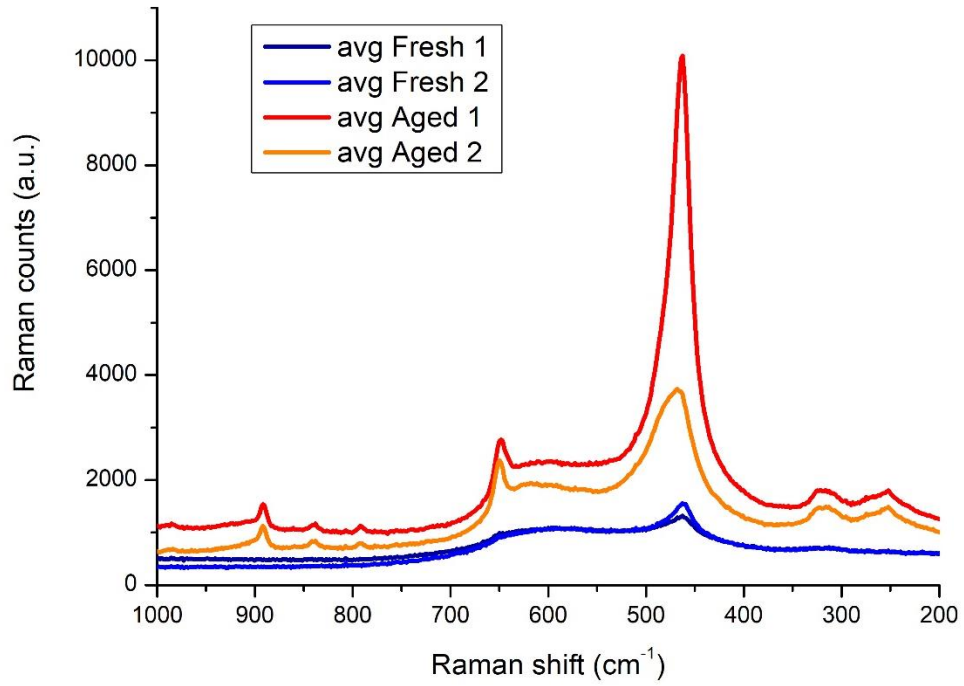


*Figure 17: Comparison between average spectra recorded on samples fresh and aged sample, in two different position.*

## 3.3 Commercial catalyst technology ageing and characterization.

Moving to fresh and aged commercial catalysts, Table 6 summarizes the result of the washcoat extraction.

| | V ($inc^3$) | Washcoat Extracted (g) | Yield |
|---|---|---|---|
| **Fresh** | 4,42 | 4,57 | 36,9% |
| **25k** | 2,65 | 2,58 | 33,6% |
| **60k** | 2,43 | 2,81 | 39,9% |
| **80k** | 2,41 | 3,04 | 43,2% |
| **FUL** | 2,21 | 4,58 | 71,6% |
| **110°C 7h - AIR** | 2,20 | 2,72 | 42,6% |
| **110°C 7h - 2% $O_2$** | 2,33 | 3,74 | 55,3% |

*Table 6: Summary of the yield of the washcoat extraction method (liquid $N_2$ + $H_2O$)*

Extraction yield was calculated considering the volume of the sample and the washcoat loading value supplied. The yield seems to be linked to the ageing of the component. The higher is the ageing, the higher is the quantity of washcoat extracted. This can be due to a greater deterioration of the coating with a loss of the adhesion on the cordierite structure caused by the thermal stress.

Before submitting the samples to washcoat extraction, was performed a visual analysis using the optical microscope on supported catalysts. The effects of ageing are immediately evident (figure 18). The washcoat progressively change its color and in the case of FUL and lab-aged samples the coating is damaged, with presence of numerous cracks and detachment of the material, likely due to the thermal stress.

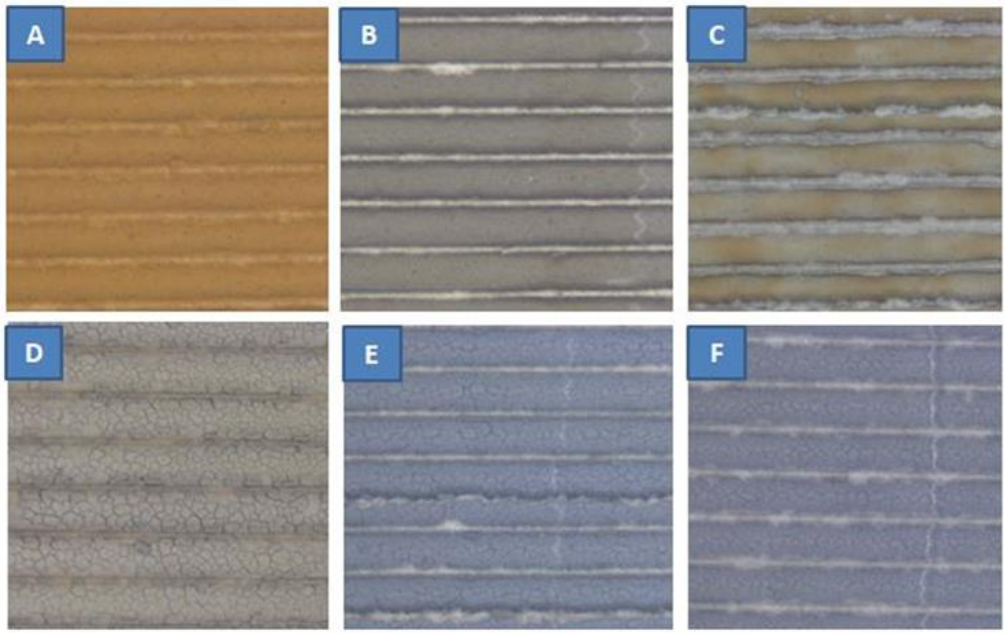


*Figure 18: Optical microscope images of TWC sample A) Fresh B) 25k km C) 60k km D) engine bench FUL E) 1100 °C 7h – AIR F) 1100°C 7h – 2% O2.*

Structural degradation is more evident observing SEM images recorded on the supported materials (figure 19).

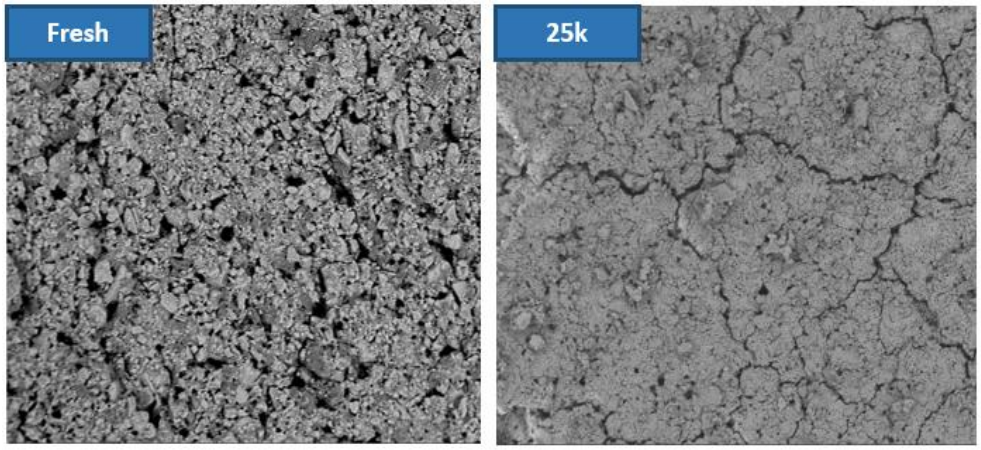

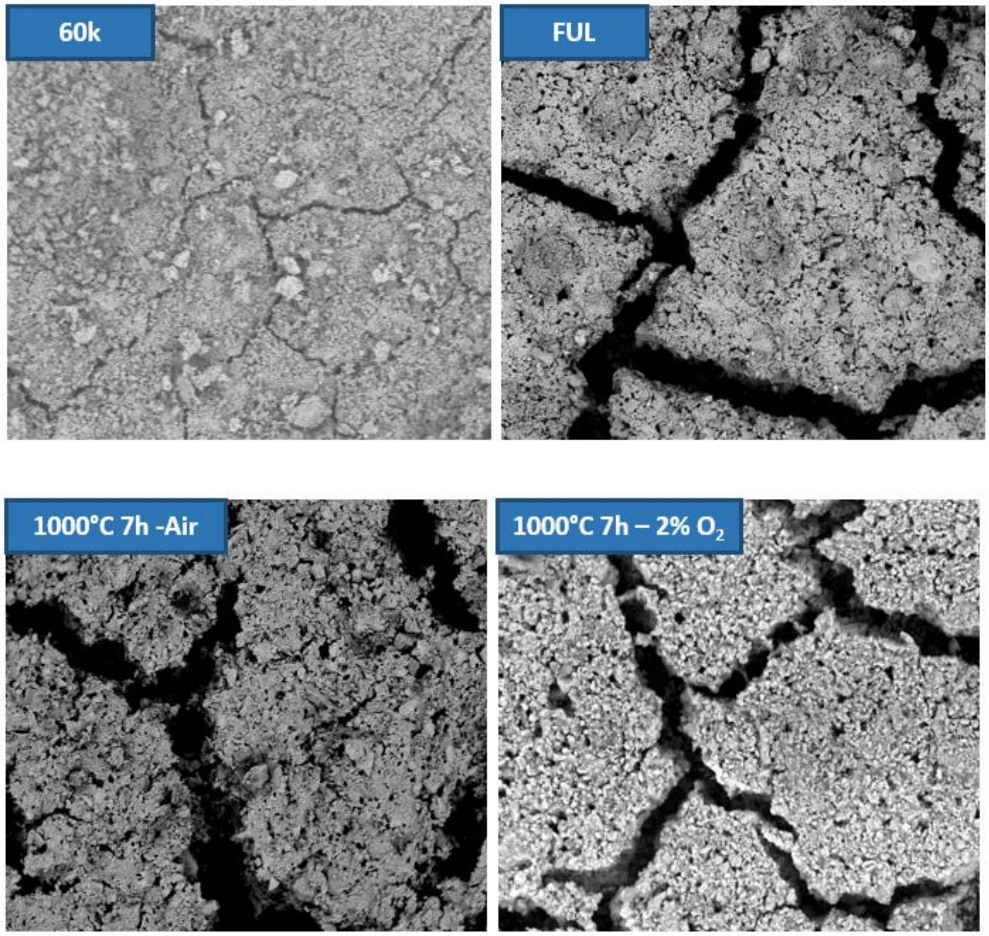


*Figure 19: SEM images of TWC Fresh, 25k km, 60k km, engine bench FUL, 1100°C 7h – AIR, 1100°C 7h - 2% O2.*

SEM images shows the presence of cracks in the washcoat layer also in vehicle-aged samples, not visible with the optical microscope. The Fresh washcoat displays a coarse morphology, with numerous dark zones associated to the deep porosity of the alumina support. This porous structure decreases with ageing, as it is possible to see in SEM images at higher magnification that shows in the residual part more compact washcoat, with lower dark zone, due to the sintering phenomena[1].

Also for these commercial catalysts, the washcoat extracted from the fresh sample was analysed using XRF. This material has a very complex composition: beside the alumina,

Ce-Zr oxides and PGMs, also numerous additives are present, typically metal oxides. The XRF analysis result are shown in table 7:

| $ZrO_2$ | $CeO_2$ | $Y_2O_3$ | BaO | $Nd_2O_3$ | $Al_2O_3$ | F | Pd | $La_2O_3$ | $HfO_2$ |
|---|---|---|---|---|---|---|---|---|---|
| 42,2 | 19,7 | 5,5 | 4,6 | 3,8 | 18,3 | 1,5 | 1 | 1 | 0,8 |

*Table 7: Semi-quantitative result, expressed in wt%, of XRF analysis performed on washcoat extracted from fresh TWC sample.*

The sample shows the presence of a high content of Ce-Zr oxides, probably in order to guarantee a solid oxygen buffer functionality, and to increase thermal stability thanks to Zr. The analysis detects also presence of Ba and a series of rare earths elements, with the function of stabilizing the support. In this case, La oxide, is present as stabilizer for the solid solution of Ce-Zr mixed oxide [17].

Moving on the morphological characterization of the washcoat, The BET results are presented in Figure 20 and Table 8, for the analyses on the full material and on the washcoat powder.

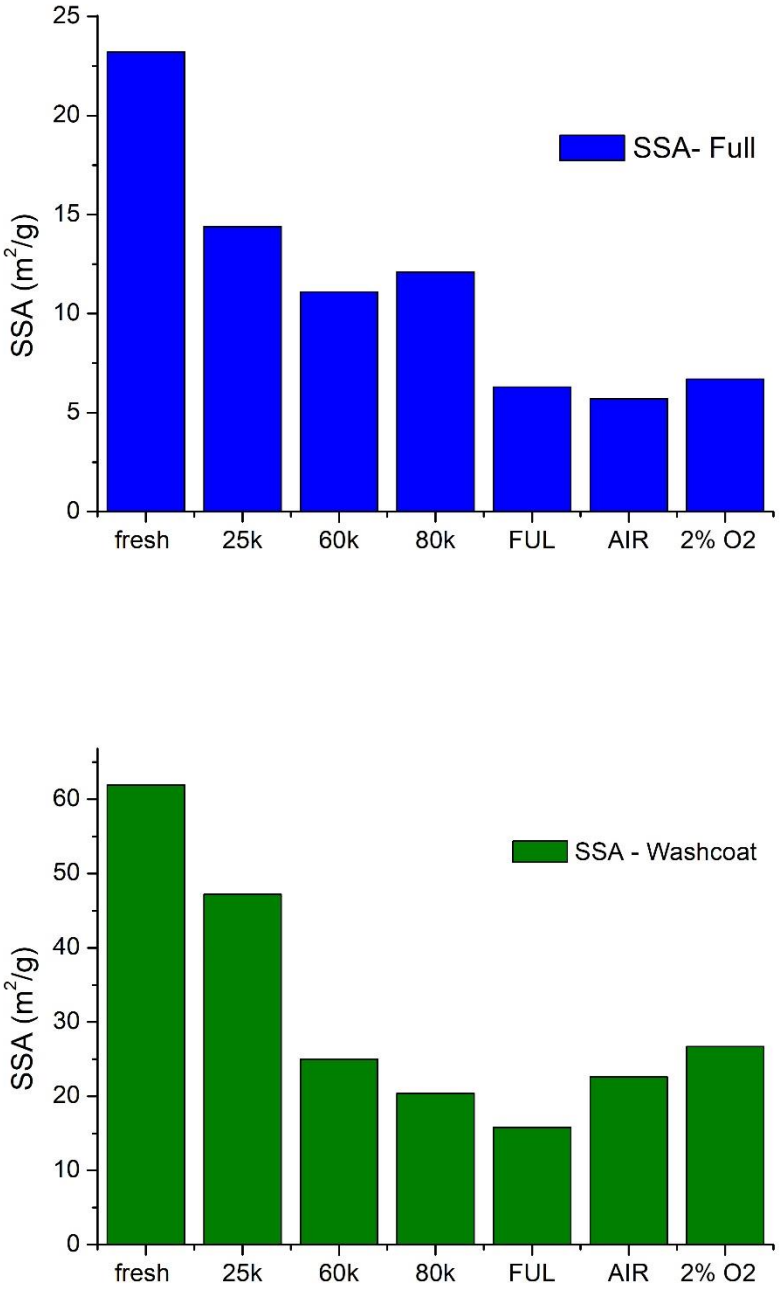


*Figure 20: Specific Surface area analysis (BET equation) measured on full samples and washcoat powder extracted from the same samples.*

| SSA (BET equation) - $m^2/g$ | Full | Washcoat |
|---|---|---|
| **Fresh** | 23,2 | 61,9 |
| **25k** | 14,4 | 47,2 |
| **60k** | 11,1 | 25 |
| **80k** | 12,1 | 20,4 |
| **FUL** | 6,3 | 15,8 |
| **AIR** | 5,7 | 22,6 |
| **2% O2** | 6,7 | 26,7 |

*Table 8: Specific Surface area analysis (BET model) measured on whole samples and washcoat powders extracted from the same samples.*

The results highlight the structural changes that take place upon thermal ageing, with a decrease of the porosity due to sintering of the support material. The full sample lab aged with air has the worst SSA, and the engine bench aged and lab aged in controlled atmosphere have similar values (less the 1 $m^2/g$ of differences). The analysis performed on the washcoat powder are more sensible. The higher values enhance the differences between the samples. In this case, the SSA value of the FUL sample are the lower, and both the lab-aged samples are near the 60k km vehicle one. The difference between the BET values of the full and extracted samples is probably due to the dilution by the cordierite, which has a very low specific surface. In this case, due to the small gap between the SSA of material, low differences in the quantity of cordierite present in the FULL sample can change significantly the results.

In Figures 21 and 22 the XRD pattern recorded on the washcoat powder samples are shown.

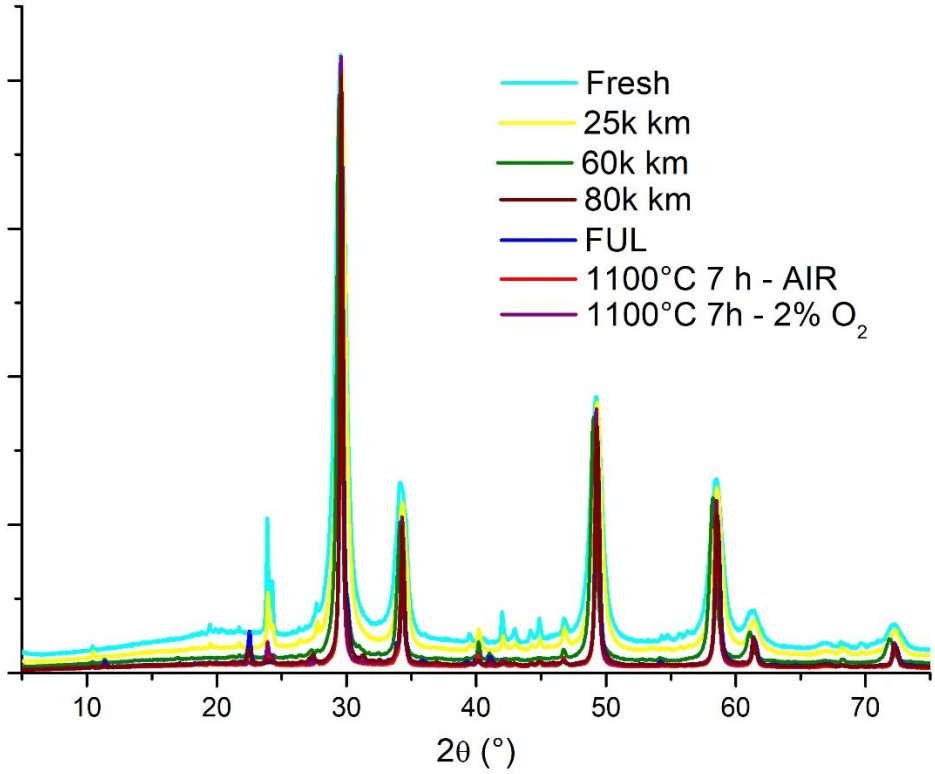


*Figure 21: XRD pattern of washcoat extracted from fresh (light blue), 25k km (yellow), 60k km (green), 80k km (brown), FUL (blue), lab aged 1100°C 7h - AIR (red) and 1100°C 7h - 2% O2 (purple) TWC samples.*

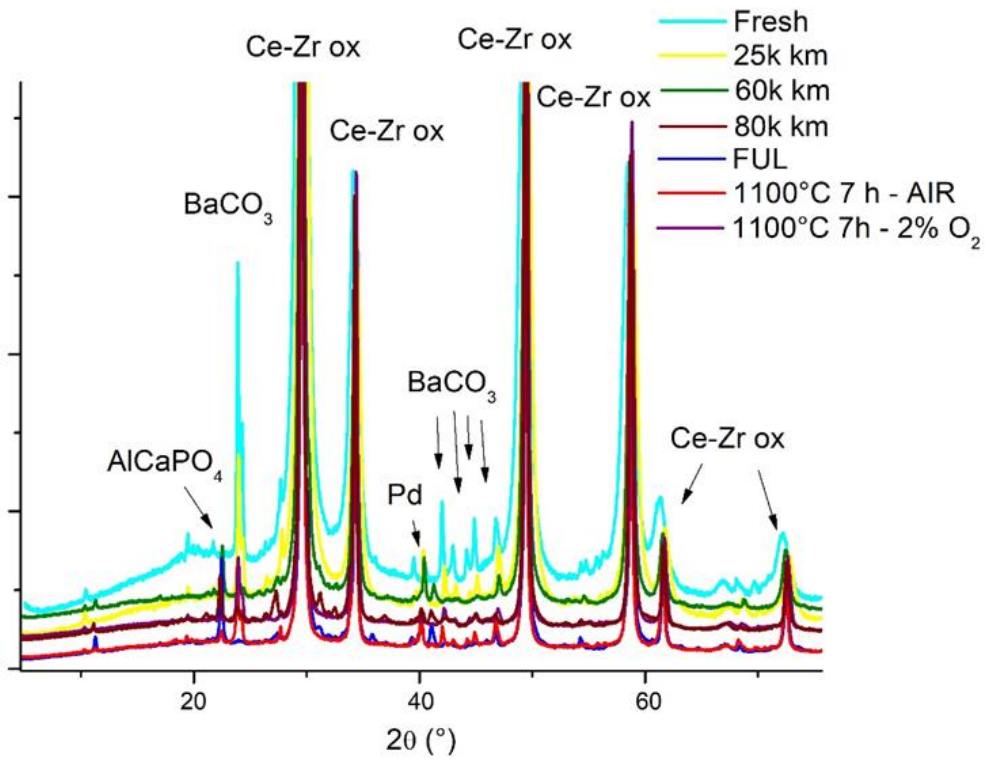


*Figure 22: normalized graph with peaks identification of XRD pattern of washcoat extracted from fresh (light blue), 25k km (yellow), 60k km (green), 80k km (brown), FUL (blue), lab aged 1100°C 7h - AIR (red) and 1100°C 7h - 2% O2 (purple) TWC samples.*

In general, the results are in agreement with XRD patterns recorded on the previous technology and with XRF analysis, with a high amount of Ce-Zr oxides and an important presence of whiterite, $BaCO_3$. The pattern does not highlight the presence of alumina oxides. For the fresh sample, this is understandable, due to the crystallographic characteristics of the $\gamma$-$AL_2O_3$: as discussed above, this polymorph typically has small crystalline grain and a not negligible amorphous content, and its pattern is characterized by low intensity peaks [6]. In addition, also the aged sample patterns do not show peaks associated to the other polymorphs of alumina, despite the higher crystallinity. This can probably due to the relatively low concentration of the alumina phase in these samples. Also in this case the Ce/Zr mixed-oxide phase display patterns with a cubic symmetry and fluorite-structure typical of $CeO_2$ [3]. The peaks become more intense and sharp with increasing ageing, which led to general increases of crystallinity and crystal dimensions.

The peaks of $BaCO_3$ decrease their intensity with the ageing probably due to the progressive conversion to other forms during ageing (maybe BaO) or to the solution of Ba in the crystal lattice of Ce-Zr oxides promoted by high temperatures. These peaks totally disappear in the samples more aged on real engine, FUL,80k and 60k km, probably because in that condition very high exothermic peaks can occur, which enhance this process. In all the aged samples patterns a peak at 40° is present, associated to Pd [12]. This is caused by the progressive sintering of noble metal particles driven by the high temperature, the environment and the presence of water [18]. The processes of migration and coalescence of PGM nanoparticles reduce the dispersion, but increase the dimensions of crystallites, making visible in to XRD pattern. The peaks are not high and sharp enough for the determination of crystal dimensions, but their presence is an important marker of the deactivation of the catalytic material. The higher vehicle aged samples (60k-80k km on vehicle, FUL on engine bench) display the presence of a peak at 22°, associated to a Ca-Al phosphate. This compound is associated to chemical ageing process, due to the accumulation of elements deriving from the combustion of fuels and engine oil and their additives, containing P, Ca and Zn. These elements can form a glassy over layer on the washcoat surface, constituted mainly of phosphates, or other compounds, and formed for example upon reaction with washcoat components, in this case alumina. The comparison between the lab-aged samples is interesting (Figure 23): the patterns are very similar, with peaks with almost the same intensity and position. There is one important difference: the peak of Pd in the sample aged in air is more intense compared to the pattern of sample aged in controlled environment. This difference can be associated to the atmosphere where the ageing takes place: air has a higher content of oxygen, so the environment is more oxidant with respect to a flux with only 2% of $O_2$. The extremely oxidant atmosphere enhanced the sintering of noble metal particles, leading to the formation of crystallite with higher dimensions.

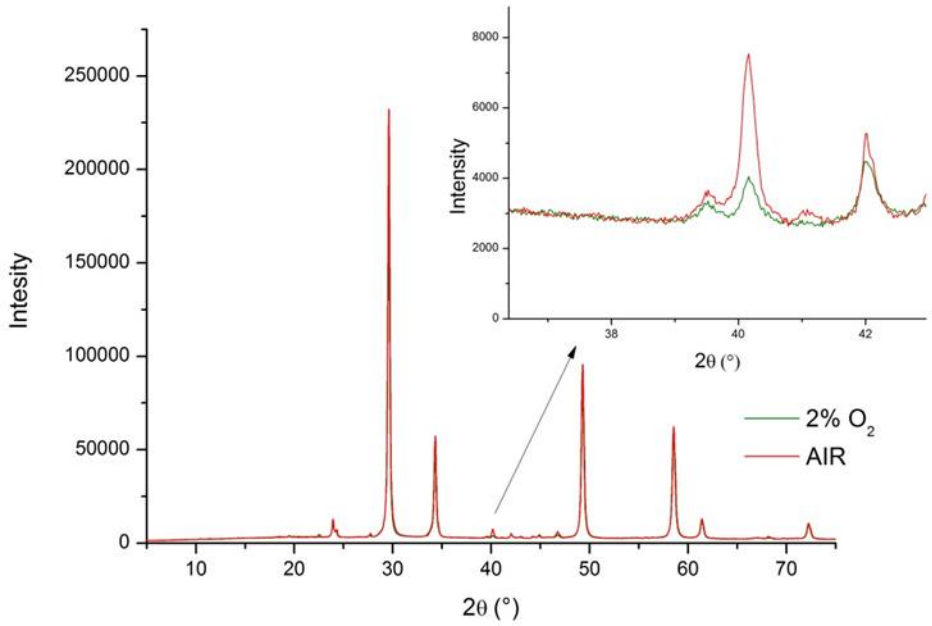


*Figure 23: Comparison between XRD patterns measured on TWC aged sample in laboratory condition: 1100°C 7 h - AIR (red) and 1100°C 7h - 2% $O_2$ (green).*

TEM images recorded on fresh and engine bench FUL aged sample highlight important morphological modifications of the washcoat material. The identification of the different phases present was performed with the help of EDX. Figure 24 presents a series of TEM images recorded on the fresh washcoat powder sample. The agglomerates are formed by a series of polygonal little structures (figure 24A), but also other phases are present, morphologically easy to identify. In figure 24B it is possible to see a massive stick-like structure, over 1 µm long. EDX analysis allows to identify this structure as Ba carbonate phase. Being a fresh sample, this can be the form that whiterite was added to washcoat during the preparation of the coating. It is possible to identify another component, a lamellar flakes structures formed by very thin crystals, almost transparent to TEM (figure 24C). That structure was identified as $Al_2O_3$ phase using EDX detector. In figure 24D it is possible to see a detail of the Ce-Zr mixed oxide structure. The crystals have regular polygonal form with dimensions above of 10 nm. In this sample it was not possible identify any Pd particles. Scanning the zones using the EDX detector the analyses

displayed always a constant low level of Pd, probably because there are numerous little particles, well dispersed.

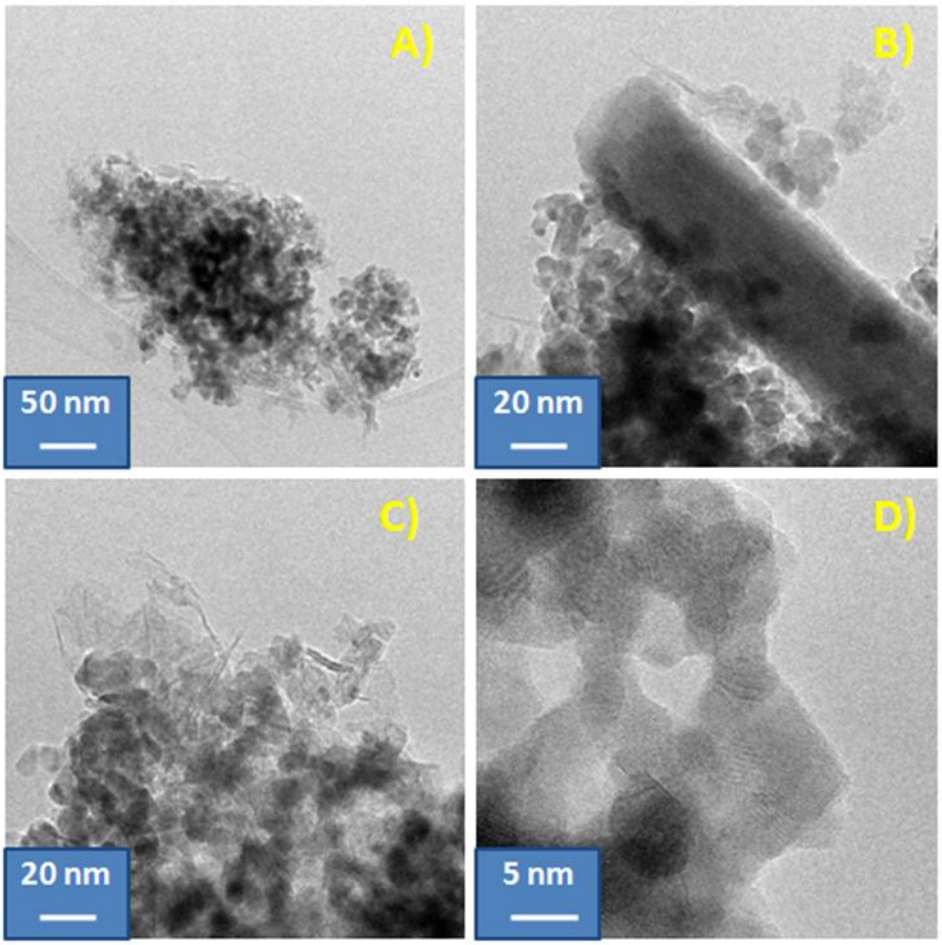


*Figure 24: TEM images of TWC washcoat powder from engine bench aged (FUL) sample. A) washcoat powder aggregates B) residues of BaCO3 (red circle) C) Pd particles on Al2O3 crystal (red circle) D) Ce-Zr mixed oxide crystals.*

FUL aged sample (Figure 25) shows numerous differences. First of all the aggregates are formed by large coarse circular structures (Figure 25A). The stick shape structures of $BaCO_3$ disappeared. Some darker spots were detected in the matrix of the particles (figure 25B, red circles). Using EDX detector on the zones, the chemical analysis highlighted high levels of Ba. These dark particles are probably residues of $BaCO_3$ that were not

integrated from Ce-Zr crystal structure. Due to their high dispersion in the sample and the very low dimensions of the particles (less than 5 nm) this phase is impossible to detect with XRD, as can be seen in the relative pattern (Figure 22). In one of the aggregates present in the sample, a dark particle with 100 nm of diameter was detected, placed on a lamellar structure, maybe $Al_2O_3$ (Figure 25C). EDX analysis allow identifying as Pd particles, likely grown due to thermal sintering. Also the Ce-Zr oxide crystal are grown in their dimensions (Figure 25D), showing a less regular shape.

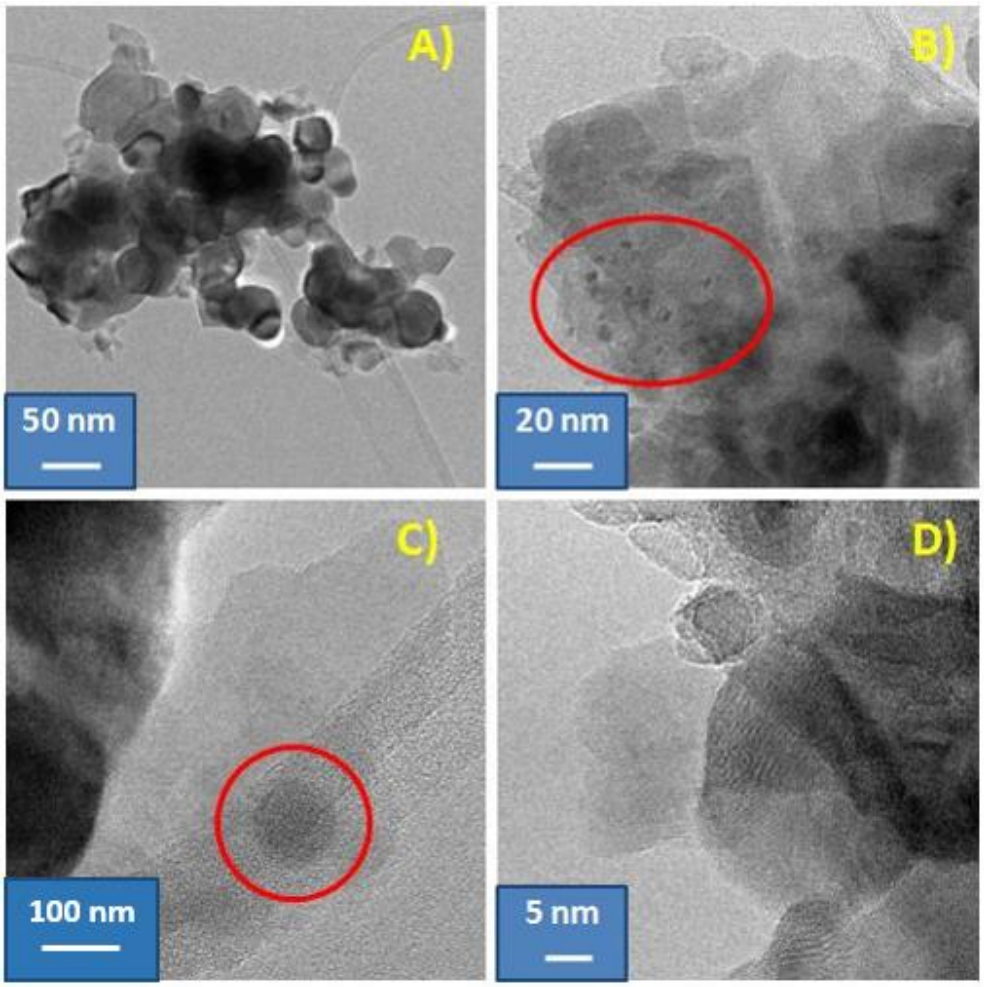


*Figure 25: TEM images of TWC washcoat powder from engine bench aged (FUL) sample. A) washcoat powder aggregates B) residues of BaCO3 (red circle) C) Pd particles on Al2O3 crystal (red circle) D) Ce-Zr mixed oxide crystals.*

Raman spectroscopy does not provides interesting result on that material. The spectra recorded on fresh and FUL samples highlight only one interesting peak, with respect the spectra recorded on previous material.

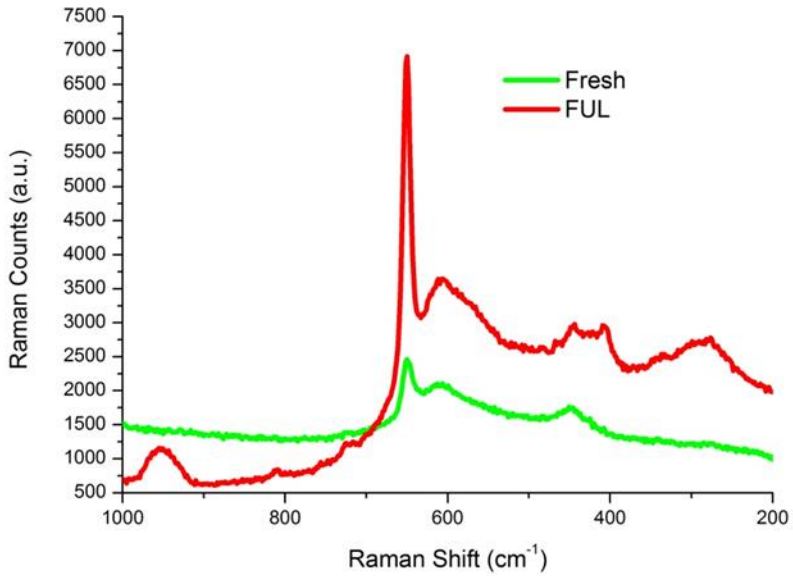


*Figure 26: Comparison between average Raman spectra recorded d on fresh (green line) and FUL sample (red line), using a 514 nm of excitation radiation.*

The peak, recorded at 650 $cm^{-1}$was associated to B2g Raman mode of PdO, native form of this noble metal in automotive catalysis [16], displays a higher intensity in the aged sample, probably due to crystal growth of noble metal particles. It is more intense with respect to the previous but it is surrounded by a very high background, with some broad peaks very difficult to identify. The aged spectra presented in the graph was recorded after an outgas treatment (100°C – 0.5 h) because the spectra previously recorded present a very intense fluorescence, which cover all the possible other peaks. This phenomenon is probably associated to the presence of carbonaceous residues in the sample, associated to the oxidation process occurred during the engine bench cycles. The peaks are interesting but it is difficult to associate them to a PdO particles dimensions, furthermore the high background does not allow performing a mapping of the sample surface.

## 3.4 Noble metals particles evolution.

In this chapter we will discuss the noble metal particles sintering phenomena, as probed with different techniques. FTIR experiments with CO as particularly informative. The first FT-IR measurements of CO adsorption at RT were performed on the washcoat powder extracted from a fresh sample outgassed in vacuum at 400 °C for 30 mins. The absorbance spectrum recorded in this condition does not show any trace of peaks associated to the interaction between CO and noble metal particles, irrespective of the pressure of CO sent to the sample. This lack of reactivity of the fresh catalyst was interpreted as originating from the low severity of the surface outgassing protocol, which did not clean the surface from foreign adsorbed species. Therefore, an activation treatment was devised. In Figure 27 the measurements performed on the fresh sample after the oxidation-reduction pretreatment described in Chapter 2 are presented.

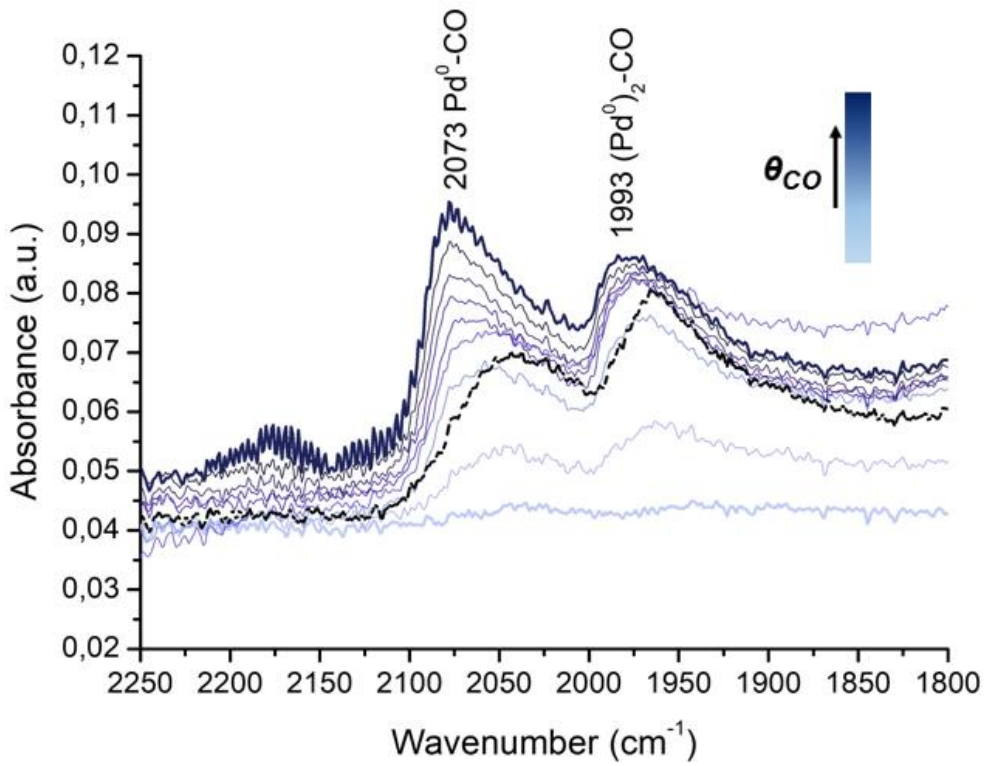


*Figure 27: FT-IR measurement of CO adsorption at RT on the fresh sample after 400°C - 0,5h oxidation-reduction ($O_2$-$H_2$) pretreatment at increasing pressure of CO and after final degassing (black line).*

IR spectra show two peaks, with intensity that increases with the increase of pressure of CO dosed to sample. The first one is around 2100–2000 $cm^{-1}$, typical of the stretching vibration of CO adsorbed in the on-top position on Pd0 site, and the second peak is around 2000–1700 $cm^{-1}$, typical of CO stretching in bridge-bonded configuration between two $Pd^0$ sites [19]. Increasing the CO pressure, the peaks gain in intensity and show a progressive shift to higher wave numbers, due to the increase of the CO coverage, which enhance the dipole coupling [20]. Upon outgassing, the CO coverage decreases and this causes a red-shift towards the original position. The relative amount of on-top vs. bridged carbonyls can provide information on metal particles dispersion. However, the quantitative determination of the distribution of CO between on-top and bridge positions is very difficult and it was not possible on the collected data due to the overlap of the peaks. However, qualitative trends could be estimated. Pd tends to form bridged carbonyls when reduced, which are more stable than the linear ones [21]. A high contribution of the linearly bonded CO is an indication of a loss of dispersion of the Pd, because the proximity of two Pd atoms is necessary to form bridges. Due to better results obtained with oxidation-reduction pretreatment, it was applied to the successive samples, which has been exposed to harsh environment (25k, 60k, 80 km, FUL, Lab-aged).

In figure 28 the IR spectra recorded at RT with increasing level of CO on a sample prepared with 25k km washcoat powder are presented

.

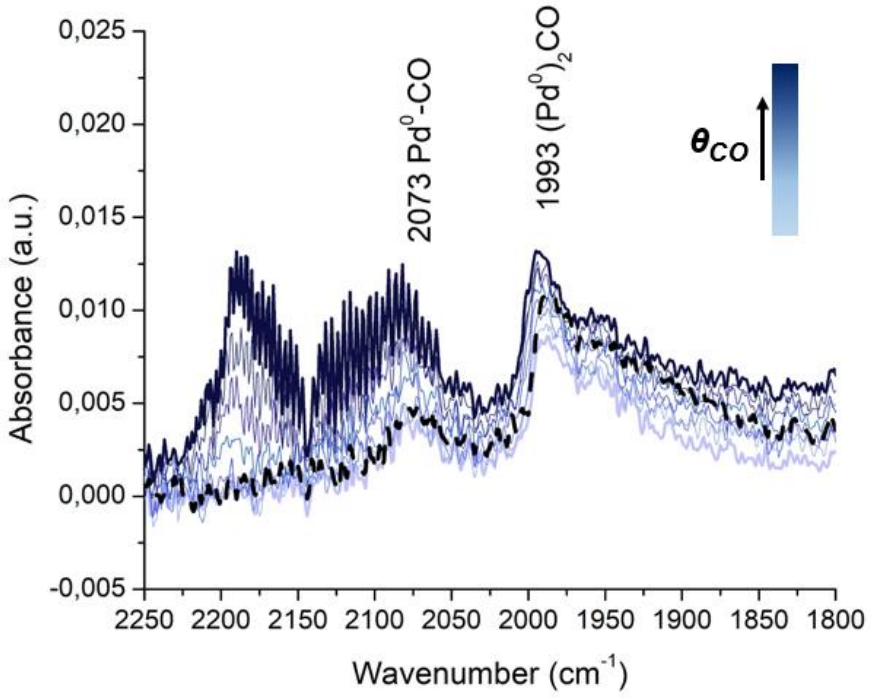


*Figure 28: FT-IR measurement of CO adsorption at RT on 25k km sample after 400°C - 0,5h oxidation-reduction ($O_2$-$H_2$) pretreatment at increasing pressure of CO and after final degassing (black dotted line).*

The overall intensity of carbonyl bands is highly decreased, indicating a loss of Pd active sites. This effect can be linked to sintering phenomena occurred at high temperature, leading to a growth of noble metal particles and to a loss of surface of the porous support, that could lead to an encapsulation of nanoparticles, making them completely inaccessible to the probe molecule. These effects are enhanced on the sample aged on vehicle for 60k km (Figure 29), where the absorbance peaks associated to CO adsorption have completely disappeared.

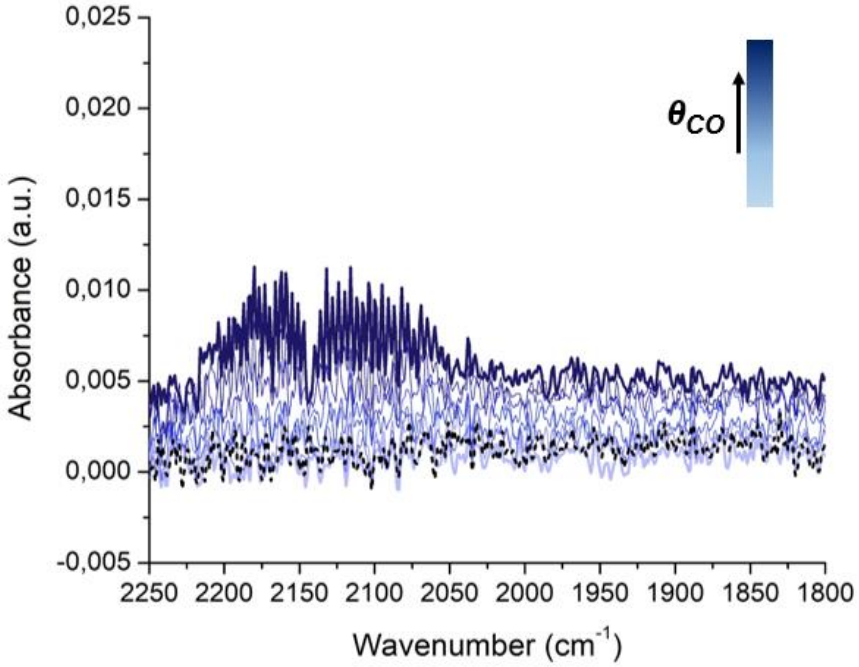


*Figure 29: FT-IR measurement of CO adsorption at RT on 60k km sample after 400°C - 0,5h oxidation-reduction ($O_2$-$H_2$) pretreatment at increasing pressure of CO and after final degassing (black dotted line).*

Previous tests indicated the good correlation between the 60k km sample and laboratory ageing 1100°C- 7h in hydrothermal condition (air) one. In order to verify this analogy, the latter was analyzed using this technique, after $O_2$-$H_2$ pretreatment (figure 30).

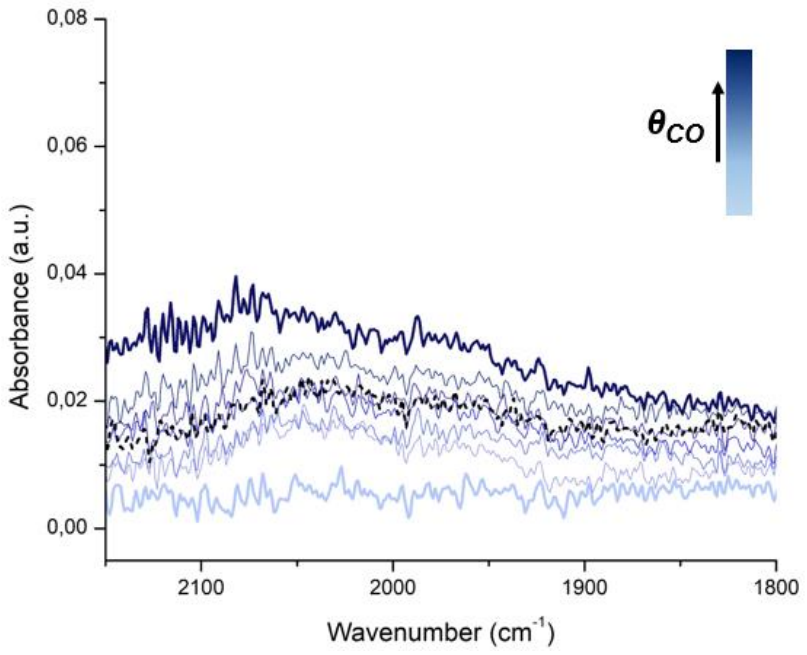


*Figure 30: FT-IR measurement of CO adsorption at RT on Laboratory aged 1100°C 7h – AIR sample after 400°C - 0,5h oxidation-reduction ($O_2$-$H_2$) pretreatment at increasing pressure of CO and after final degassing (black dotted line).*

The IR spectra recorded in this case do not have the same trend of 60k km one, but this could be associated to the different condition that two sample has been exposed during their ageing. Even in this case the stretching peaks of CO is not detectable, probably due to successive sintering of noble metal particles, as seen above in 60k km sample. Given the non-detectability of CO on metal particles on the 60k sample, the more aged samples 80k and FUL were not studied with this technique in order to avoid redundant and unsuccessful analysis. Finally, it is worth noticing that the CO adsorption experiments did not detect distinct peaks for CO adsorption on Rh, which is present on the catalyst with 1:11 ratio with Pd, clearly too low for detection. This is a limitation of our study, due to the great importance of Rh for NOx reduction functionality and to its peculiar deactivation mechanism [22], which should be addressed with more sensitive methods.

The analysis performed at liquid nitrogen temperature (LNT) allow to detect the weaker adsorption phenomena happening on the oxides of the washcoat.

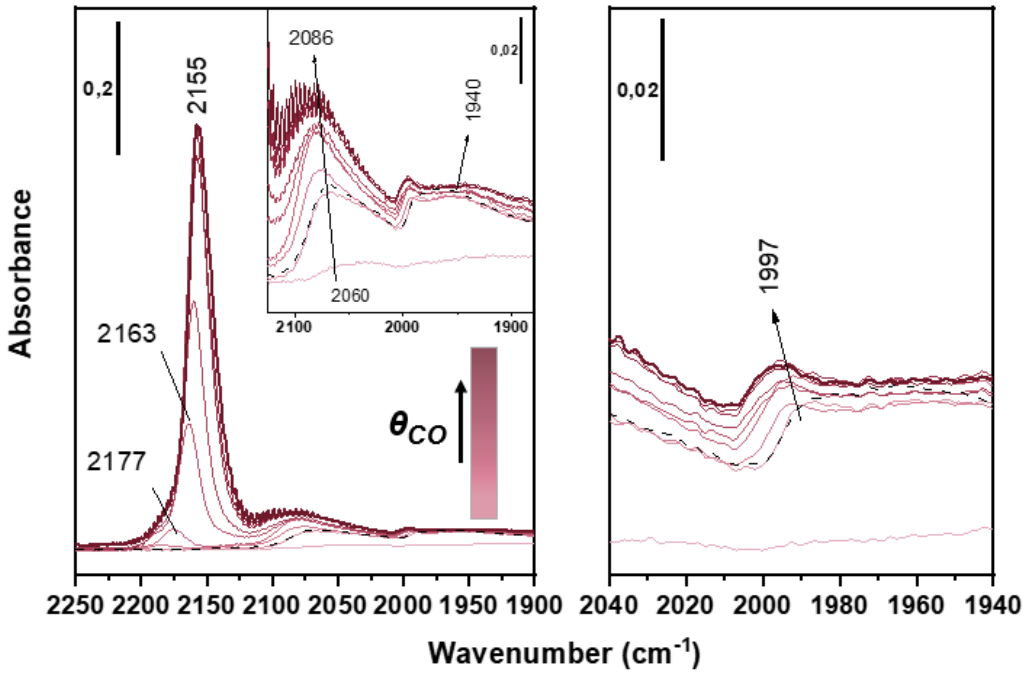


*Figure 31: FT-IR measurement of CO adsorption at LNT on fresh sample after 400°C - 0,5h oxidation-reduction ($O_2$-$H_2$) pretreatment at increasing pressure of CO and after final degassing (black dotted line).*

Figure 31 shows the spectra recorded on the fresh sample. They show an intense peak in the range 2200–2100 $cm^{-1}$, whose intensity increases with CO pressure. The peak red-shifts from 2177 to 2155 $cm^{-1}$ upon increasing CO coverage due to chemical effect, i.e., on increasing CO adsorbed on the surface, the σ-donation decreases. Consequently, electron density in the slightly antibonding HOMO orbital of CO increases and the CO stretching decreases. This peak is probably generated by the superposition of different contributions of CO adsorbed on $Ce^{4+}$ and $Zr^{4+}$ cations, since their stretching vibrations fall in this spectral region [23]. The convolution in one peak of these contributions, which should be separated in the pure oxides, can be associated to a compositionally homogeneous solid solution of the Ce and Zr oxides, with negligible contribution of segregated pure oxide phases. At lower wavenumbers bands related to on-top (2086 $cm^{-1}$) and bridged (1997 and 1940 $cm^{-1}$) $Pd^0$ carbonyls are present [24]. Differently from measurements performed at RT, at LNT the bridged carbonyl region shows complex features with the presence of two bands. Typically the IR spectra of CO adsorbed on

reduced Pd are interpretable on the basis of what occurs on the most stable Pd faces, Pd(111) and Pd(100) [25, 26]. The peak at 1997 $cm^{-1}$ is assigned to bridged carbonyls on Pd (100) faces, while the peak at 1940 $cm^{-1}$ is related to bridged species on Pd (111) face. The band at 2086 $cm^{-1}$ (2060 $cm^{-1}$ for very low CO coverage) is related to linear carbonyls on Pd (111) face. As observable at RT as well, the band of linear carbonyls is asymmetrical due to a shoulder on the low wavenumber side. This shoulder is reasonably due to the presence of defects such as edges, corners and kinks, on noble metal particle surface [27]. The stability of the carbonyl species during the outgassing (dashed lines in the figures) further helps to discriminate between CO bonded to Pd and to the support. Pd carbonyls are more stable than carbonyls of the support, since Pd0 bonds CO both by σ-donation and π-backdonation, while Zr and Ce cations bond CO exclusively via σ-donation and the related bands are completely removed by outgassing. These peaks display the same behavior observed at RT in aged samples, with a progressive disappearance of the signal due to sintering of noble metal particles.

The peaks associated to adsorption on the support material display a similar behavior: the intensity decreases upon ageing, due to the sintering of Ce-Zr oxides. This phenomenon causes not only a loss in intensity of the band but also a decrease in the chemical effect that causes a shift to higher frequencies at maximum coverage with respect to the fresh case, as can be seen in figure 32, which shows the spectra recorded on the 25k km sample.

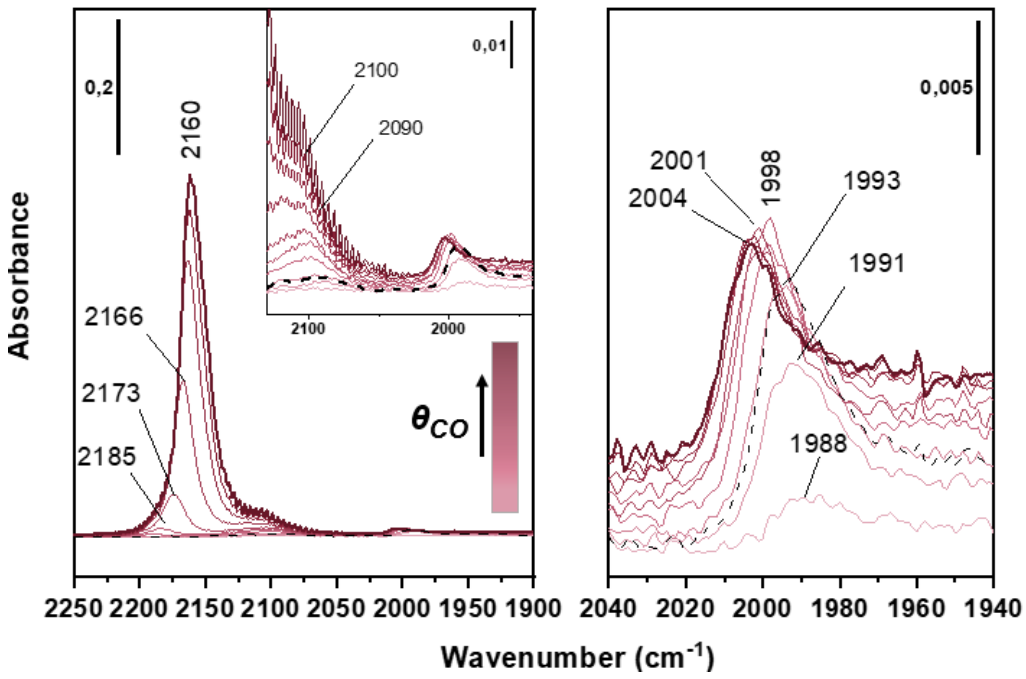


*Figure 32: FT-IR measurement of CO adsorption at LNT on 25k km sample after 400°C - 0,5h oxidation-reduction ($O_2$-$H_2$) pretreatment at increasing pressure of CO and after final degassing (black dotted line).*

In the 60 k sample (Figure 33) a peak assigned to mono carbonyls on re-duced $Ce^{3+}$ species appears at 2116 $cm^{-1}$. The assignment of this band to the carbonyls on the support cation is corroborated by the low stability of the species, which are removed by outgassing (dashed line in Figure 33). The appearance of this peak can be linked to the effects of ageing: the high temperature sintering of these components hindered the $Ce^{4+}$ to $Ce^{3+}$ redox reaction [28]. In addition, there may be a contribution of chemical ageing, with Ce reacting with the phosphate compound present in the engine out gas, coming from the combustion of engine oil additives, forming the very stable $CePO_4$ phase [29]. These effects lead to immobilization of Ce, hindering its participation to redox reactions necessary for oxygen storage.

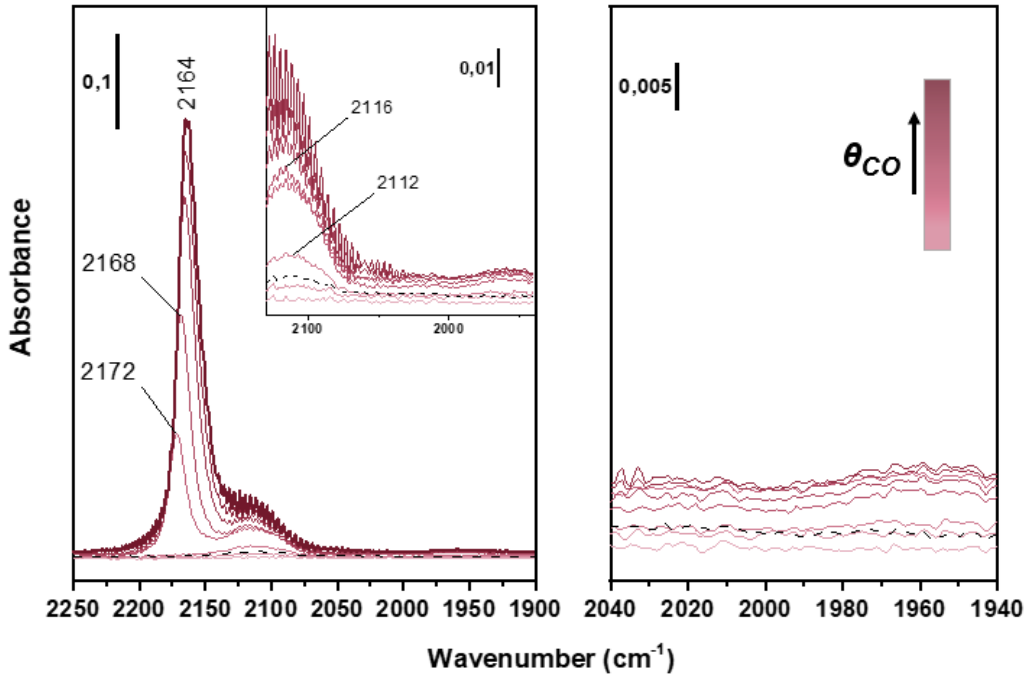


*Figure 33: FT-IR measurement of CO adsorption at LNT on 60k km sample after 400°C - 0,5h oxidation-reduction ($O_2$-$H_2$) pretreatment at increasing pressure of CO and after final degassing (black dotted line).*

The laboratory-aged (Figure 34) show a less intense peak associated to $Ce^{3+}$, probably because in this case there is only the support sintering contribution. This sample has not been in contact with chemical species deriving from the combustion, so the chemical ageing effects in this case are not expected. As for the laboratory-aged sample, the contribution of $Pd^0$-CO at 2096 $cm^{-1}$ is quite evident. Moreover, it is worth to note that in the 60,000 km sample $Pd^0$-CO might be associated to the shoulder of the peak at 2116 $cm^{-1}$, the $Ce^{3+}$-CO band, which is absent for the laboratory aged one.

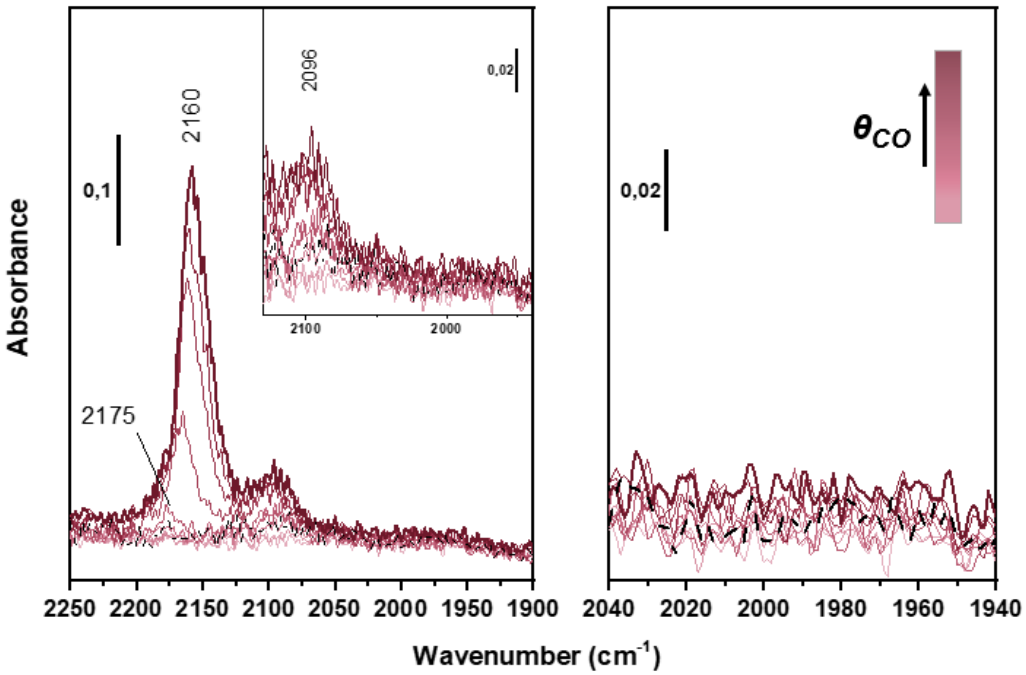


*Figure 34: FT-IR measurement of CO adsorption at LNT on laboratory aged 1100°C 7h – AIR sample after 400°C - 0,5h oxidation-reduction (O2-H2) pretreatment at increasing pressure of CO and after final degassing (black dotted line).*

Moving to pulse CO pulse chemisorption experiments, before the measurement, a reduction pretreatment was performed not only to activate the noble metal surface, but also for to follow the $H_2$ consumption during the heating of sample, in order to record the reduction peak and perform a TPR (Temperature Programmed Reduction) test. In figure 35 the TRP trend recorded on the fresh sample is presented.

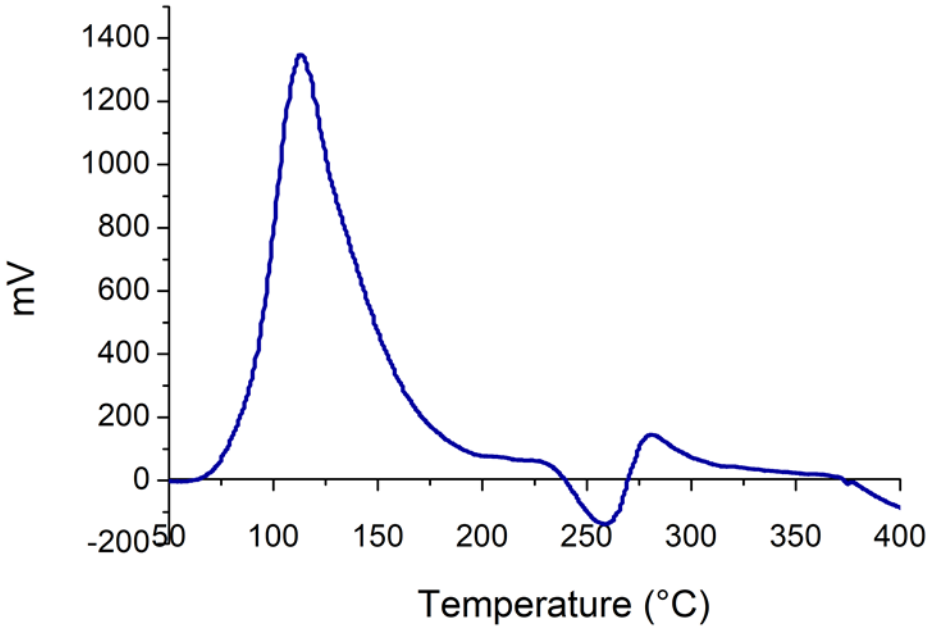


*Figure 35: Temperature programmed reduction trend recorded on the fresh sample during heating from RT to 400°C (10°C/min) in 20 ml/min flow of 5% $H_2$ in Ar.*

The $H_2$ reduction trend displays a reduction peak between 100 and 150°C. The noble metal is completely reduced over 300°C, so this temperature was chosen as set-point temperature for the subsequent pre-treatment. TPR trend presents a first intense peak, related to the reduction of highly dispersed PdO. The second positive peak at 280°C is ascribed to the reduction of relatively stable PdO interacting with the Ce-Zr support. Between them, a negative peak is present, due to a release of $H_2$ that could be attributed to the decomposition of Pd-$H_x$, palladium hydride alloy [30]. The results of the CO-pulse experiment on fresh sample are presented in figure 36A-B, reporting the instantaneous and integrated TCD signal (proportional to the CO concentration at the reactor outlet).

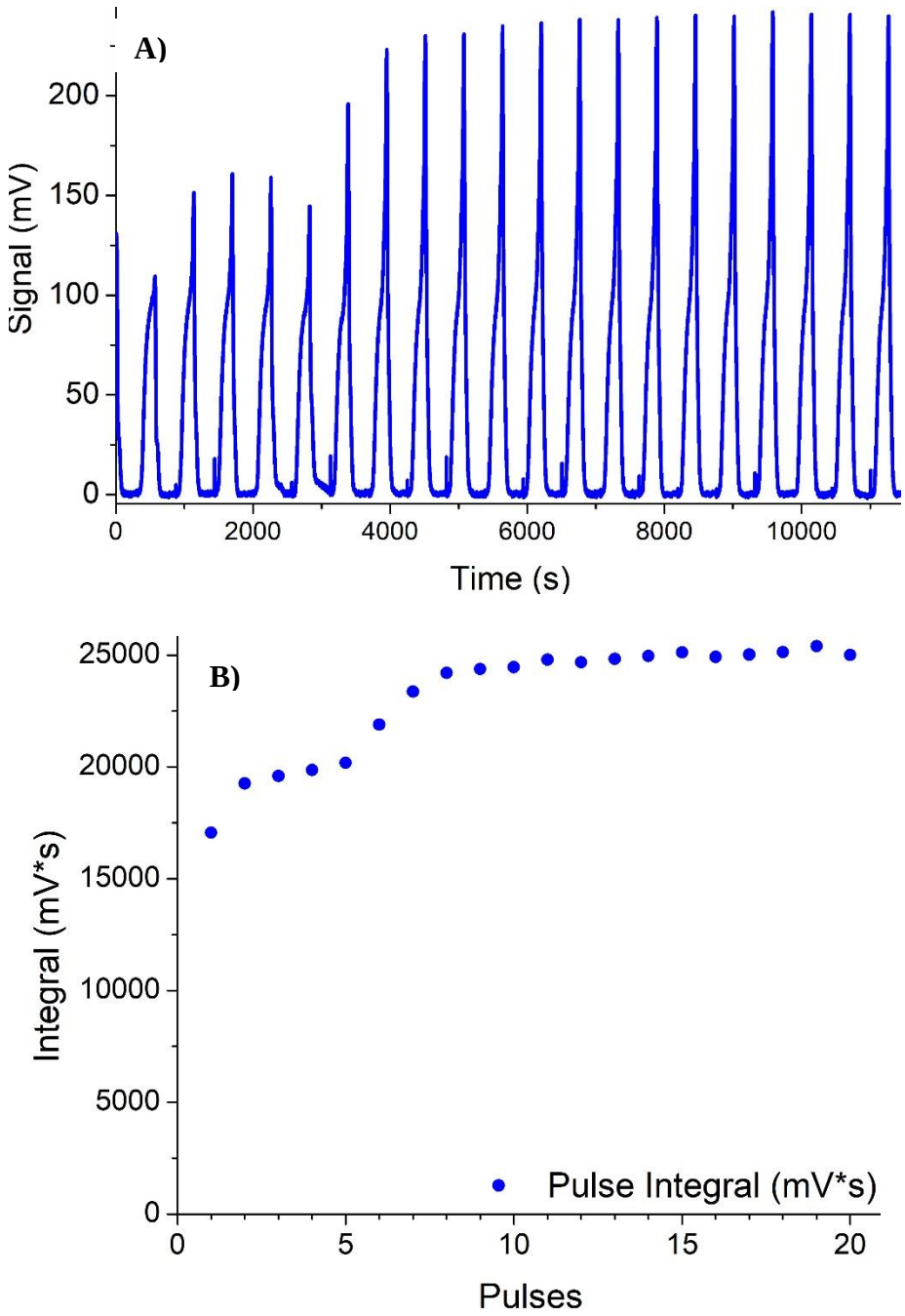


*Figure 36: A) TCD signal (mV) recorded during successive sending of pulses of 800 µl of 10% CO in He carrier until saturation on fresh sample B) Value of integral of the peaks recorded.*

The first peaks are attenuated due to the chemisorption of CO on the surface of noble metal particles, while successive pulses gradually increase until saturation of the adsorption capacity of the metal, when the peaks reach a constant intensity. The CO uptake was calculated from the integral of the peaks (Figure 4b). The dispersion of Pd particles was calculated from the Pd:CO ratio. CO molecules can chemisorb on superficial Pd atoms in linear or bridged form and the coexistence of both the configurations was confirmed by IR spectroscopy. Since two IR peaks with similar intensities appearing after exposing the catalyst to CO, were ascribed to the two CO chemisorbed species, and considering their very similar extinction coefficient (accordingly with literature), a Pd:CO ratio of 1,5 can be suitably assumed for calculations [31]. Using this assumption, from the amount of chemisorbed CO it is possible to calculate the number of Pd sites involved in the reaction and evaluate the ratio between this value and the quantity of Pd present inside the sample, obtained from chemical analysis (1% Pd in weight). The fresh sample exhibits a quite high palladium dispersion, around 51%, expressed in terms of ratio between the moles of Pd involved in total CO uptake and total Pd moles in the sample. This result indicate that the noble metal is distributed on the support in very small particles, consistently with the absence of visible Pd particles in the SEM observations reported in the following. In fact, an average metal particle size of about 2 nm can be estimated from CO chemisorption [32]. For the 25k km sample the situation changes significantly: the differences between the intensity of the first peaks and the peaks at saturation become negligible and difficult to determine. To increase the sensitivity a new test was done, performing the CO pulse manually using a gas syringe in order to increase the concentration of signal peaks. Similarly, in this case the adsorption is barely observable, but measuring the integral of the peaks it was possible detect a little attenuation of first three peaks, as it can be seen in figure 37.

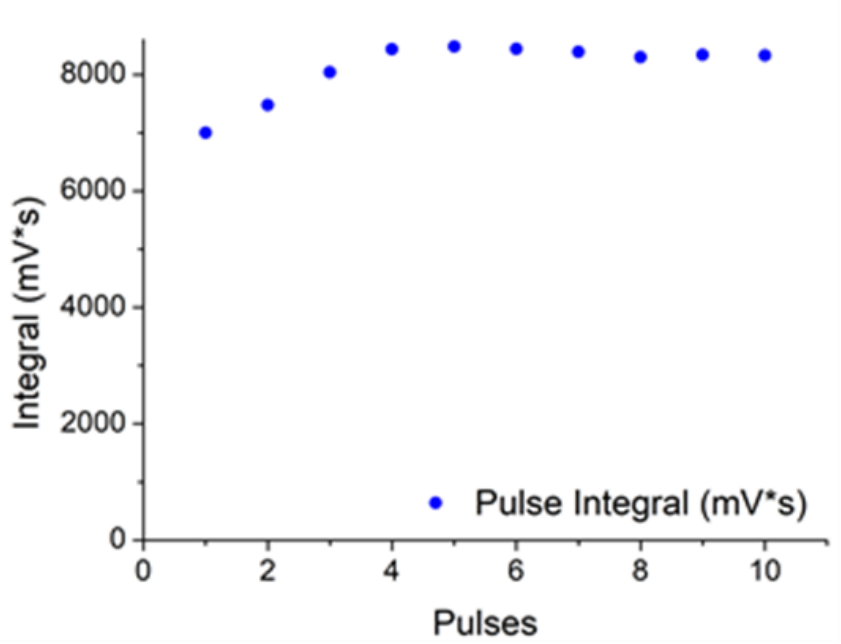


*Figure 37: Integrals of TCD signal peaks recorded during successive sending of pulse of 800 µl of 10% CO in He carrier until saturation on 25k km.*

The dispersion of Pd in this sample is decreased to 8% and for 60K catalyst, it is below 1%, although in the latter cases the CO uptake is too low to obtain reliable values (figure 38A). These results point out that the metal particles are sensitive to sintering during the catalyst life cycle, as suggested by FT-IR measurement. The CO chemisorption test was performed also on the sample laboratory-aged 1100°C – 7h in air, in order to verify the correlation with the 60k km sample. Even in this case the data obtained do not allow to evaluate the dispersion, which is below 1% (figure 38B). Due to the results obtained on this sample, sample with higher level of ageing (80K and FUL) were not analyzed because the sintering of noble metal was probably higher and the results obtained would have been under the detection limits of the method.

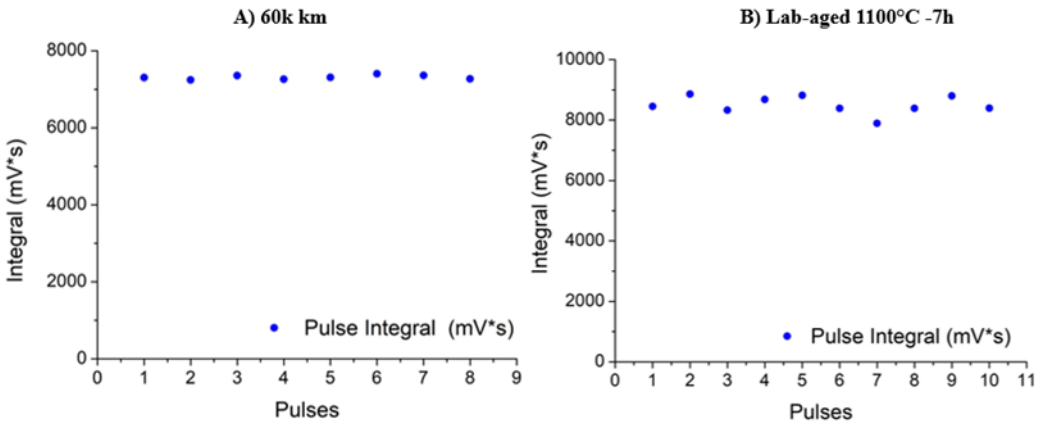


*Figure 38: Integrals of TCD signal peaks recorded during successive sending of pulse of 800 µl of 10% CO in He carrier until saturation on A) 60k km and B) laboratory-aged 1100°C-7h AIR sample.*

The images recorded on FESEM-HR on different samples highlight the sintering phenomena (figure 39).

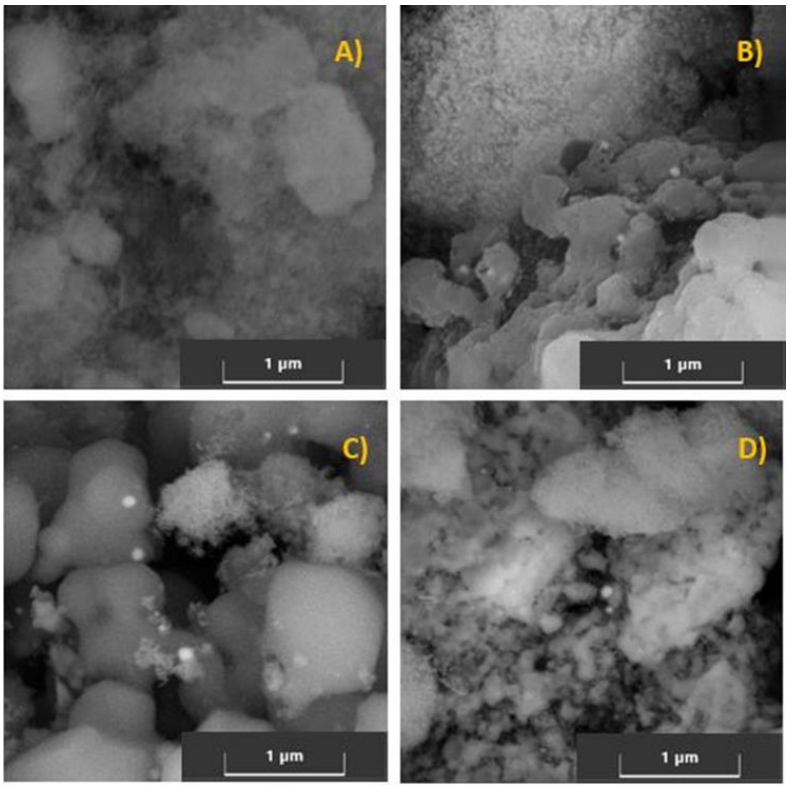

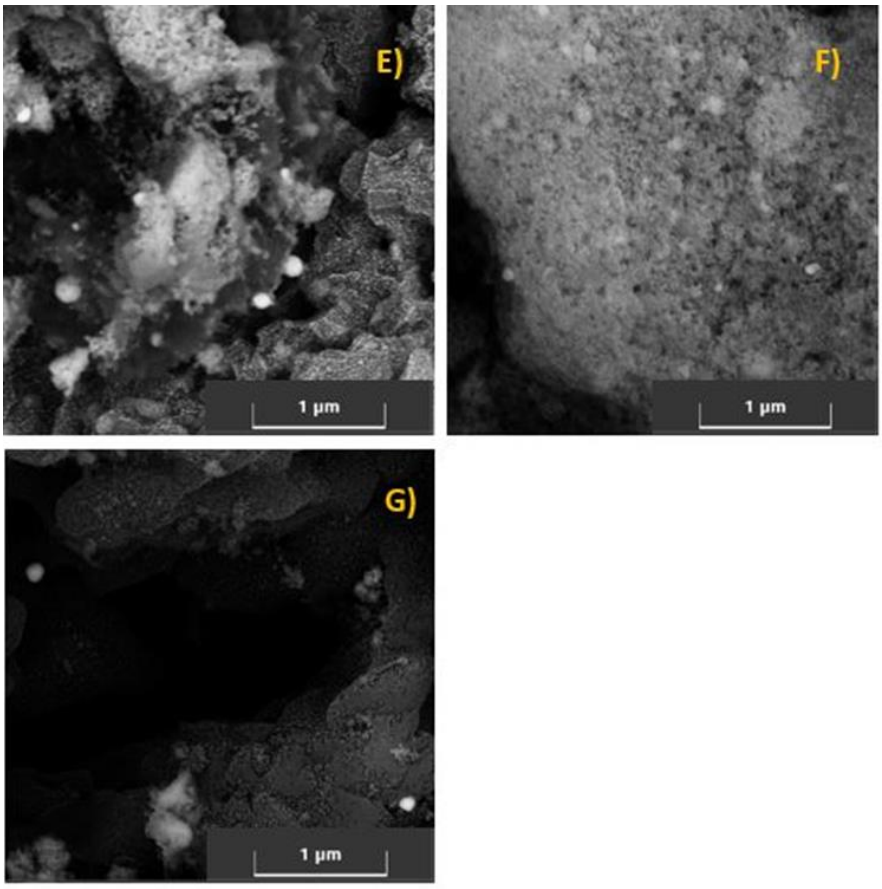


*Figure 39: FESEM images of TWC sample A) Fresh B) 25k km C) 60k km D) 80k km E) FUL F) 1100°C 7h - 2% O2 G) 1100°C 7h – AIR.*

The fresh washcoat displays a coarse morphology, with numerous dark zones associated to the porosity of support. This porous structure disappears with ageing, as it can see in following SEM images, which show a more compact washcoat, with lesser dark zones, due to the sintering phenomena [1]. In all the aged samples images it is possible to observe the presence of light little particles, dispersed in the washcoat support, not detected in images recorded with previous SEM instrument. In order to identify this components a series of EDX measurement, analyzing punctually this particles and recording a mapping on whole samples were performed.

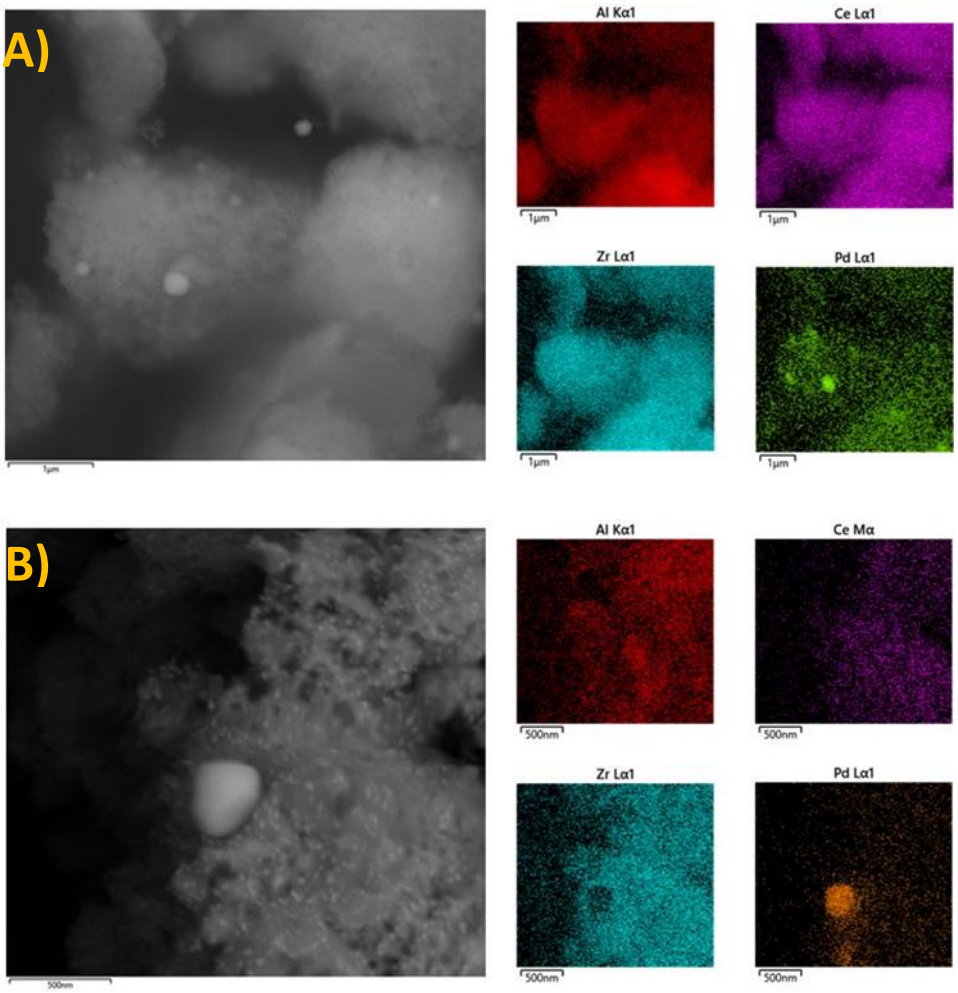


*Figure 40: EDX mapping recorded on SEM images of A) 60k km B) FUL samples.*

The elements mapping performed with EDX detector highlight a high concentration of Pd in correspondence of light particles (figure 40), and performing a single-point analysis on this lighter zone, the spectra recorded highlight presence only of Pd, O and C (figure 41) where the dimensions of particles are sufficiently large to have no contribution from support. In other cases, the intensity of the peak associated to Pd is higher than in the spectrum recorded in the washcoat support area.

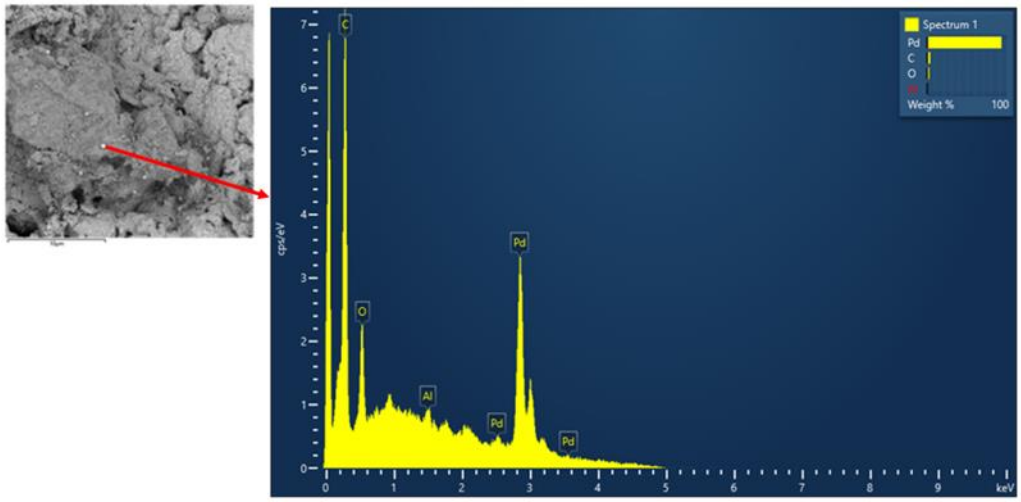


*Figure 41: analysis performed sampling a single light particle, detected in FUL sample.*

Therefore, it is possible to identify these components as Pd/PdO particles, grown due to sintering of catalytic material. In the fresh sample no particles were detected, but performing EDX analysis in different sampling points, a constant Pd signal was recorded, probably because there were numerous well dispersed small particles. This is in agreement with the CO chemisorption analysis which highlighted a good dispersion of very small particles, with diameters below 2 nm in the fresh washcoat sample. Once the identification of noble metal particles in images recorded through this instrumentation was confirmed, a series of diameter measurement was performed, in order to quantify the particles growth process upon ageing. An example of the measurement performed is present in figure 42.

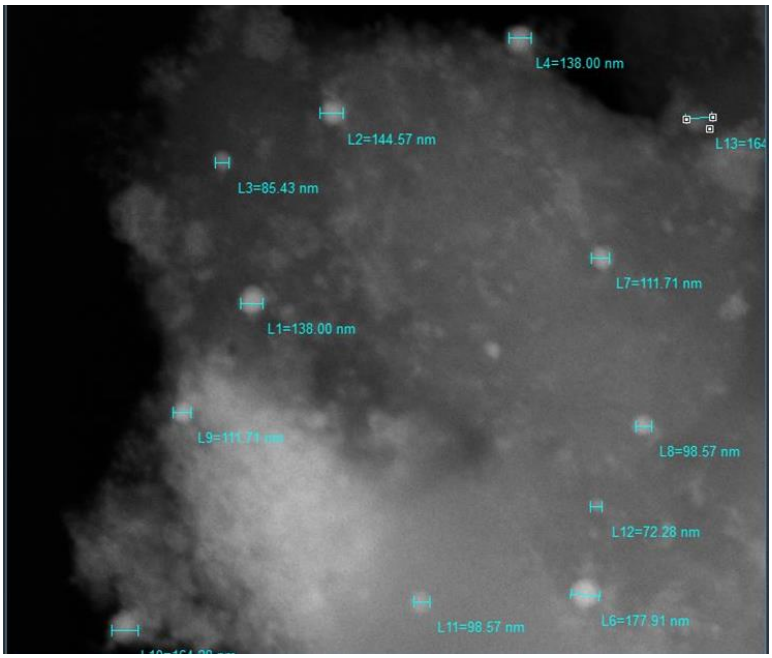


*Figure 42: particles diameter measurements performed on 1100°C -7 h AIR laboratory aged sample.*

In Table 9 are presented the minimum-maximum diameter value registered on samples analyzed and the average value.

| | d min (nm) | d max (nm) | average (nm) |
|---|---|---|---|
| **25k km** | 74 | 115 | 92 |
| **60k km** | 102 | 149 | 121 |
| **80k km** | 131 | 197 | 150 |
| **FUL** | 210 | 800 | 398 |
| **1100°C - 7 h AIR** | 85 | 177 | 130 |
| **1100°C – 7 h 2% $O_2$** | 79 | 118 | 101 |

*Table 9: Minimum, maximum and average value of noble metal particles diameter measured via SEM software.*

The diameter of noble metal particles increases with ageing, overcoming 100 nm of average value from 60k km sample. This is in agreement with FT-IR and CO chemisorption results, which highlighted a high sintering of noble metal particles starting from 25k km, with a great reduction of CO stretching signals and Pd dispersion, up to 60k km sample, which did not show sufficient results. With a particle diameter above 100 nm the interaction of CO is limited, not enough to have to a complete deactivation of catalyst material, but leading to results below the detection limits of the applied techniques. FUL sample is confirmed to be the worst case of the study, with Pd cluster diameter up to 0.8 µm. Particle dimensions measurements confirm also the previous hypothesis about the laboratory-ageing environment. Comparing the XRD patterns recorded on washcoat powder extracted from the catalyst aged with air and in presence of low level of $O_2$, the peaks associated to Pd are higher in the first case, indicating a higher growth of noble metal particles in presence of higher concentration of oxygen. The diameter measurement confirms this result, with sample aged in low oxygen condition that present clusters with lower dimensions, but anyway above 100 nm.

## 3.5 Chemical ageing contribution evaluation.

The chemical ageing effects detected in previous analyses were evaluated using ICP-OES, focused on the principal elements coming from engine oil additives (Ca, P, and Zn) and on S [33]. Fresh and laboratory aged samples show very low level of these elements, below the detection limits of the instrument. Engine aged samples display increasing levels of P and Ca, in particular for 60k, 80k and FUL, and this is consistent with XRD results. S contribution is negligible, probably due to the very low level of sulfur content in the automotive fuels required by the current regulations (Figure 43 – Table 10).

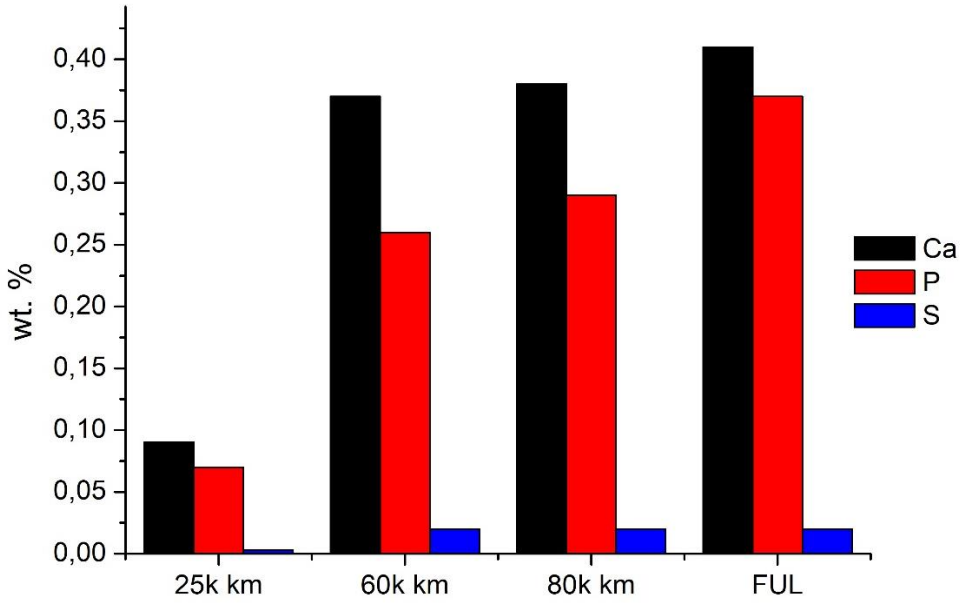


*Figure 43: quantitative results, expressed in wt%, of ICP-OES analysis performed on washcoat powder samples.*

| | Ca | P | S |
|---|---|---|---|
| **25k km** | 0,09 | 0,07 | 0,003 |
| **60k km** | 0,37 | 0,26 | 0,02 |
| **80k km** | 0,38 | 0,29 | 0,02 |
| **FUL** | 0,41 | 0,37 | 0,02 |

*Table 10: quantitative results, expressed in wt%, of ICP-OES analysis performed on washcoat powder samples.*

Phosphorus presence could be probably attributable to combustion products of a widely used engine oil additive, zinc dialkyldithiophosphate (ZDDP), added as anti-wear and antioxidant agent, which produces $P_2O_5$ in the exhaust gas. Ca and Zn are associated to several oil detergent additives [34].

## 3.6 Functional characterization of catalysts samples.

In this chapter we will discuss the results of the tests of catalytic function of the samples. Please refer to Chapter 2 for a description of the test apparatus and operating conditions. Figures 44 and 45 present the efficiency curves for CO and HC oxidation.

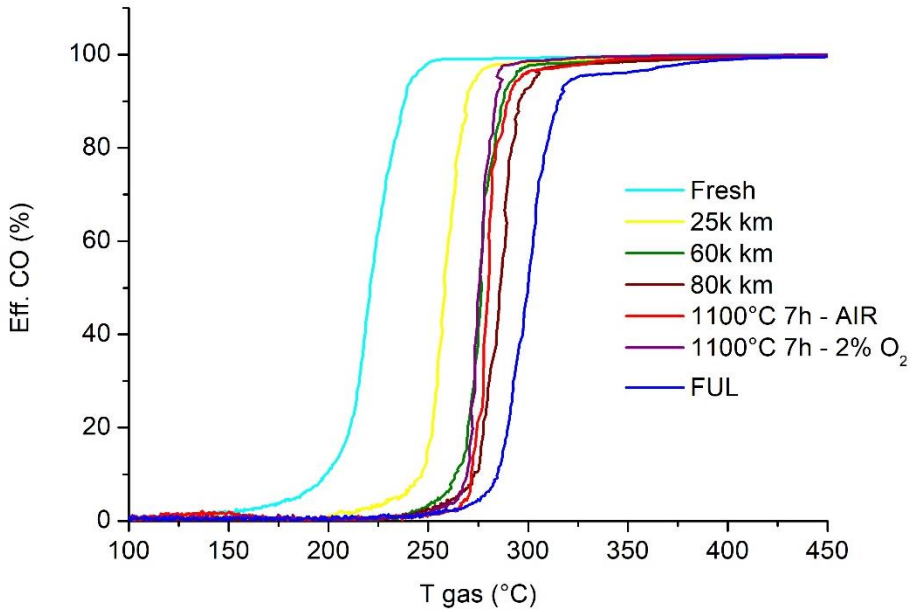


*Figure 44: Efficiency conversion curve for CO oxidation.*

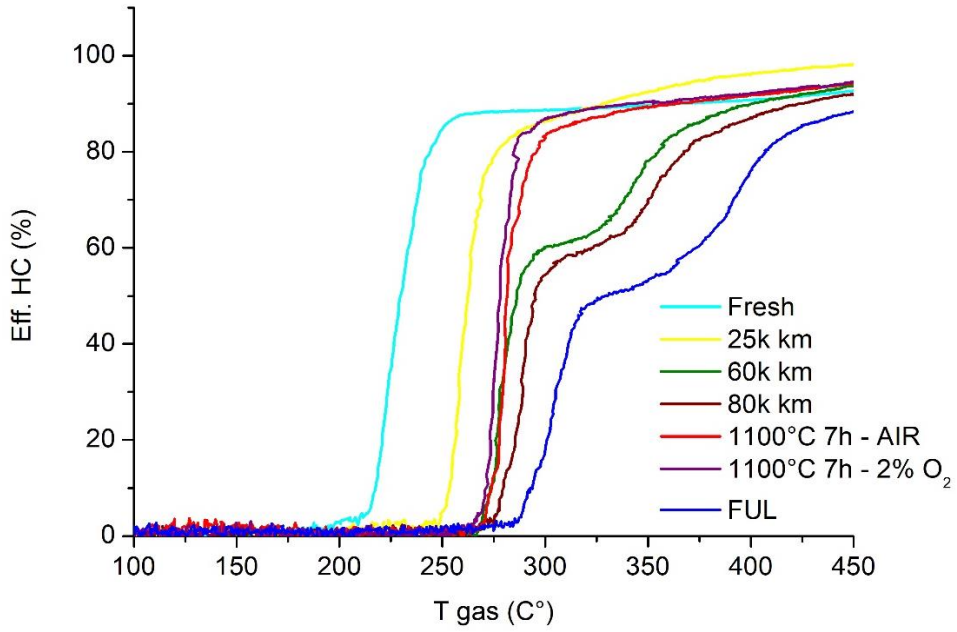


*Figure 45: Efficiency conversion curve for HC oxidation.*

Both the graphs highlight the effect of the catalysts deactivation due to ageing. The conversion starts progressively at higher temperature, as long as the ageing increases. For CO oxidation at high temperature, the reactions reach 100% conversion in all the samples, although the FUL sample reaches full conversion only above 400°C. HCs are harder to convert, in particular $CH_4$, and the oxidation starts at higher temperature with respect to CO in all the samples. FUL 60k and 80k km sample, all aged in real condition, present an evident step of the curve above 300°C, with an almost flat region. This behavior could be linked to a contribution of chemical ageing effect. Sintering of noble metal particles reduce the contact between active site of active material and the reactant present in the stream, leading to an increase of the activation energy of the reactions, causing in turn an increase of the temperature at which they occur. The reaction between the washcoat materials with substances coming from the engine out gas provoke series of transformation (conversion in inactive compound, masking of catalysts surface) that, added to thermal ageing effects, could lead to this particular this behavior in HC

efficiency curves [35]. In Figure 46 and Table 10 the light off temperatures for the oxidation of CO and HC, recorded during the efficiency tests are presented.

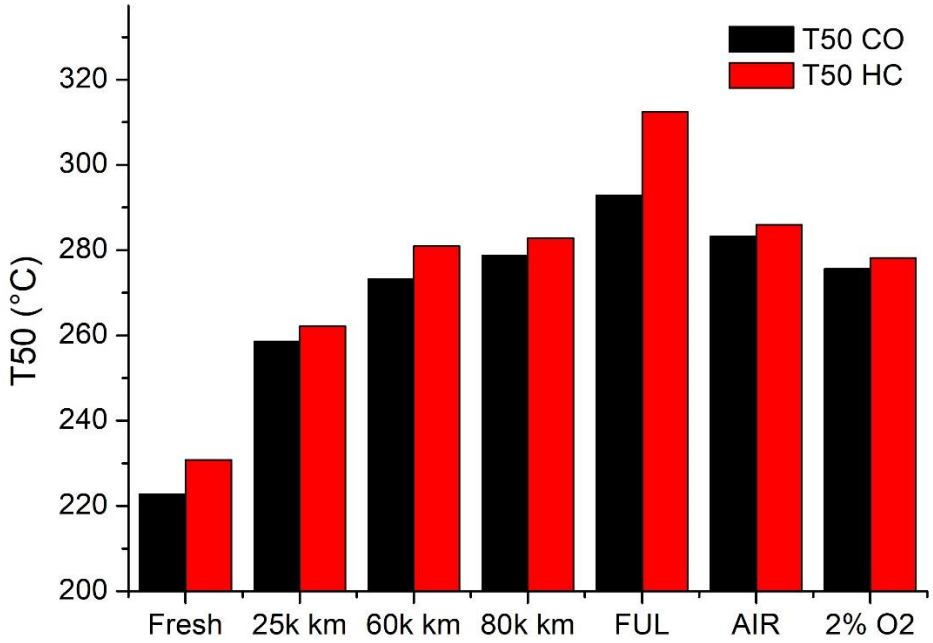


*Figure 46: light-off temperature recorded during the efficiency tests for the oxidation of CO (black) and HC (red)*

The light off temperatures increase with the ageing for both the reactions. The differences between CO and HC T50 are low, less than 10°C in almost all the sample tested, except in the case of the engine bench FUL aged. The oxygen storage capacity decreases significantly along the ageing, as it can be seen in Figure 47 and Table 11.

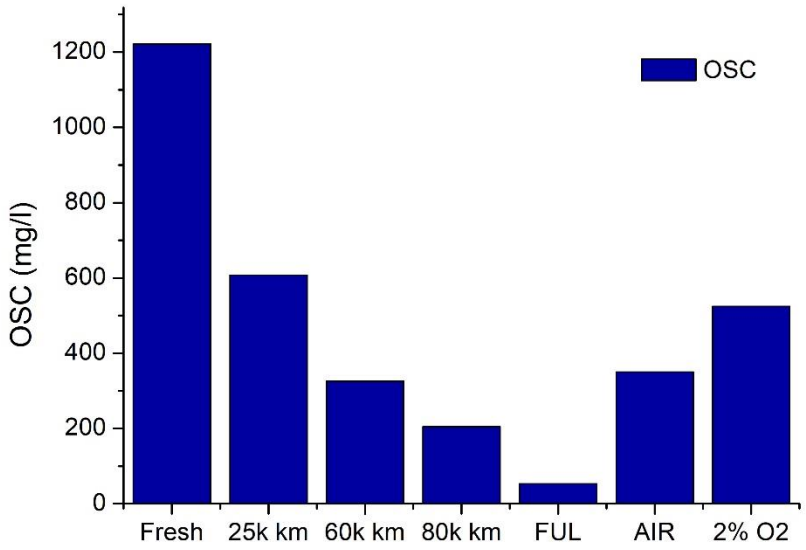


*Figure 47: Oxygen Storage Capacity (OSC) measured in all the samples.*

| | T50 CO (°C) | T50 HC (°C) | OSC (mg/l) |
|---|---|---|---|
| **Fresh** | 222,8 | 230,8 | 1221 |
| **25k km** | 258,6 | 262,2 | 608 |
| **60k km** | 273,3 | 281,0 | 326 |
| **80k km** | 278,8 | 282,8 | 205 |
| **FUL** | 292,9 | 312,4 | 53 |
| **1100°C 7h - AIR** | 283,2 | 286,0 | 350 |
| **1100°C 7h - 2% $O_2$** | 275,6 | 278,2 | 524 |

*Table 11: Light-off temperature and Oxygen storage capacity measured on catalysts samples.*

The OSC for the 25k km sample is half of that of the fresh one and it is furthermore halved at 60k km. This phenomenon is linked to the redox properties of the oxygen

storage components that were found to drastically change with increasing aging. Thermal and chemical ageing of these components decrease their functionality [23]. In terms of performances, both the laboratory-aged samples are quite similar to the 60k km sample, with almost equal light-off temperatures. The OSC of sample aged in controlled atmosphere (2% $O_2$) is higher than air-aged and 60k km, resulting therefore less representative. Observing the conversion curves, lab aged samples display the same trend at low temperature, but above 300°C they do not show the same step present in the engine-aged sample. This is consistent with the hypothesis that the step is caused by chemical ageing. In fact, the laboratory ageing protocol is a purely hydrothermal process, so it cannot simulate the effects of the chemical ageing.

- REFERENCES:


1. Neyestanaki, A. K.; Klingstedt, F.; Salmi, T.; Murzin, D. Y. Deactivation of Postcombustion Catalysts, a Review. *Fuel* **2004**, *83* (4–5), 395–408.
2. Talo, A.; Lahtinen, J.; Hautojärvi, P. An XPS Study of Metallic Three-Way Catalysts: The Effect of Additives on Platinum, Rhodium, and Cerium. *Applied Catalysis B: Environmental* **1995**, *5* (3), 221–231.
3. Terribile, D. The Preparation of High Surface Area CeO2–ZrO2 Mixed Oxides by a Surfactant-Assisted Approach. *Catalysis Today* **1998**, *43* (1–2), 79–88.
4. Wu, X.; Xu, L.; Weng, D. The Thermal Stability and Catalytic Performance of Ce-Zr Promoted Rh-Pd/γ-Al2O3 Automotive Catalysts. *Applied Surface Science* **2004**, *221* (1–4), 375–383.
5. Fernández-García, M.; Martínez-Arias, A.; Iglesias-Juez, A.; Belver, C.; Hungría, A. B.; Conesa, J. C.; Soria, J. Structural Characteristics and Redox Behavior of CeO2–ZrO2/Al2O3 Supports. *Journal of Catalysis* **2000**, *194* (2), 385–392.
6. Cava, S.; Tebcherani, S. M.; Souza, I. A.; Pianaro, S. A.; Paskocimas, C. A.; Longo, E.; Varela, J. A. Structural Characterization of Phase Transition of Al2O3 Nanopowders Obtained by Polymeric Precursor Method. *Materials Chemistry and Physics* **2007**, *103* (2–3), 394–399.
7. Guo, J.; Gong, M.; Yuan, S.; Chen, Y. Effect of BaO on Catalytic Activity of Pt-Rh TWC. *Journal of Rare Earths* **2006**, *24* (5), 554–559.
8. Gangwar, J.; Gupta, B. K.; Tripathi, S. K.; Srivastava, A. K. Phase Dependent Thermal and Spectroscopic Responses of $Al_2O_3$ Nanostructures with Different Morphogenesis. *Nanoscale* **2015**, *7* (32), 13313–13344.
9. Fernández-García, M.; Martínez-Arias, A.; Hungría, A. B.; Iglesias-Juez, A.; Conesa, J. C.; Soria, J. Thermal Behavior of (Ce,Zr)Ox/Al2O3 Complex Oxides Prepared by a Microemulsion Method. *Phys. Chem. Chem. Phys.* **2002**, *4* (11), 2473–2481.
10. Schaper, H., E. B. M. Doesburg, and L. L. Van Reijen. "The influence of lanthanum oxide on the thermal stability of gamma alumina catalyst supports." *Applied Catalysis* 7.2 (1983): 211-220.
11. Hietikko, M.; Lassi, U.; Kallinen, K.; Savimäki, A.; Härkönen, M.; Pursiainen, J.; Laitinen, R. S.; Keiski, R. L. Effect of the Ageing Atmosphere on Catalytic Activity and Textural Properties of Pd/Rh Exhaust Gas Catalysts Studied by XRD. *Applied Catalysis A: General* **2004**, *277* (1–2), 107–117.
12. Baylet, A.; Marécot, P.; Duprez, D.; Castellazzi, P.; Groppi, G.; Forzatti, P. In Situ Raman and in Situ XRD Analysis of PdO Reduction and Pd° Oxidation Supported on γ-Al2O3 Catalyst under Different Atmospheres. *Phys. Chem. Chem. Phys.* **2011**, *13* (10), 4607.

13. Chen, J. J.; Ruckenstein, E. Role of Interfacial Phenomena in the Behavior of Alumina-Supported Palladium Crystallites in Oxygen. *J. Phys. Chem.* **1981**, *85* (11), 1606–1612.
14. Boullosa-Eiras, S.; Vanhaecke, E.; Zhao, T.; Chen, D.; Holmen, A. Raman Spectroscopy and X-Ray Diffraction Study of the Phase Transformation of ZrO2–Al2O3 and CeO2–Al2O3 Nanocomposites. *Catalysis Today* **2011**, *166* (1), 10–17.
15. de Oliveira, L. F. C.; Faulstich, F. R. L.; Zotin, F. M. Z. Comment on "Raman Spectroscopy and X-Ray Diffraction Study of the Phase Transformation of ZrO2–Al2O3 and CeO2–Al2O3 Nanocomposites" by S. Boullosa-Eiras, E. Vanhaecke, T. Zhao, D. Chen, A. Holmen (Catalysis Today, 166 (2011) 10–17). *Catalysis Today* **2012**, *187* (1), 215–216.
16. Iglesias-Juez, A. Metal–Promoter Interface in Pd/(Ce,Zr)Ox/Al2O3 Catalysts: Effect of Thermal Aging. *Journal of Catalysis* **2004**, *221* (1), 148–161.
17. Wang, Qiuyan, et al. "Application of rare earth modified Zr-based ceria-zirconia solid solution in three-way catalyst for automotive emission control." *Environmental science & technology* 44.10 (2010): 3870-3875.
18. Lassi, Ulla, et al. "Deactivation correlations over Pd/Rh monoliths: the role of gas phase composition." *Topics in catalysis* 30.1-4 (2004): 457-462.
19. Fernández-García, M., et al. "New Pd/CexZr1− xO2/Al2O3 three-way catalysts prepared by microemulsion: Part 1. Characterization and catalytic behavior for CO oxidation." *Applied Catalysis B: Environmental* 31.1 (2001): 39-50.
20. Bensalem, Abdelhamid, et al. "Spectroscopic study of CO adsorption on palladium–ceria catalysts." *Journal of the Chemical Society, Faraday Transactions* 92.17 (1996): 3233-3237.
21. Bergeret, Gérard, and Pierre Gallezot. "Particle size and dispersion measurements." *Handbook of Heterogeneous Catalysis: Online* (2008): 738-765.
22. Vedyagin, A.A.; Volodin, A.M.; Stoyanovskii, V.O.; Kenzhin, R.M.; Slavinskaya, E.M.; Mishakov, I.V.; Plyusnin, P.E.; Shubin, Y.V. Stabilization of active sites in alloyed Pd–Rh catalysts on γ-Al2O3 support. *Catal. Today* **2014**, *238*, 80–86.
23. Hadjiivanov, Konstantin I., and Georgi N. Vayssilov. "Characterization of oxide surfaces and zeolites by carbon monoxide as an IR probe molecule." (2002): 307-511.
24. Groppo, E., et al. "Role of the support in determining the vibrational properties of carbonyls formed on Pd supported on SiO2− Al2O3, Al2O3, and MgO." *The Journal of Physical Chemistry C* 111.19 (2007): 7021-7028.
25. Surnev, S.; Sock, M.; Ramsey M.G.; Netzer, F.P.; Wiklund, M.; Borg, M.; Andersen, J.N. CO adsorption on Pd(111): a high-resolution core level photoemission and electron energy loss spectroscopy study. *Surf. Sci.* **2000**, *470*, 171–185, doi.org/10.1016/S0039-6028(00)00853-0.
26. Xu, X.; Goodman, D.W. An infrared and kinetic study of carbon monoxide oxidation on model silica-supported palladium catalysts from 10-9 to 15 Torr. *J. Phys. Chem.* **1993**, *97*, 7711–7718, doi:10.1021/j100131a047.
27. Hollins, P. The influence of surface defects on the infrared spectra of adsorbed species. *Surf. Sci. Rep.* **1992**, *16*, 51–94, doi:10.1016/0167-5729(92)90008-y.
28. Gong, Jian, et al. "An experimental and kinetic modeling study of aging impact on surface and subsurface oxygen storage in three-way catalysts." *Catalysis Today* 320 (2019): 51-60.
29. Christou, Stavroula Y., et al. "Suppression of the oxygen storage and release kinetics in Ce0. 5Zr0. 5O2 induced by P, Ca and Zn chemical poisoning." *Applied Catalysis B: Environmental* 106.1-2 (2011): 103-113.
30. Cao, Yidan, et al. "Comparative study of ageing condition effects on Pd/Ce0. 5Zr0. 5O2 and Pd/Al2O3 catalysts: Catalytic activity, palladium nanoparticle structure and Pd-support interaction." *Applied Catalysis A: General* 457 (2013): 52-61.
31. Beck, A., et al. "Pd nanoparticles prepared by "controlled colloidal synthesis" in solid/liquid interfacial layer on silica. I. Particle size regulation by reduction time." *Catalysis letters* 65.1-3 (2000): 33-42.

32. Borodziński, Andrzej, and Magdalena Bonarowska. "Relation between crystallite size and dispersion on supported metal catalysts." *Langmuir* 13.21 (1997): 5613-5620.
33. Fernández-Ruiz, R., et al. "TXRF analysis of aged three way catalysts." *Analyst* 131.4 (2006): 590-594.
34. Larese, C., et al. "Deactivation of real three way catalysts by $CePO_4$ formation." *Applied Catalysis B: Environmental* 40.4 (2003): 305-317.
35. Heck, Ronald M., Robert J. Farrauto, and Suresh T. Gulati. *Catalytic air pollution control: commercial technology*. John Wiley & Sons, 2016.

# 4 Results Discussion & Conclusions.

In the previous chapters we have described a series of convergent characterization studies of a variety of samples aged with different protocols, both on vehicle and on the laboratory. All the samples highlights a clear series of phenomena linked to the deactivation of the catalysts: sintering of the oxide support, with loss of its porous structure, crystal growth process of Ce-Zr oxides and growth of the noble metals particles, with loss of homogeneity of their distribution in the matrix. The loss of efficiency was quantified with a series of functional test, which highlight the increase in the temperature of light off and the loss in the OSC of the materials upon ageing. The growth of noble metal particles and the loss of dispersion in the washcoat material was followed with different techniques, showing a significant sintering already in the less aged sample (25k km), with the formation of large clusters with dimensions above 100 nm in both the 60k and h the laboratory-aged samples. These results are in agreement with the results of FT-IR analysis, showing the progressive disappearance of the signals associated to the interaction of the probe molecule (CO) with Pd active sites, and with pulse adsorption results, that underline the progressive loss of dispersion of the nanoparticles. Chemical ageing has an important role, in particular for samples aged on real engines exhausts. Its contribution is evident from XRD patterns, with the presence of the typical peaks associated to phosphates. Chemical ageing is also responsible for the presence of the evident step in the HC conversion curves in all the higher aged samples on real engines. FT-IR analysis at liquid $N_2$ temperature allowed to understand the different contributions of thermal and chemical ageing on Ce-Zr mixed oxide. The high temperature sintering of these components hinders the redox capability of Ce and reduces the interaction with the engine out gases. The reaction with phosphorous compounds present in engine out gas leads to the formation of redox inactive $Ce^{3+}$ phosphates.

The ultimate purpose of the studies presented in this thesis is the development of accurate simulated ageing protocols, reproducing the ageing occurring with real vehicle usage. In this respect, the data collected in this study constitute a reference frame which can be used for the validation of proposed new ageing methods. In order to summarize the

correlations between real and simulated ageing results, in the following is presented an attempt to correlate some key observables parameters with ageing mileage (Figures 48-52).

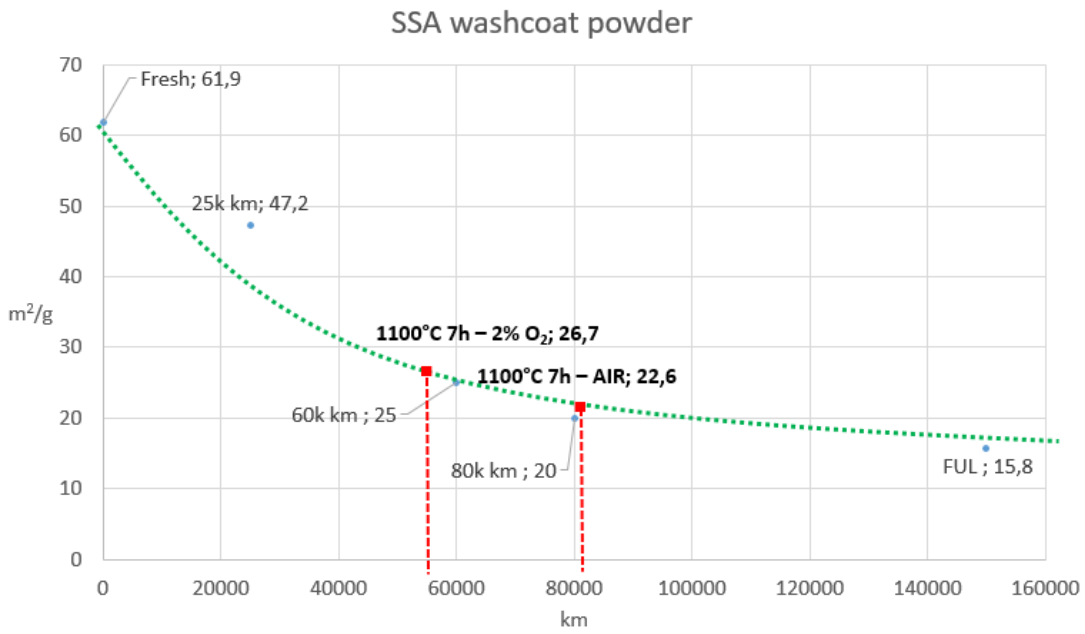


*Figure 48: Specific Surface Area value (BET equation) plotted vs. mileage of real vehicle samples.*

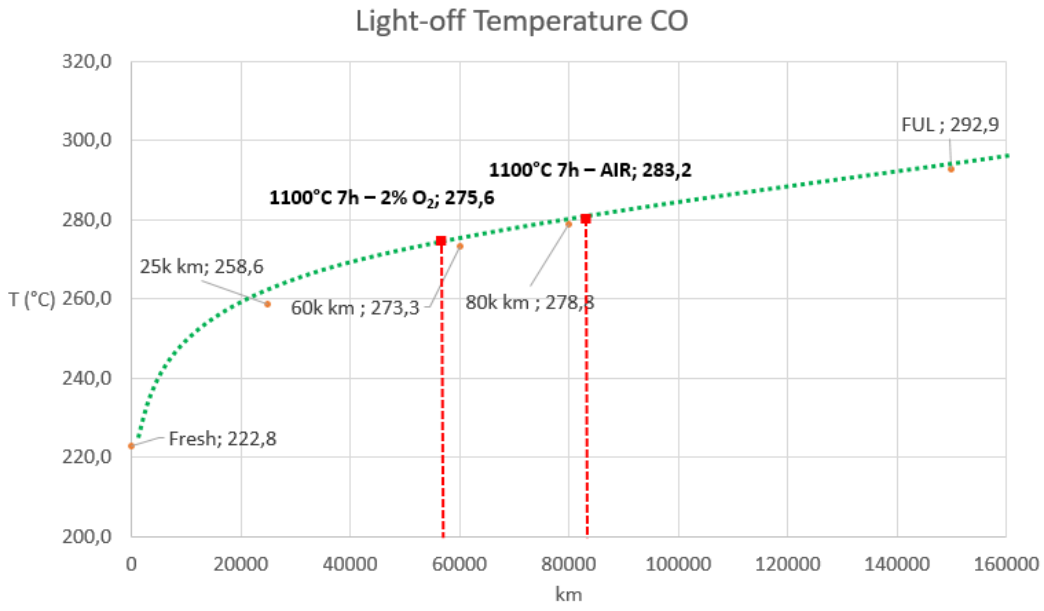


*Figure 49: CO Light-off temperature plotted vs. mileage of real vehicle samples.*

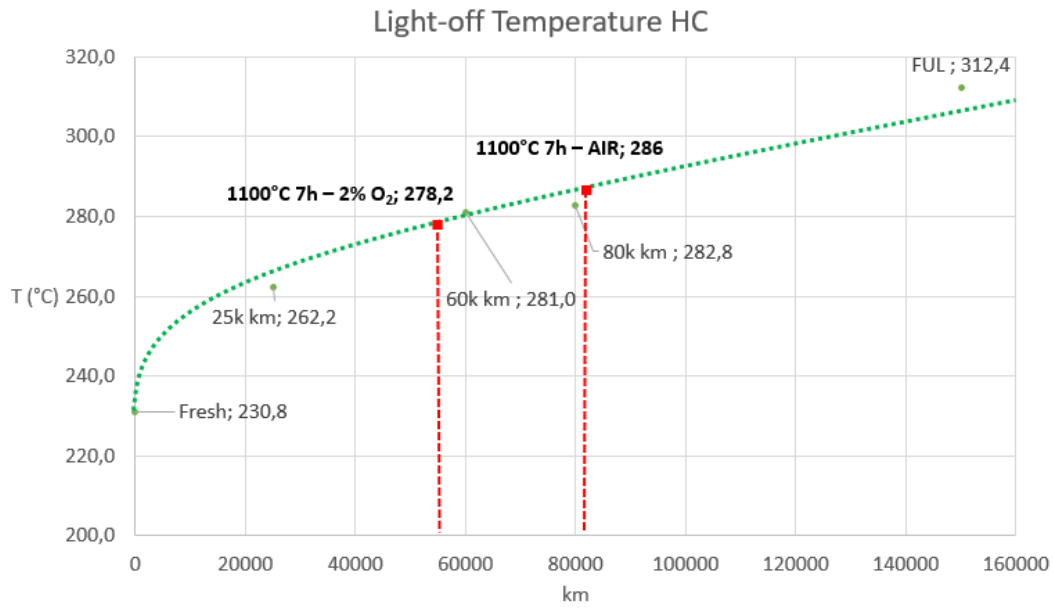


*Figure 50: HC Light-off temperature plotted vs. mileage of real vehicle samples.*

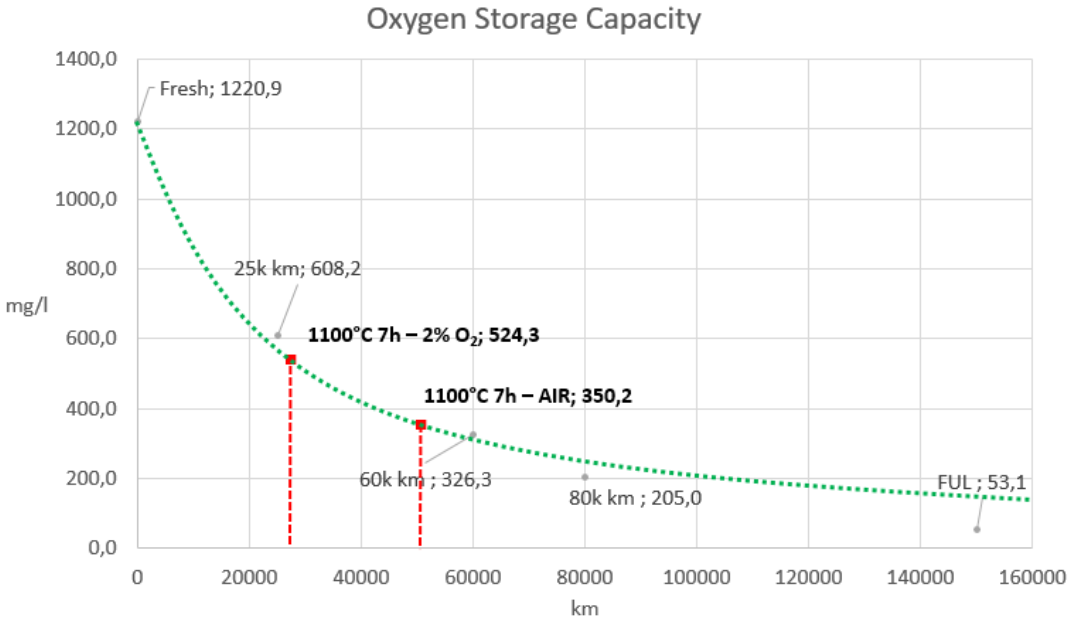


*Figure 51: Oxygen Storage capacity plotted vs. mileage of real vehicle samples.*

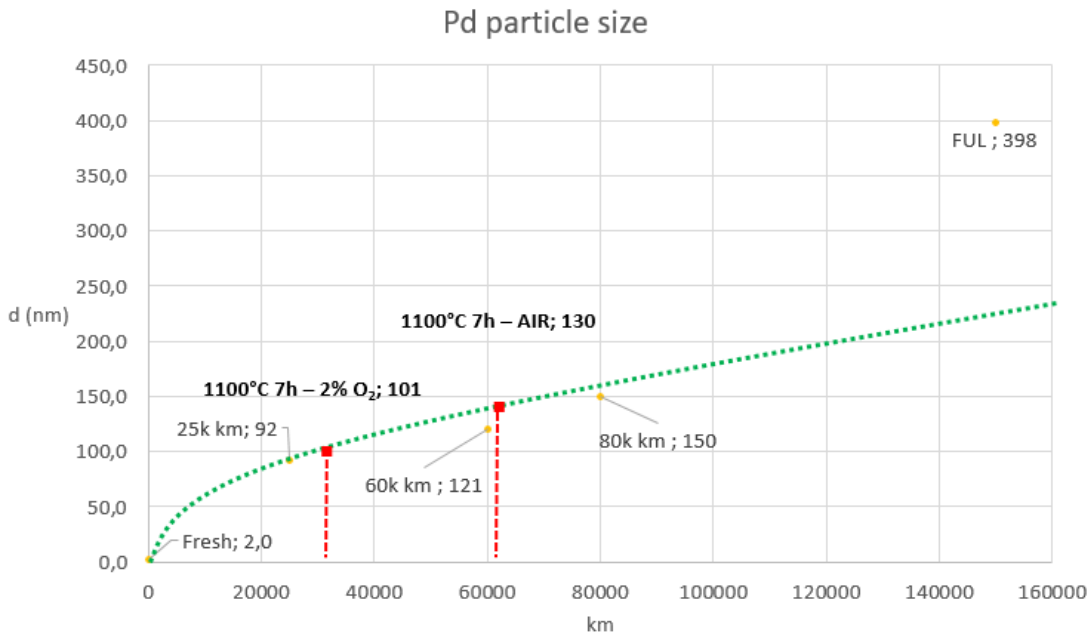


*Figure 52: Pd nanoparticles size (diameter) plotted vs. mileage of real vehicle sample.*

The correlation between vehicle aged samples allow to estimate and "equivalent mileage" for the samples aged with laboratory protocols. In particular, the plotted parameters show that the proposed ageing protocol display results comparable with mileage around 40 and 80k km, depending on the parameter considered. For the SSA and light-off temperature for CO and HC oxidation the estimated mileage in between 60 and 80k km, while for OSC and Pd particles size the estimated mileage are around 40 and 60k km, probably because these parameter are more affected by engine environment. The sample aged in a low oxygen environment presents in general a good correlation with lower mileage ageing, probably due to lower severity linked to the lower oxidant environment. The lower equivalent mileage attributable to OSC value registered on real samples could be linked to the chemical ageing contribution. As explained before, the reaction of Ce with elements contained in engine out gas lead to formation of inert species, enabling to participate to redox reaction useful to the oxygen buffer function. The chemical ageing contribution remains the major problem of the accelerated ageing protocol performed in

laboratory because is very difficult replicate the condition where take place. In addiction also the growth of Pd nanoparticles results more severe in terms of correlation with simulated ageing protocol, probably because the variable environment condition increase the growth rate of PGM particles. The engine bench aged sample represents a limit case, displaying in many cases result worse than expected, in particular in terms of particles dimension. This is remarkable considering the fact that this protocol was originally conceived as a full useful life condition testing method, representative of very high mileage levels. On the contrary, they proved to be more detrimental compared to general trend coming from the analysis of real vehicle samples. In order to understand the ageing of the catalysts at very high mileage and improve the capacity to design representative laboratory testing methods, further testing of high mileage real samples is needed. In particular, samples coming from a vehicles with over 100k km of road accumulation were expected for further characterization. All the information acquired during this characterization will be employed to develop a new accelerated ageing protocol, using a particular facilities specially developed for this topics. This instrument, called “Lab-Cat”, allow to flux in a full-scale catalytic component a high quantity of a synthetic gas mixture at high temperature, with a controlled and adjustable concentration, order to perform ageing protocol in variable condition, similar to a real engine environment.

# 5 Annex 1: Published material.

The results presented previously has been partially published on some scientific publications:

*International Journal of Automotive Technology*, Vol. 21, No. 2, pp. 329–337 (2020)
DOI 10.1007/s12239–020–0031–x


pISSN 1229–9138/ eISSN 1976–3832

## THERMAL AGEING EFFECTS IN A COMMERCIAL THREE-WAY CATALYST: PHYSICAL CHARACTERIZATION OF WASHCOAT AND ACTIVE METAL EVOLUTION

Mattia Giuliano[1, 2)*], Gabriele Ricchiardi[1)], Alessandro Damin[1)], Mauro Sgroi[2)], Giovanna Nicol[2)] and Flavio Parussa[2)]

[1)]Department of Chemistry, NIS and INSTM Reference Centre, University of Torino, Torino 10135, Italy
[2)]Fiat Research Center, Group Materials Labs, Environment & Chemical Analysis, Innovation Aftertreatment & Batteries, Strada Torino 50, Orbassano 10043, Italy

*(Received 28 February 2019; Revised 9 May 2019; Accepted 10 June 2019)*

DOI: https://doi.org/10.1007/s12239-020-0031-x

*International Journal of Automotive Technology*, Vol. 22, No. 1, pp. 131–139 (2021)
DOI 10.1007/s12239–021–0014–6


pISSN 1229–9138/ eISSN 1976–3832

## CHARACTERIZATION OF VEHICLE AND LABORATORY AGED COMMERCIAL THREE WAY CATALYST: A MORPHOLOGICAL AND FUNCTIONAL CORRELATION BETWEEN REAL AND SIMULATED AGEING

Mattia Giuliano[1, 2)*], Gabriele Ricchiardi[1)], Maria Carmen Valsania[1)], Flavio Parussa[2)], Giovanna Nicol[2)] and Mauro Sgroi[2)]

[1)]Department of Chemistry, NIS and INSTM Reference Centre, University of Torino, Torino 10125, Italy
[2)]Fiat Research Center, Group Material Labs, Environment & Chemical Analysis, Innovation Aftertreatment & Batteries, Strada Torino 50, Orbassano 10043, Italy

*(Received 30 March 2020; Revised 30 April 2020; Accepted 5 May 2020)*

DOI: https://doi.org/10.1007/s12239–021–0014–6

catalysts

MDPI

*Article*

# Characterization of the Evolution of Noble Metal Particles in a Commercial Three-Way Catalyst: Correlation between Real and Simulated Ageing

**Mattia Giuliano [1,2*], Maria Carmen Valsania [1], Pierfrancesco Ticali [1], Enrico Sartoretti [3], Sara Morandi [1], Samir Bensaid [3], Gabriele Ricchiardi [1] and Mauro Sgroi [2]**

[1] Department of Chemistry, NIS and INSTM Reference Centre, University of Torino, Via G. Quarello 15, I-10135 and Via P. Giuria 7, I-10125 Torino, Italy; mariacarmen.valsania@unito.it (M.C.V.); pierfrancesco.ticali@unito.it (P.T.); sara.morandi@unito.it (S.M.); gabriele.ricchiardi@unito.it (G.R.)

[2] Batteries & Aftertreatment, E/E & Multifunctional Materials, Materials Engineering Methods & Tools, Fiat Research Center, Strada Torino 50, 10043 Orbassano, Italy; mauro.sgroi@crf.it

[3] Department of Applied Science and Technology, Politecnico di Torino, Corso Duca degli Abruzzi 24, 10129 Turin, Italy; enrico.sartoretti@polito.it (E.S.); samir.bensaid@polito.it (S.B.);

* Correspondence: mattia.giuliano@crf.it; Tel.: +39-011-908-3605

DOI: https://doi.org/10.3390/catal11020247